MAR 31 1971

THE UNIVERSITY OF MANITOBA

THE VARIATION OF DIFFUSER EFFICIENCY WITH MASS INJECTION NORMAL TO THE ENTRY FLOW

by

B. W. WILTON

A THESIS

SUBMITTED TO THE FACULTY OF GRADUATE STUDIES

IN PARTIAL FULFILMENT OF THE REQUIREMENTS FOR THE DEGREE

OF MASTER OF SCIENCE IN MECHANICAL ENGINEERING

DEPARTMENT OF MECHANICAL ENGINEERING

WINNIPEG, MANITOBA

MAY, 1971

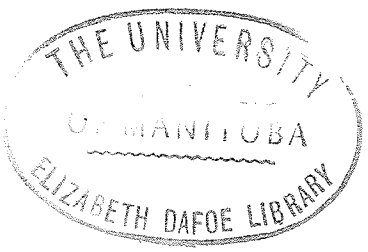

© B. W. Wilton 1971

TABLE OF CONTENTS

		Page
LIST OF NOTATION		iii
SUMMARY		iv
1.	INTRODUCTION	1
2.	THEORETICAL AND EXPERIMENTAL BACKGROUND TO THE WORK	3
	2.1 Diffuser Efficiency	3
	2.2 Diffuser Design	6
	2.3 Turbulent Flow in Rectangular Channels	9
	2.4 Separation of the Turbulent Boundary Layer	10
	2.5 Diffuser Flow Mechanisms	14
	2.6 The Reattachment of a Two Dimensional Jet to a Flat Surface	18
	2.7 The Configuration of a Jet in a Deflecting Flow	19
	2.8 A Stubby Circular Cylinder Within a Boundary Layer	21
3.	EXPERIMENTAL TECHNIQUE	21
	3.1 Apparatus	21
	3.2 Flow Visualization	23
	3.3 Investigation of Diffuser Flow Mechanisms	25
4.	DEVELOPMENT OF THE MASS INJECTION SYSTEM	26
	4.1 Variations in the Method of Injection	26
	4.2 Variations in the Configuration of Injection	28
	4.3 Variations in the Position of Injection	29
	4.4 The Injection System	30
5.	DISCUSSION OF RESULTS	31
	5.1 Diffuser Efficiency and Its Correlation With Published Values	31
	5.2 The Flow Mechanisms Created By Jets Normal to the Mainstream	32
	5.2.1 The Single Jet	33
	5.2.2 The Double Jet	35
	5.2.3 Variations in Flow Mechanisms With Bleed Rate	37

Page

5.3 Variation of Efficiency With the Configuration 38

5.4 Variations in Diffuser Flow Mechanisms With Mass Injection Rate 41

5.5 Variations in Diffuser Efficiency With Mass Flow Rate 43

6. GENERAL CONCLUSIONS 44

APPENDIX A

A Fluidic Windtunnel Speed Stabilization System. 47

APPENDIX B

Design Considerations for the Full Scale Windtunnel. 51

LIST OF REFERENCES. 55

FIGURES

LIST OF NOTATION

A	cross-sectional area at the section in question
A^1	total cross-sectional area of the jets
m	ratio of the areas at the inlet and exit of the diffuser
$\dot{M}_b$	bleed mass flow rate in the jet
$\dot{M}_\infty$	mass flow rate in the mainstream
P_1	static pressure at the diffuser inlet
P_2	static pressure at the diffuser exit
ΔP	change in static pressure between the diffuser inlet and the diffuser exit
ΔP^1	pressure rise to the section of maximum pressure in the straight duct following the diffuser
ΔP_f^1	pressure rise to an assumed pipe friction in the straight duct following the diffuser
u_1	local velocity at a point in the cross-section at the diffuser inlet
u_2	local velocity at a point in the cross-section at the diffuser exit
$\overline{u}_1$	mean velocity at the diffuser inlet
$\overline{u}_2$	mean velocity at the diffuser exit
α_1	kinetic energy coefficient at the diffuser inlet
α_2	kinetic energy coefficient at the diffuser exit
θ	angle of flow expansion within the diffuser
η_p	pressure efficiency
η_E	energy efficiency
η_o	overall efficiency
$\Delta\eta$	maximum change in diffuser efficiency
ρ	density of air

SUMMARY

Variations in diffuser efficiency are created by injecting mass in the form of circular jets just upstream of the diffuser inlet. Diffuser efficiency can be decreased from 82.5% to 74.0% with the mass flow in the jets 2.3% of the mainstream mass flow. The flow mechanisms around the jets were visualized using the liquid film technique. Pitot traverses were performed to evaluate the flow mechanisms within the diffuser. Decreasing the mass flow in the jet results in a simple decrease in the magnitude of the flow mechanisms around the jet and within the diffuser.

ACKNOWLEDGEMENTS

The author wishes to acknowledge his appreciation to Dr. Jeff Tinkler for suggesting the topic and for his valuable criticisms given as thesis advisor. Special thanks to Mr. Gus Bertels, Dr. Ram Azad, and Messrs. Frank Christian, Les Wilkins, Fred Buccini and Fred Wilton for their advice and technical assistance.

1. INTRODUCTION

A diffuser as its name implies, is a device used to slow down the mainstream flow usually with the least possible loss in energy. As the area ratio increases, continuity demands that the mass flow remain constant and therefore the velocity of the fluid must decrease. However, as the velocity decreases, the static pressure in the diffuser rises. The adverse pressure gradient (i.e. rising pressure) in a diffuser causes considerable problems in the boundary layer of the flow. If the velocity distribution upstream of the diffuser is non-uniform or if the angle of divergence of the diffuser is too great, then a thick boundary layer will be formed in the diffuser. At a point very close to the wall, the flow has been slowed almost to a standstill. The increasing pressure however calls for a further retardation. The fluid near the wall responds by moving slightly upstream. Thus a zone of recirculation has been established causing a deflection of the mainstream (i.e. the mainstream has "separated" from the wall). Separation creates irregular turbulent eddies downstream which cannot reconvert their kinetic energy of rotation into a pressure rise. Therefore, the diffuser operates inefficiently.

Diffuser efficiency is a measure of how effectively a diffuser converts the kinetic energy at its inlet to static pressure at its outlet. If no separation occurs within the diffuser, losses will be low with good pressure recovery. However, if separation does occur, the flow is highly disturbed and losses are significant. It has long been noted that leakage into a diffuser is detrimental to its pressure recovery, thereby lowering its efficiency. In effect, the leakage would take the form of small jets at the flanged joints on either end of the diffuser. It would seem plausible

then that jets could be used to control diffuser efficiency.

The present study to produce variations in efficiency by injecting air normal to the flow in a diffuser is part of a program to stabilize speed fluctuations in an open circuit wind tunnel at the University of Manitoba. The speed stabilization system has four basic components.

- a speed sensor
- a comparator
- a power amplifier
- a variable tunnel resistance.

A speed sensor incorporating the comparator has been developed and its performance investigated [1]. The power amplifier is under investigation. Variable tunnel resistance is to be controlled by two means: (1) variation of the drag of blunt bodies by means of base bleed, and (2) diffuser efficiency control by blowing normal to the flow entering the diffuser. Comprehensive tests have been done to determine the variation of drag with base bleed [2 & 3]. The present study is concerned with controlling diffuser efficiency.

Should a loss in tunnel speed be detected by the speed sensor, a pressure output from the comparator is relayed to the fluidic amplifier to produce relatively large input flow changes to the diffuser efficiency control and base bleed cylinders. This system is unique in that fluidic (rather than electro-mechanical) means are used to control the flow. The attractive feature of all fluidic devices is that they contain no moving parts and they can operate under widely varying environmental conditions for indefinite lengths of time. In most fluidic devices, use is made of interaction of jets and phenomena relating to separated and reattached

flows. Since their development in 1960, new and varied applications have been found for these devices. The present study is one such application.

A more detailed description of the speed stabilization system and the role fluidics play in it is presented in Appendix A.

2. THEORETICAL AND EXPERIMENTAL BACKGROUND TO THE PRESENT STUDY

2.1 Diffuser Efficiency

The efficiency of a diffuser in converting the kinetic energy at its inlet to pressure, can be defined in several ways and the suitability of any particular definition depends upon the purpose for which the diffuser is used. Basically, diffuser performance may be described by: (1) pressure efficiency; (2) energy efficiency; and (3) overall efficiency.

The simplest definition of efficiency is based on the assumption that the local velocity u_1 entering the diffuser at any point in the section is uniform across the throat section and that the velocity u_2 through its exit section is also uniform and equal to mu_1 where m is the ratio of the area at the diffuser entrance to that at the exit. The efficiency of pressure recovery can be expressed as

$$\eta_p = (P_2 - P_1) / (\tfrac{1}{2}\rho u_1^2 - \tfrac{1}{2}\rho u_2^2)$$

$$= \Delta P / \tfrac{1}{2}\rho u_1^2 (1 - m^2).$$

In determining the efficiency, it is necessary to measure only the pressure rise ΔP and the inlet dynamic pressure.

No flow confined within the walls of a pipe has a perfectly uniform velocity across its section. Velocities near the boundary are less than the mean and near the center of the passage velocities are usually greater than the mean. The true kinetic energy entering the diffuser is therefore greater than that obtained by using the mean velocity (where the mean velocity is found by integrating the local velocities over the section and dividing by the area of the section), but less than that obtained by measuring the total head on the center line and subtracting the static pressure. If the true kinetic energy flowing through the inlet section is $\alpha_1 \ (\frac{1}{2}\rho\bar{u}_1^2)$ then

$\alpha_1 = \frac{1}{A}\int (u_1/\bar{U}_1)^3 dA$ where A is the total cross sectional area, u, the local velocity, and $\bar{U}_1$ the mean velocity. Precise values of α_1 can be determined only by measurement of the inlet velocity distribution. In fully developed turbulent pipe flow, α_1 is of the order of 1.04 but it can rise above 1.1 in very rough walled ducts [4]. The velocity distribution at the outlet of a diffuser is usually very disturbed and the mean kinetic energy is usually greater than $\frac{1}{2}\rho\bar{U}_2^2$. The kinetic energy coefficient at the exit (α_2) is therefore very sensitive both to the flow conditions entering the diffuser and within it. A true energy efficiency can be written

$$\eta_E = (P_2 - P_1) \ / \ (\alpha_1 \tfrac{1}{2}\rho\bar{U}_1^2 - \alpha_2 \tfrac{1}{2}\rho\bar{U}_2^2)$$

$$= \Delta P \ / \ \alpha_1 \tfrac{1}{2}\rho\bar{U}_1^2 \ \left(1 - \frac{\alpha_2}{\alpha_1} \cdot m^2 \right)$$

provided that the pressure is uniform across the two cross sections considered. The experimental determination of this efficiency is tedious since, in addition to the pressure rise and the mean entry velocity, it is necessary to establish both α_1 and α_2 by velocity traverses at the entry and exit sections of the diffuser. The velocities at the exit of a diffuser can

fluctuate very severely and, if the flow has separated and is oscillating from one side to another, very deceptive results can be obtained with ordinary slow traversing of a single pitot tube across the whole section.

Yet a third definition of efficiency is possible when a diffuser is followed by a length of straight parallel pipe in which the bad velocity distribution emerging from the diffuser is allowed to straighten itself out. For a short distance following the diffuser, static pressure rises in spite of wall friction and, because of the smoothing of the velocity distribution, the kinetic energy diminishes. Gibson [5] reports that this smoothing out of the flow is very rapid. His work on a 10.2^{o} rectangular diffuser showed that only 2.5 widths of the diffuser were required downstream of the diffuser exit so that α_2 would fall from 1.20 to 1.035. An efficiency based on the pressure rise to the highest pressure point in the duct following the diffuser should be slightly below the energy efficiency due to the energy lost in the flow evening process. However, the usual correction for pipe friction losses in the downstream section of the duct is an over-correction because of the abnormally low velocities near the walls. Tests on diffusers carried out this way are sufficient for many practical purposes and very much easier since no great error is involved by assuming the downstream kinetic energy factor α_2 equal to about 1.03. This overall efficiency can be written

$$\eta_o = (\Delta P^1 + \Delta P_f{}^1) \; / \; \tfrac{1}{2}\rho \bar{U}_1{}^2 \; (\alpha_1 - \alpha_2 m^2)$$

where ΔP^1 is the pressure rise from the diffuser-entry to the section of maximum pressure in the downstream duct, α_2 is the kinetic energy factor for the velocity distribution in this section and $\Delta P_f{}^1$ is the pressure credit due to the assumed pipe friction in the downstream section of the duct (it would seldom exceed 1% of ΔP^1).

Of these three definitions, the simplest to use would be η_p, provided that the mean velocity obtained by integrating over the diffuser inlet did not vary significantly from the centerline velocity. Otherwise, velocity traverses would have to be taken at the diffuser inlet for each condition at which the efficiency was checked.

2.2 Diffuser Design

One of the most important causes of low efficiency in duct systems is the large loss which accompanies a transformation from kinetic energy to pressure. Exit cones of wind tunnels and turbines, expanding entries to cooling ducts, and air intakes on aircraft, all require efficient expansions of flow. It is well known that the effect of an opposing pressure gradient on the boundary layer at a wall is to increase the thickness of the layer and, when the pressure gradient is large, to produce a separation of the flow from the wall. These phenomena occur in diffusers where the pressure rises and the velocity falls as the section diverges. Large loss of head results from a separation and this constitutes the main design problem. If the diffuser is properly designed, a high efficiency is obtainable.

The efficiency depends upon various factors, the most important of which is the rate of expansion of the flow, as this factor determines the magnitude of the opposing pressure gradient. Some results of experiments on the flow between straight diverging walls by Gibson and Peters [5 & 6] are summarized in Figure 1. Pressure efficiency η is plotted against 2θ, as in Figure 2. The efficiency is high at small angles only and drops off rapidly as 2θ increases. The angle of divergence (2θ) at which maximum

efficiency occurs depends upon the shape of the tunnel. For conical diffusers the angle of maximum efficiency lies in the range of 2θ = 5 degrees to 2θ = 8 degrees. In general the efficiency decreases rapidly after 10 degrees. Diffusers of rectangular section have been investigated by Gibson and Vedernikov as reported in Reference 7. The expansion was carried out between one pair of walls, the other pair remaining parallel. Maximum efficiency occurs at 2θ = 11 degrees. Similarly Gibson also considered the case of a diverging duct having a square section throughout. Here maximum efficiency occurs at 2θ = 6 degrees. Figure 3 is a comparison of the efficiency of two versus four diverging walls for various angles of expansion.

The effects of these three sectional shapes on the efficiency may be compared at the same rate of expansion (i.e. the same increase in area per unit lenght of duct) as in Figure 4. At a given rate of expansion, the conical diffuser is the most efficient of the three.

It has been shown that the flow conditions in a diffuser and the downstream duct depend on the velocity distribution at the inlet of the diffuser (i.e. the initial state of the boundary layer, which may be measured in terms of displacement, momentum, and energy thicknesses). Worster [4] reports that Winternitz has recently shown a good correlation between diffuser efficiency and the inlet momentum thickness of the boundary layer. Various velocity distributions can be created by using different lengths of inlet pipe (l_1 in Fig. 2). With $l_1 = 0$, the velocity is very nearly constant over the whole inlet section and when l_1 = 30 times the diameter of the initial section (D_1 in Fig. 2), the velocity varied as the 1/7th power of the distance from the wall (i.e. fully developed turbulent

flow). Comparing the values of η in Figure 5, it is seen that a turbulent boundary layer at the diffuser inlet reduces the efficiency by about 7% in the range 5 deg $\leq 2\theta \leq$ 30 deg.

A factor which is also very important is the length of duct following the diffuser. It has been shown that the rise in pressure during the transformation from kinetic energy to pressure is not complete at the final section of the diffuser. The pressure continues to rise in the duct following the cone, reaching a maximum at a position two to six times the maximum diameter (D_2 in Figure 2) from the outlet of the diffuser. A complete investigation of the effect of varying the outlet length of duct (l_2 in Figure 2) has been completed and the results are shown in Figure 6. It has further been shown that the position of maximum pressure depends on the angle of expansion and on the flow conditions at the entry to the diffuser. It can be seen from Figure 6 that when there is fully developed turbulent flow at the entry ($l_1 / D_1 = 30$), the length of duct following the final section of the diffuser is about $6D_2$ for all values of 2θ. On the other hand, when the velocity distribution over the inlet section is very nearly constant (i.e. the boundary layer is very thin), l_2 may be shorter (e.g. at $2\theta = 8$ deg, $l_2 / D_2 = 4$).

The rise in pressure in the duct following the outlet of the diffuser is a result of a mixing of the flow which produces a change in the velocity distribution between the exit of the diffuser and the position of maximum pressure. It has been found that the velocity distribution over the section where the pressure is a maximum is very similar to the velocity distribution of fully developed turbulent pipe flow and that it is approximately independent of the angle of expansion and of the velocity distribution at the entry section.

No extensive tests on the effect of the Reynolds number on the efficiency appear to have been made. Gibson and Peters [5 & 6] both indicate that there was no appreciable scale effect in the range $0.5 \times 10^5 \leq R_e \leq 2.5 \times 10^5$ in which their experiments were made.

A careful consideration of the above factors will lead to an efficient diffuser design. The necessity for a small angle of divergence however often implies that diffusers of very long length will be required. Such designs are not always possible, particularly on aircraft where considerations of weight, compactness and cost are important. This problem leads to variations in the rate of curvature, the use of vanes and deflectors, and the use of suction, any one of which may be incorporated in the diffuser design. As the present study is unconcerned with such problems, these considerations in diffuser design will be by-passed.

2.3 Turbulent Flow in Rectangular Channels

As all the ducts on the experimental apparatus in the present study are square or rectangular in shape, it may be well to consider some aspects of the type of flow one would expect from them.

Fully developed turbulent flow in straight channels of a non-circular cross-section is a three dimensional problem both in mean flow and the turbulence structure. The mean flow velocity vector at each point in the flow field is generally composed of a component in the axial flow direction and transverse components in a plane normal to this direction. The transverse components at all points form a flow pattern known as secondary flow and which can be regarded as being superimposed upon the axial mean flow.

For fully developed laminar flow in straight non-circular channels, secondary flow is non-existent. For discussion purposes however, consider fully developed turbulent flow in a square channel. From experimental measurements it is known that secondary flow in this type of channel distorts isotachs as shown in Figure 7 [8] where an isotach is defined to be a line of constant axial mean-flow velocity. For comparison purposes a typical isotach for fully developed laminar flow is also shown in Figure 7. If quantitative measurements of secondary flow are made, it is possible to construct secondary flow streamlines. Typical secondary flow streamline patterns are shown in Figure 8 where ψ is the stream function (defined in terms of the channel half-width, the centerline velocity, and the secondary flow components in the y and z directions) and C_1, C_2,... are constant values. Investigations by Nikuradse (1926), Hoagland (1960) and Gilbert (1960) indicate typical secondary flow velocities of the order of 1% of the maximum axial mean flow velocity [8]. Furthermore it has been shown that secondary flow, although a small fraction of the total mean flow, has a pronounced effect on isotach distributions as in Figure 7.

2.4 Separation of the Turbulent Boundary Layer

Boundary layer flow has the peculiar property that under certain conditions the flow in the immediate neighbourhood of a solid wall becomes reversed causing the boundary layer to separate from it. In order to understand this phenomenon, a detailed study of the processes involved within the boundary layer will be presented.

Adjacent to a wall, the motion of a thin stratum of fluid lying wholly inside the boundary layer is determined by three factors:

1) The forward pull of the outer free-moving fluid, transmitted through the laminar boundary layer by viscous shear and through the turbulent boundary layer by bulk momentum transfer.
2) The viscous retarding of the solid boundary which must, by definition, hold the first stratum adjacent to it at rest.
3) The pressure gradient along the boundary. The stratum is accelerated by a negative pressure gradient (i.e. pressure decreasing in the direction of flow) and retarded by a positive gradient, provided the viscous stresses are not too large.

Consider the flow about a circular cylinder along with its accompanying pressure distribution as shown in Figure 9. In the presence of a negative pressure gradient (as from D to E Figure 9) the boundary layer follows the contour of the surface. If a particle enters the boundary layer near the forward stagnation point (D) with a low velocity and high pressure, its velocity will increase as it flows into the lower pressure region along the side of the cylinder. However, there will be some retardation from wall friction so that its total useful energy will be reduced by a corresponding conversion into thermal energy. At E the pressure is at a minimum and from E to F the pressure would increase as shown in Figure 9.

What happens next may best be explained by reference to Figure 10. Let A represent a point in the region of accelerated flow, with a normal velocity distribution in the boundary layer while C, D and E are points

downstream on the curved surface along which the pressure is increasing. When the particle in the boundary layer passes the point of minimum pressure and maximum velocity (B), it cannot regain its original pressure and velocity values because of the energy it has converted to heat. The velocity of the layer close to the wall is reduced at C and finally brought to a stop at D. The increasing pressure calls for a further retardation. As the flow is at a standstill (making further retardation virtually impossible), the boundary layer separates from the wall. At E there is a back flow next to the wall, driven in the direction of decreasing pressure- opposite to the direction of the mainstream - feeding fluid into the boundary layer which has left the wall at D.

Downstream from the point of separation, the flow is characterized by irregular turbulent eddies, formed as the separated boundary layer becomes rolled up in the reversed flow. This condition usually extends for some distance downstream until the eddies are worn away by viscous attrition. Because the eddies cannot convert their kinetic energy of rotation into an increased pressure, the pressure downstream remains close to that at the separation point.

Recently, a new concept has been developed to aid in the explanation of turbulent boundary layer separation. The theory by Stratford [9] postulates that the turbulent boundary layer in a pressure rise may be divided into two distinct regions. The outer is an historical region in which the pressure rise just causes a lowering of the dynamic head profile, the losses due to the shear stresses being almost the same as for flow on a flat plate. In the inner layer on the other hand, the inertia forces are small so that the velocity profile is distorted by the pressure gradient until the latter

is largely balanced by the transverse gradient of shear stress. It has been found that for the inner layer at the separation position, the velocity close to the wall is proportional to the square root of the distance from the wall. The velocity profile is in contrast to that for the laminar boundary layer at separation where the velocity is proportional to the square of the distance from the wall. A summary of the treatment and a picture of the flow is sketched in Figures 11 and 12.

In the outer layer in a rapid pressure rise, the shear forces in the outer part of the boundary layer are small compared with either the inertia forces or the pressure gradient. Shear forces however do cause a decrease in total pressure along any one streamline, but this decrease is uniform across the whole velocity profile as shown in Figure 11. Therefore the effect of the pressure rise in the outer part of the boundary layer in this region is to cause a general lowering of the velocity profile rather than a change in shape.

In the inner layer the effect of the fluid inertia is too small for the above mechanism to be possible. In particular, the inertial forces at the wall are zero so that the pressure forces must be balanced entirely by the gradient of the shear force, i.e.

$$\frac{\partial P}{\partial x} = \frac{\partial T}{\partial y} \quad \text{at } y = 0$$

This balance at the wall can only occur after there has been a change in the profile shape. When the sudden pressure gradient is reached at a point $x = x_o$, the dynamic head and hence the general level of velocity would start to fall everywhere, were it not for the no slip condition at the wall. This, as it were, anchors the velocity profile, which distorts

instantaneously at $x = x_o$, $y = 0$, until, just at the wall, the required balance is attained. The inner layer commences its growth at the discontinuity at $x = x_o$, $y = 0$ and is the region in which the slope of the velocity profile has changed. In the inner layer there is a transition between fluid at the wall, for which the pressure force is balanced entirely by the shear force gradient, and fluid in the outer layer, where the pressure forces causes simply a direct reduction of dynamic head. Thus the concept of an "inner" and "outer" region in a turbulent boundary layer aids greatly in the understanding of separation and its related phenomena.

2.5 Diffuser Flow Mechanisms

As has been shown in § 2.2, the flow in a diffuser depends upon: the inlet velocity profile; the total divergence angle; the area ratio; and several other design factors. As a function of the parameters listed above, there are also four regimes of flow found in the diffuser. Holding all inlet conditions constant and holding the ratio of wall length to throat width constant, increasing the angle of divergence from zero to 100 or more degrees causes these four regimes to appear in the following order: (1) no appreciable stall or transitory stall (where "stall" is synonymous with the term "separation"); (2) large transitory stall; (3) fully developed stall; and (4) jet flow. These regimes are sketched in Figure 13 and are shown as a function of the parameters listed above in Figure 14.

According to Kline, Moore and Cochran [10] transitory stall is not a two dimensional flow but clearly a three dimensional transient flow. Furthermore it exists over a very wide range of conditions as can be seen in Figure 14. In this flow regime, transient "spots of stall" appear and

disappear first in one location and then in another. The extent of this regime of flow was found to be strongly influenced by inlet free-stream turbulence as well as by diffuser divergence angle and area ratio. In the early work the regimes of flow were mapped using a conventional dye injection system. Subsequently, it began to be clear that transitory stall existed at much lower angles than those at which it had already been observed. Kline [11] in his study of plane walled diffusers with two parallel walls made the following "tentative" conclusions:

(a) Spots of transitory stall may exist down to at least very low values of adverse pressure gradient.

(b) These spots originate very near the wall, probably in the laminar sublayer.

(c) The spots grow in size, number and time of duration as the adverse pressure gradient is increased in magnitude or in length of application.

(d) The means by which the spots are carried back downstream is by leaving the wall and being caught up by the inertia of the mainstream.

Kline further reports that careful observations of the wall layers using the dye persistence technique show that small local transient backflows to exist near the wall even for surprisingly mild adverse pressure gradients. For example, back flows or spots of stall have been clearly seen by several observers at a total divergence angle of 5 degrees with a ratio of wall length to throat width of 6.7 and a thin inlet boundary layer. In some instances spots of stall have been observed at even lower angles. The actual minimum value of angle at which spots of stall can first be discerned

apparently depends both on the number of observations made and on the free-stream turbulence level. As such the occurrence is statistical in nature thereby requiring more detailed studies before more exact information is available.

When found at very small adverse pressure gradients the spots of stall are very small and appear for only short periods of time. Typically, on a 4 inch wall, one spot might appear in a matter of 2 minutes at a given cross-section and might be 1/16 of an inch in diameter. As the adverse pressure gradient is increased, the spots grow; several spots may appear at once at a given cross-section, and they may extend through the boundary layer into the main flow. Finally the spots coalesce and destabilize the entire flow pattern. A fully developed stall then ensues with flow moving upstream all along one wall. The growth of these spots of stall correlates with the increase in losses of the diffuser. This phenomenon can be used to explain many well-known but previously inexplicable facts such as: (1) large pressure pulsations in diffusing passages; (2) the large losses in diffusers which cannot be accounted for by wall friction and turbulence; (3) the differing observations made by previous observers about the nature of stall; and (4) the consistent failure of two dimensional boundary layer theory to predict the separation of the turbulent boundary layer.

It is now generally believed that the inception of stall is usually a three dimensional transient phenomenon called transitory stall. Kline concludes that transitory spots of stall are viewed as a mechanism that is adopted by the fluid to supply the energy needed by the very slow moving layers near the wall in order to negotiate an adverse pressure gradient.

The regime of flow called steady stall on Figure 14 corresponds to the classical picture of stall of a two dimensional boundary layer. It has a recirculating flow region occupying most of the diffuser; the through-flow follows down one wall and the performance is very poor. The fully developed stall regime is a relatively steady, stable, flow condition. The region of large fluctuations recorded by some observers is believed to be the region of large transitory stall. The distinction between the two regimes is clearly defined. In fully developed stall, one wall has a large area of back-flow all the time; in transitory stall, any given wall area has forward flow part of the time and backward flow part of the time.

The last flow regime to be considered is jet flow. The jet flow region occurs only at very high angles of divergence. It is characterized by a fully developed stall on both walls. It is less stable than the regime called two dimensional steady stall, and thus one finds an overlap region on the flow mechanism chart of Figure 14. If the angle is increased, transition to jet flow occurs at the upper line; if the angle is decreased the transition is found at the lower line. The flow mechanism chart of Figure 14 can be used not only to explain the known data and performance of diffusers over the range of interest but also can be used as a basis for the design of wide-angled diffusers of high performance. In addition, the chart provides basic information about the nature of turbulent boundary layer flows in adverse pressure gradients.

2.6 The Reattachment of a Two Dimensional Jet to a Flat Surface

Although the present study is concerned with a three dimensional jet in a streaming flow, the flow mechanisms involved in a two dimensional jet should aid in the more complex three dimensional case.

Jets are frequently observed to adhere to and flow around nearby solid boundaries. This is seen, for example, when one's finger is held close to a thin stream of water issuing from a tap, or when tea is poured from a badly-designed teapot. This general class of phenomena which may be observed in both liquid and gaseous jets, has become known as the Coanda effect, after Henri Coanda who applied it in many inventions.

Although a jet is probably deflected more effectively by a curved surface, there is nevertheless considerable interest in Coanda's particular wall geometry, the simplest form of which consists of a single flat plate displaced a short distance from a two dimensional slot and inclined at an angle to the axis of the slot. After leaving the slot the flow separates from the surface and, if the plate is sufficiently long and its inclination is sufficiently small, the jet curves toward the plate and eventually reattaches to it, enclosing a separation bubble. The forces on the flat plate have been measured by von Glahn and a physical explanation of the behaviour has been given by Squire as reported in [12]. It is imagined that the jet is flowing freely, completely separated from the plate. After leaving the slot the highly unstable shear layers on both sides of the jet quickly become turbulent and the surrounding fluid is rapidly entrained. That fluid which is entrained near the wall is slightly accelerated. The presence of the wall impedes the replacement of the entrained fluid and thus the static pressure on the wall becomes less than that of the

surroundings. In consequence the jet curves toward the wall. This in turn impedes the return flow still more and the static pressure drops further. Thus eventually, if the wall is long enough, the flow reattaches to it, enclosing a separation bubble. An equilibrium condition is reached when the mass flow entrained from the bubble by the inner portion of the jet balances the mass flow returned to the bubble at reattachment where the jet divides into forward and reversed flows as in Figure 15.

2.7 The Configuration of a Jet in a Deflecting Flow

In a number of cases it is necessary to deal with a jet expanding into a stream of fluid at an angle to it. For example, in the combustion chamber of a gas-turbine engine, a significant part of the air necessary for combustion and all the air used for cooling the combustion products are introduced through inlets located in the side walls of the hot tube.

A jet of fluid entering a flow which is moving at an angle to the jet's axis, is curved in the direction of flow of the mainstream. The mainstream flow is retarded by entrainment of the jet at its leading edge, thereby creating an increased pressure, while at the rear of the jet rarefaction occurs as explained in § 2.6. The pressure difference across the jet creates the necessary centripetal force to deform the jet. The velocity and pressure fields of a curved jet of air in the plane of symmetry of the jet are represented in Figure 16 [14]. The measurements were made by means of a cylindrical probe traversed along directions normal to the local axis of the jet which is represented by the geometric location of the points with the maximum velocity values. The profile of the total pressure is given by the solid line; the static pressure profile by the dotted line; the arrows designating velocity vectors. The total pressure changes sharply, decreasing

at the edges of the jet. Because of the inflow of fluid to the jet, the increase in pressure at its forward edge is somewhat less than it would be at the wall of a solid body of the same form as the curved jet. In the jet itself, the static pressure continuously decreases from the forward edge to the rear.

In Figure 17 from the work of G.S. Shandorov as reported in Ref. 14, the cross-sectional contours of a jet are shown for the initial and subsequent sections. If a jet is initially axisymmetric, then as it moves away from the nozzle, it will acquire the shape of a horseshoe. The deformation of the jet's section is explained by the character of its interaction with the flow. Because of the intensive intermixing of the air as it emerges from the nozzle with that of the air of the deflecting flow, a turbulent layer develops at once. Peripheral particles of the jet, having less velocity than the particles of the core are more forcefully bent by the deflecting flow away from their initial direction and are moved along more curved trajectories, which leads to the development of a horseshoe.

As a result of the action of the deflecting flow and the circulatory zones, the particles of the jet all branch out more and more from the plane of symmetry. The legs of the "horseshoe" move farther apart, giving rise to the possibility of additional circulatory motion in the jet itself (i.e. of vortex pairs with axes parallel to the aerodynamic axis of the jet). The corresponding flow diagram is shown in Figure 18.

2.8 A Stubby Circular Cylinder Within a Boundary Layer

During the flow visualization portion of the present study, it was found that interaction of the jet with the boundary layer was similar to that of a circular cylinder protruding a short distance into the boundary layer.

Gregory and Walker (1951) made some experiments on this type of flow as part of an investigation into the effect of very small excrescences in promoting transition from laminar to turbulent flow [13]. They showed (as in Figure 19) that the horseshoe vortex passes around the front of the cylinder in both directions and leads to a vortex pair trailing off downstream. This vortex induces in turn a smaller pair of vortices rotating in the opposite sense and passing downstream in the same way. Later in § 5.2, the similarities between the flow pattern produced by a stubby cylinder and that produced by a cylindrical jet, will be presented.

3. EXPERIMENTAL TECHNIQUE

3.1 Apparatus

The tests for the present study were conducted at the University of Manitoba on a square diffuser: initial section 6" x 6"; divergence angle 2θ = 6 degrees and area ratio A_1/A_2 = 0.25. Construction was of 1/4" plywood with the exception of one side which was 1/4" plexiglass.

Immediately upstream of the diffuser (Figure 20) a 3" long section of 1/2" thick plexiglass on all four sides of the tunnel served as an aid in visualizing the jet flow as it interacted with the mainstream. This

section also served as the injection site for the jets and therefore connections were made to this section to monitor the mass flow rate to the jets. The diffuser was supplied with air from a 3 H.P. centrifugal fan at approximately 80 ft/sec. A honeycomb at the fan exhaust as well as two wire screens (32 Mesh) on either end of the effuser caused a considerable straightening of the flow. A 7" length of straight duct following the effuser allowed some of the disturbances coming from the fan to subside further.

Immediately downstream of the diffuser a two foot length of duct helped in pressure recovery.

Pitot traversing mechanisms were installed along the tunnel, one upstream of the diffuser, three within the diffuser and one downstream of the diffuser exit. Basically, these mechanisms consisted of a wooden slide for movement in the vertical plane and a pitot tube which could be traversed in the horizontal plane. Station 1 was located 3" upstream of the diffuser inlet; stations 2, 3, 4 and 5 were located 4", 16", 28" and 58" downstream of the diffuser inlet respectively. Static pressure taps were installed at stations 1 to 5 as well as at 6" intervals down both the top and bottom of the diffuser for its entire length. The static taps were connected to a multi-tube manometer to facilitate the reading of pressures. The mass flow rates of the jets were also monitored on the multi-tube manometer.

3.2 Flow Visualization

Several different methods of flow visualization were used with varying degrees of success in order to help interpret the flow within the diffuser.

Initially, tufts were spaced at two-inch intervals for the full length of the diffuser on three of the four walls. The tufts were made from a 1 1/4" length of cotton string which was tied and cemented to a 1/4" length of nylon thread. The thread was fastened to the diffuser wall by a small piece of masking tape. The nylon thread allowed the tuft to pivot in the direction of the flow in the diffuser. The length of the tuft itself determines to some extent the type of flow it will record. If the tuft was too short, it would be more sensitive to the randomness of the turbulence in the diffuser than a longer tuft, which would tend to record more of an average direction. Figure 22 demonstrates the use of the tuft as it indicates separation occurring approximately half-way down the diffuser.

Once the mass injection system had been installed, limited trials were made using smoke for visualizing the jet in the mainstream. As it was physically impossible to generate enough smoke to make the jet visible in a mainstream whose velocity was of the order of 80 ft/sec, an alternate technique was used. By quickly turning the fan on and off, an impulse of air was sent into the tunnel which when coupled with smoke issuing from the mass injection hole produced a trace such as in Figure 23. The jet can be seen reasonably well even though its leading edge is partially obscured by a reflection. This technique however provided only limited information on the jet in the mainstream and therefore another technique was proposed.

The liquid film technique has long been used in flow visualization. Generally, a suspension of lampblack in kerosene is painted on an airfoil which has been placed in an airstream. The kerosene flows over the surface, evaporating as it does so, leaving the lampblack deposited on the surface as streamlines. Several modifications of this method were used to suit the present study. Rather than lampblack, a commercial flourescent paint powder pigment* was used. As well as being readily available, this powder is flourescent under ultra violet light which enables better resolution than ordinary incandescent light can provide. This property was found unnecessary however, as the photographs obtained with the Polaroid Land Camera were generally of a high quality. Rather than painting the suspension on in the tunnel, a stainless steel plate (coated with the suspension) was placed in the tunnel on top of the plexiglass. Holes were drilled in the plate to coincide with those in the plexiglass bottom. The jet then passed through both the plexiglass and steel plates, leaving a trace on the steel plate which could then be removed from the tunnel and photographed. Another plate configuration entailed suspending a plate in the plane of symmetry of the jet. These two plate configurations are shown in Figure 24. A third configuration, that of a plate in the plane of symmetry of the two sets of jets in the corner (i.e. along the diagonal of the tunnel section), provided no further information as there was no visible trace on the plate.

The proper suspension of Day-Glo in kerosene was determined by trial and error. Three and one-half parts of Day-Glo to one part of kerosene by volume provided a thin enough coating to flow readily and yet concentrated

* Manufactured by the Day-Glo Color Corporation, Cleveland, Ohio.

enough to leave a good trace on the surface. It was also noted that a concentration of fluid (as in a vortex core) would gradually evaporate leaving a small build-up of powder on the surface as a good indication of zones of recirculation.

Of the three methods of flow visualization attempted, the liquid film technique proved the most satisfactory.

3.3 Investigation of Diffuser Flow Mechanisms

In order to assess the effect of the jet on the flow in the diffuser, some means of investigating the internal flow within the diffuser had to be established. As was mentioned earlier, five pitot-traversing stations were constructed: one upstream of the diffuser; one downstream of the diffuser; and three within the diffuser itself. Traverses were taken at each station and the resulting data was plotted as velocity contours by the CALCOMP PLOTTER of the IBM SYSTEM 360 computer. The contours were plotted at 2 ft/sec intervals which represented the order of the error involved in reading the manometer. Traverses at each station were taken at three different bleed rates: (1) no bleed; (2) one-half bleed; and (3) full bleed.

The venturi-meters on each of the injection units were calibrated such that by throttling the flow behind the venturi, equal mass flows could be supplied to each set of four jets. This adjustment was accomplished by means of constant reference to the manometer until all four injections systems were receiving the same amount of mass flow. Once the tunnel had stabilized, efficiency readings were taken and diffuser efficiencies calculated. The process was then repeated at a higher injection rate until the whole spectrum of mass flow rates, from no bleed to full bleed had been

covered. In order to check for possible hysterisis effects inherent in the system, the complete test was rerun in the reverse order (i.e. from full bleed to no bleed). As the amount of mass injected into the tunnel is dependent upon the depression of the static pressure in the tunnel below atmospheric pressure, the test was rerun again with the fan throttled to produce an upstream velocity of the order of one-half of its former value, in order to determine how a decrease in the static pressure would affect the injected mass flow rate and its related diffuser efficiency.

4. DEVELOPMENT OF THE MASS INJECTION SYSTEM

Three distinct stages were encountered in the development of the mass injection system. First, the type of jet to be used, whether a circular jet, a rectangular jet, or a peripheral slotted jet, had to be decided upon. Then having established which jet was most effective in decreasing the diffuser efficiency, the optimum configuration for the jets at any cross-section was determined. Finally, the position of the jets was varied downstream in the diffuser to detect an optimum point to disturb the flow.

4.1 Variations in the Method of Injection

Initially, a mass injection system was installed in the tunnel immediately upstream of the throat of the diffuser. Twenty-eight 1/4" I.D. tubes (7 per side) were mounted normal to the walls of the section. With the holes uncovered, the mass injected through each hole was strictly a function of the depression of the pressure in the tunnel below the ambient. With all the holes uncovered (i.e. full bleed) the diffuser efficiency was

80.2%, whereas, with all the holes covered (i.e. no bleed) efficiency rose to 86.5%. Thus using jets equally spaced around the periphery of the section, a maximum change of 6.3% could be produced. A slot around the periphery seemed the most logical extension of the peripheral circular jets and therefore its characteristics were investigated.

Variations in diffuser efficiency were performed over a range of slot size, the mass flow was varied by successively uncovering one side of the slot at a time until at full bleed, mass was being injected from all four sides. An approximation to the mass flow rate was made by assuming a constant static pressure across the injection section within the tunnel. Therefore, the mass that could be driven across any slot area was strictly a function of the pressure differential that existed between the ambient pressure outside of, and the constant static pressure within, the tunnel. The results are shown in Figure 25. One final variation was tried, that of a slot with spacers in it, creating in effect a series of rectangular jets around the periphery. The mass flow rate was varied in a similar fashion to that of the slot.

For comparison purposes, the performance of the three different types of jets are plotted in Figure 26 on the basis of equal bleed area (i.e. the size of the slot and rectangular jets were adjusted such that their total bleed area would equal the total bleed area of the circular jets). Two important considerations emerged from Figure 26. First and foremost, the round jets produced the greatest change in efficiency per unit mass injected. From no bleed to full bleed the round jets produced a 6.8% decrease in efficiency versus a 6.1% and 5.6% decrease for the rectangular and slotted jets respectively. Secondly, injecting air in a

symmetric manner from all four sides seemed to create the greatest efficiency decrease possible. Therefore at this point it was known that the jets should be circular in shape and placed symmetrically about the diffuser entrance.

4.2 Variations in the Configuration of Injection

Having established that circular jets were to be used in a symmetrical manner, it remained to decide what configuration of jets would best disrupt the flow. Maintaining the condition of symmetry, all possible combinations of the circular jets (seven per side just upstream of the diffuser inlet) were tried. In Figure 27, an X indicates a covered bleed hole while an O indicates an open hole with mass being injected at that point. The two points of interest are points 6 and 7. Point 7 seems to indicate that two holes in a corner cause a sharp drop in efficiency. This was not the case when the holes were moved away from the corner as at point 9. Point 6 again suggests that blowing in the corners is more efficient at disrupting the flow (this time with three holes in the corner) than using all 7 holes (point 5). It was concluded therefore that injecting the mass through four jets in each corner (two per side) seemed a promising method of disrupting the flow.

The corner blowing configuration (00XXX00) was then duplicated at 1 7/8" and 1/8" upstream as well as 1 3/4" downstream of the throat of the diffuser. This allowed a check on the performance of this configuration at positions other than right at the throat as well as allowing more sophisticated combinations of injection points to be tried as in Figure 28(a) to (e). The most promising configuration seemed to be that of Figure 28(a) using a single hole upstream to initially disrupt the flow and then followed by two

holes farther downstream. However, when comparing the efficiency change on a unit area basis (i.e. $\Delta \eta/A'$ where A' is the total cross-sectional area of the jets) no superior decrease in efficiency was found.

Once the corner configuration (OOXXXOO) had been reproduced down the length of the diffuser, further combinations of three and four holes were tried (Figures 28(f) - (i)) but none produced a greater percentage decrease per unit area than the corner configuration.

One final configuration test was tried in order to determine the proper spacing of the two jets in the corner. Here it was found that two jets spaced longitudinally about 1 3/4" apart and 5/8" from the corner would cause a greater decrease than any lateral spacing of the corner configuration formerly used. This new configuration (Figure 28(j)) was in fact the best to date and was the one subsequently used in the mass injection system.

4.3 Variations in the Position of Injection

During the course of experiments to optimize the best configuration for injecting mass, the best position in the tunnel (i.e. upstream of the throat, at the throat, or downstream of the throat of the diffuser) to inject was also investigated. The corner blowing configuration was placed at 6" intervals down the entire length of the diffuser, but it was found however, that as the air was slowed in the diffuser, the static pressure rose rapidly resulting in a decreased injection rate. There was no advantage therefore, to injecting mass at stations downstream of the diffuser entry. As a result, it was found best to have one injection site sitting at the throat of the diffuser and the other, a short distance upstream to disturb the flow before it reached the throat. It was concluded therefore that the

configuration shown in Figure 28(j) was the optimum design placed in the best possible position to disturb the flow in the diffuser.

4.4 The Injection System

Although several mass injection systems were designed to measure the mass flow rate in the jet, the device subsequently selected and manufactured is shown in Figure 21. Each unit consists of a venturi-meter followed by a flexible hose and clamp (to act as a throttling device) which is subsequently connected to a fiberglass diffuser. The end of the diffuser is covered with a metal plate to which four hose connections are made. The hoses supply each of the four nozzles in one corner with an equal mass of air. The entire system from the venturi-inlet to the nozzles on the end of the hose for each jet was designed to ensure an equal distribution of mass to each jet and also to avoid losses by keeping the velocity of the bleed air below 3 ft/sec.

Although it was possible to inject as high as fifty percent of the mainstream mass flow normal to the mainstream, it was considered more practical to use a smaller mass flow rate in the jets. Injecting 3% of the mainstream mass flow was considered the optimum for the jets. If more than 3% of the flow were taken from the settling chamber (the air supply for the fluidic amplifiers is taken from the settling chamber) the flow in the settling chamber would be too disturbed. The physical size of the apparatus such as the pipe leading from the settling chamber to the injection point (6" diameter for a 3% bleed rate) also placed restrictions on the bleed range. In actuality, there were some losses inherent in the mass injection apparatus which decreased the bleed range to 2.3%.

5 DISCUSSION OF RESULTS

5.1 Diffuser Efficiency and Its Correlation With Published Values

In Chapter 2.1, three different definitions for diffuser efficiency were presented, namely:

1) pressure efficiency

$$\eta_p = (P_2 - P_1) \,/\, \tfrac{1}{2}\rho\bar{U}_1^{\,2}\,(1 - m^2);$$

2) energy efficiency

$$\eta_E = (P_2 - P_1) \,/\, \alpha_1\,\tfrac{1}{2}\rho\bar{U}_1^{\,2}\,\left(1 - \frac{\alpha_2}{\alpha_1}\,m^2\right);$$

and 3) overall efficiency

$$\eta_o = (P_2 - P_1 + \Delta P_f^{\,1}) \,/\, \tfrac{1}{2}\rho\bar{U}_1^{\,2}\,(\alpha_1 - \alpha_2\,m^2)$$

Overall efficiency (as in (3)) was considered unusable as the downstream portion of the square duct was not long enough to ensure a maximum pressure recovery. A comparison was then made between the pressure efficiency and the energy efficiency. Integration over the velocity field at the diffuser inlet in order to evaluate the average velocity led to a pressure efficiency of 73.1% at full bleed. Further integration over the velocity fields at both the diffuser inlet and exit led to the evaluation of the kinetic energy coefficients $\alpha_1 = 1.16$ and $\alpha_2 = 2.25$. The energy efficiency was calculated as 67.2%, a significant drop from the pressure efficiency. These results are misleading however, as the slow traversing of the velocity field at the diffuser exit (where the flow fluctuates rapidly) caused an erroneous value for α_2. Thus it was deemed inadvisable to use the energy definition for diffuser efficiency.

A final comparison was made between pressure efficiency based on the mean inlet velocity and pressure efficiency based on the center-line velocity at the throat of the diffuser. It was found that at full bleed for example, the diffuser efficiency was 4.33% higher at the mean velocity conditions than that based on the center-line velocity. This error was considered acceptable however when compared to the sixty-odd time consuming traverses that would be necessary were this error not ignored. Thus the diffuser efficiency was determined by measuring the pressure drop along the diffuser and the center-line dynamic head at the diffuser inlet.

Patterson in Figure 4, compares diffuser efficiencies between various types and lengths of diffusers with area ratios of 4/1. For $A_2/A_1 = 4.0$ and $L/D = 8.4$ as in the present study, Figure 4 suggests that a square diffuser should be operating nearly 90% efficiently. The diffuser in the present study operated at 83.4% efficiency with no bleed, based on the center-line velocity. Therefore the diffuser performance does correlate reasonably well with published values if allowance is made for the inlet boundary layer.

5.2 The Flow Mechanisms Created by Jets Normal to the Mainstream

One of the most important aspects of the present study was to determine how the jet interacted with the mainstream to create a loss in diffuser efficiency. Generally, studies of this nature require some form of visualization of the jet in the mainstream in order to obtain some understanding of the various processes involved. The liquid film technique was used in this study and the results are shown in Figures 29 to 34. Using these photographs as a guide, a three dimensional clay model of the flow was built as shown in Figure 35. In order to gain an understanding of the fundamentals behind the jet flow, the obvious case to examine first would be that of the single jet.

5.2.1 The Single Jet

Figure 29 is a photograph of a liquid film plate held in the vertical plane of symmetry of a jet discharging from the duct floor. The mainstream flow travels from left to right along the plate while the jet intersects the mainstream at the position indicated with the arrow. The flow can be seen to separate upstream of the leading edge of the jet and then be entrained by the jet as it moves upward into the mainstream. The jet is deflected through 90^{o} by the mainstream by means of a pressure gradient across the jet as explained in § 2.6 and § 2.7. The light elliptically shaped region just beneath the jet is caused by a build-up of pigment on the plate which indicates a region of intense recirculation (i.e. a vortex core). Figure 30 is a liquid film plate taken on the duct floor with the jet issuing through a hole in the plate between the 2 1/4" and 2 1/2" points on the scale. The separation point upstream is well defined as are the two vortex cores on either side of the downstream edge of the jet. The size of the region of recirculation associated with each vortex is clearly defined and can be seen not to extend much beyond the 3" mark. Between the 3" and 3 1/2" marks there appears to be a region of relatively low velocity indicated by a lack of perceptible streamlines. From the 3 1/2" mark the flow appears to resume its motion in the downstream direction. However, upon closer scrutiny, a more complex flow pattern was uncovered.

Figure 30 indicates that a clearly defined region exists outside the region of influence of the two vortices on either side of the jet. A very definite line of fluid exists in much the same manner as the flow about a stubby circular cylinder (as in § 2.8). Comparison of Figures 19 and 30 suggests that just as in the case of a stubby circular cylinder, a jet will

cause the formation of a horseshoe vortex which bends around the region of recirculation and then gradually lifts and travels on downstream. Figure 35 illustrates the formation of the horseshoe vortex for the case of the double jet.

Consider for the moment the leading configuration in Figure 35 as representing the reaction of the flow to a single jet. Notice that rather than two vortices recirculating on either side of the jet, there is a surface (or volume) of recirculation moving as indicated. Notice also that the horseshoe vortex spirals inwards toward the recirculating surface. Thus the rotation of the horseshoe vortex and the motion on the recirculation surface (or separation bubble) are in the same sense, except at the leading edge of the jet. It is physically impossible for a viscous fluid to have two adjacent portions of fluid moving in the opposite direction without some form of linkage between them to reconcile the discrepency. With reference to Figure 35, it would seem only natural that a small vortex would be formed at the leading edge of the jet which would rotate counterclockwise upstream from the jet to match the clockwise rotation downstream of the horseshoe vortex. This is in fact the case as the fine line of stagnant fluid between these two vortices can be seen to be sitting very close to the upstream edge of the jet in Figures 30 and 32. This small vortex has the same sense of rotation as the recirculating surface behind the jet and therefore unites with this region by following the periphery of the jet aperture.

As the horseshoe vortex is rotating inwards (as in the plan view, Figure 35), it is constantly pumping fluid (from the mainstream and adjacent jet) into the region underneath it. As the fluid in the vortex is rotating

very rapidly, a particle of fluid would tend to gain a substantial component of velocity normal to the axis of the vortex. Thus a particle beneath the horseshoe vortex would move almost at right angles to the axis of the vortex until it reached the region of influence of the mainstream. It would then gradually change its direction and move downstream with the flow. The region in which the particle changes direction shows on the plate (Figure 30) as a clearly defined line adjacent to the region of recirculation.

It is apparent from both Figures 30 and 35 that following the downstream end of the recirculation region a flow in the mainstream direction is restablished. This it is believed, is due to the horseshoe vortex lifting off the surface while at the same time pumping fluid beneath it which results in a flow downstream. Above this flow the jet is nestled between and a little above the horseshoe vortex. Moving downstream, the jet and vortex spread out as they travel until finally they degenerate into turbulent eddies whose rotational energy is irretrievable.

5.2.2 The Double Jet

The case of the double jet is identical to that of a single jet with only a few exceptions. As the horseshoe vortex of the leading jet lifts, it pumps fluid beneath it, which, in this case is immediately entrained by either the second horseshoe vortex or the second jet (Figures 31 and 32). Figures 31 and 32 also indicate that the region of recirculation behind the second jet is considerably smaller than that of the first jet. Furthermore, the second jet has a larger radius of curvature than the first jet which would indicate a decreased pressure gradient across the jet.

Notice in Figure 31 the distinct areas of entrainment on the downstream edge of the first jet and the upstream and downstream edges of the second jet. In Figure 33, the leading edge of the plate was given an excessive coating of liquid and placed in the airflow. The mainstream was diverted above the jet flow, the dark regions indicating the areas within the influence of the jet (the areas in the upper right-hand quadrant having insufficient fluid to cover the entire surface). After the plate had dried, it was replaced in the tunnel with a daub of fluid at the x = 3.3" mark. A portion of the fluid was entrained in the recirculating region and the remainder was entrained in the jet as shown. This method then, gave a reasonable idea of the position of the jet relative to the mainstream. The plate was then placed once again in the tunnel with daubs of fluid at x = 2.35" and x = 2.75" marks respectively. The result is shown in Figure 34. This photograph is interesting in several respects. Firstly, it shows the entrainment region for the second horseshoe vortex at approximately the x = 2.80" position. Secondly, it shows how the first and second jets position themselves relative to one another with an entrained layer between them. Thirdly, and most important, it shows the extent to which the region of recirculation downstream of the second jet occupies almost the entire jet aperture. The jet is not cylindrical as it leaves the aperture, but is in all probability somewhat elliptically shaped. The reduced size of the jet aperture as well as the reduced size of the zone of recirculation behind the jet, suggest that the mass flow rate of the second jet is considerably smaller than that of the first jet. As the mass flow in the jet is controlled by the static pressure in the tunnel, one may conclude that the static pressure in the neighbourhood of the second jet has risen above that in the neighbourhood of the first jet. Figure 35 points out the shape of the

jet aperture and the size of the recirculation region. Once again the second horseshoe vortex will lift as it reaches the end of the zone of recirculation. Similarly the second jet stacks itself below the first with its horseshoe vortex slightly lower, and on either side of itself.

5.2.3 Variations in Flow Mechanisms With Bleed Rate

In order to bring the consideration of the interaction between the jet and mainstream to a close, one final parameter was varied: the bleed rate. Plates were taken at full bleed, three-quarters bleed, one-half bleed, and one-quarter bleed to determine the flow mechanisms at conditions other than full bleed. Corresponding portions of Figure 36 to 43 are scaled to the same degree in order to facilitate comparison.

Figures 36 and 37 illustrate once again the case of the double jet at full bleed. In Figures 38 and 39 the jets are blowing at three-quarters of their maximum. Differences between three-quarters bleed and full bleed are slight, with the exception that the recirculation regions behind the jets are smaller and the jets themselves have a smaller radius of curvature. It should also be noted that momentum effects play a role in determining the radius of curvature of a jet. If the momentum flux per unit area were large compared to that of the mainstream, the jet could be expected to penetrate a considerable distance into the flow. Decreasing the momentum by decreasing the mass flow rate of the jet would decrease the depth of penetration of the jet. This factor is further evident at one-half bleed in Figures 40 and 41. Once again the zone of recirculation is decreased in size and the radius of curvature is decreased. Finally in Figures 42 and 43, at one-quarter of the maximum bleed rate, the recirculation region is

detectable only on the horizontal plate. The deflection of the mainstream is minimal but still indicates that all the flow mechanisms (i.e. the main horseshoe vortex, and the smaller leading edge vortex and separation bubble) which operated at full bleed, operate as low as one-quarter bleed as well.

5.3 Variation of Efficiency with the Configuration of Blowing

Initially, the testing was concerned with three different configurations, the circular jet, the rectangular jet, and the slotted jet. The slotted jet brought a number of interesting points to light. In general, it was found that the slotted jet induced separation along one, two, three and sometimes all four walls. The variation in efficiency with slot sizes from 1/16" to 1" is shown in Figure 25. In general, the larger the size of the slot (i.e. greater bleed mass flow) the larger the range of control of diffuser efficiency. Notice also that the initial gradient (i.e. blowing from one side only) is steeper than the gradient at any other point on the curves. Some evidence was also found that the diffuser efficiency (at no bleed) improved with slot size up to approximately 3/8". In effect, a rectangular groove was formed just upstream of the throat of the diffuser when the rectangular bleed slot was sealed off to produce the no bleed condition. It is suspected that a recirculation was set up in the sealed off slot which prevented a further thickening of the boundary layer as the no-slip condition at the wall no longer applied. The larger the size of the groove the greater the length of "non-growth" of the boundary layer, and therefore the thinner the boundary layer entering the diffuser. In general however, on a unit mass basis, the slotted jet could not create as

great a loss in efficiency as the circular jets.

In Figure 26, a comparison is made between the slotted jet and the circular jets. If the area of the slot was made to coincide with the total area of the seven jets spaced along the wall and if the pressure difference sustained across the jet aperture can be assumed to be the same for both the slot and the circular jets, then the differences shown in Figure 26 can be attributed to the manner in which the two different types of jets affect the mainstream flow. The graph suggests that the circular jets are the most efficient ($\Delta\eta$ = 6.8%) and the slotted jets the least efficient ($\Delta\eta$ = 5.6%) method of controlling diffuser efficiency. Although sufficient information is lacking to present a clear picture of how the jet configuration controls the efficiency, a possible interpretation is suggested below.

In order to simplify the problem consider the slotted jet as a two dimensional jet as in [12]. The boundary layer upstream of the jet is completely entrained by the jet and lifted over the separation bubble. Once the jet has reattached a certain portion of the flow will move downstream forming a new boundary layer and the remaining fluid will be recirculated in the separation bubble. The new boundary layer downstream will be considerably thicker than it formerly was as it now consists of flow from the turbulent jet as well as the old boundary layer which was entrained and accelerated by the jet. Spalding [15] suggests that the position of stall in an adverse pressure gradient is proportional to the thickness of the boundary layer as the flow approaches the adverse pressure gradient. It may be deduced therefore that diffuser performance relies heavily on the thickness of the boundary layer at its inlet.

Consider the case of the slotted jet versus the circular jet. In one case, the jet may be considered essentially two dimensional; in the other, the jet and other related phenomena are three dimensional. Rather than a two dimensional separation bubble, a recirculation region is formed behind the circular jet. A strong horseshoe vortex is set up around the jet and trails off downstream. These new flow mechanisms have two important effects on the flow in the diffuser.

First, there is a decrease in the component of momentum in the downstream direction as the rotational component of momentum of the horseshoe vortex increases in magnitude. Thus the net rate of change of momentum downstream is decreasing resulting in a component of resistive force in the upstream direction. The resistive force in the upstream direction has a tendency to retard the flow and thicken the boundary layer as it moves downstream. Secondly, and perhaps most important, separation may be induced in the corners of the diffuser by positioning the two sets of jets in close proximity to each other as in Figure 45. The horseshoe vortices tend to combine to pump fluid out of the corner. This results in a pair of vortices recirculating in the separation region as shown. This separation region can be detected in Figure 44 along the lower edge of the plate.

Disregarding for the moment the fact that the circular jets gave the greatest decrease in efficiency per unit bleed mass, there were several other factors which made the choice of a circular jet more preferable than a slotted jet. Circular holes could be quite easily and accurately placed in the full scale tunnel, but not so for a slot. Circular holes would cause far less structural weakness than a slot across the entire side or sides of the diffusing section in the windtunnel. Lastly, a manifold for a

slot which would ensure a uniform distribution of bleed mass to the slot would be difficult to design and construct.

5.4 Variations in Diffuser Flow Mechanisms With Mass Injection Rate

Having investigated the effect of the jets on the mainstream at the point of injection, the next series of tests were concerned with the resultant flow behaviour in the diffuser downstream of the jets. Pitot traverses were taken at five stations: one upstream of the diffuser; three within the diffuser; and one downstream of the diffuser in the straight duct. The traverses were performed for the no bleed, one-half bleed and full bleed conditions. The resulting contour plots of the velocity fields are shown in Figures 46 to 60.

Figures 46 to 50 deal with the velocity fields at stations 1 to 5 with no mass being injected (i.e. the no bleed condition). The inlet velocity field at station 1 shown in Figure 46 is highly non-uniform (as it is in Figures 51 and 56 for the one-half and full bleed conditions respectively). Screens downstream of the fan break up the large vortices created by the centrifugal fan but the resulting flow lacks consistency between the three different bleed conditions at this station. The vortices off the screens die out as the flow moves through the 7" settling region prior to the diffuser inlet. This results in a flow with a high speed core and a relatively thin boundary layer entering the diffuser. As the area of the diffuser increases downstream, the velocity decreases and the boundary layer thickens. The boundary layer thickness may be approximated by that portion of the fluid closest to the wall where there seems to be the highest concentration of contour lines. In general, the flow in the diffuser at the no bleed condition is well behaved with no separation in the corners or along

the walls.

The flow pattern changes with the presence of a jet blowing into the stream. At one-half bleed, the velocity field is once again highly uniform at station 1 (Figure 51). At stations 2, 3 and 4 however the plots of Figures 52, 53 and 54 indicate a zone of separation in each corner. This local separation is thought to be caused by the horseshoe vortices being carried downstream setting up a recirculation zone as suggested in Figure 45. Figure 55 shows that there is no separation indicated in the corners at station 5. Thus even though the flow is under the influence of an adverse pressure gradient, reattachment occurs at some distance downstream. This reattachment process bears closer scrutiny.

Consider a particle of fluid very close to the wall approaching the zone of separation in the corner. Prior to encountering the recirculating flow this particle would have a negligible velocity. However, once it reaches the recirculating zone it is entrained by the recirculating flow and accelerated out into the mainstream. Thus the fluid which once constituted the lower edge of the boundary layer, now has a finite velocity. The point (or line) of zero velocity (i.e. the location of the new lower edge of the boundary layer) has been displaced toward the wall to the point where the lower boundary of the upper portion of the recirculating zone meets the upper boundary of the lower portion of the recirculating zone (i.e. approximately the middle of the recirculation region). Joining the points of zero velocity along the length of the recirculation zone results in a new boundary layer thickness equivalent to the old boundary layer (since accelerated) plus approximately one-half of the thickness of the recirculating flow. At the downstream end of the circulation region the point of zero velocity is once again very close to the wall. At this point however, the flow splits:

the flow above the recirculation zone continues downstream along the wall, whereas the flow moving downstream in the separation bubble is recirculated upstream once again. The flow has therefore reattached.

Much the same process occurs at the full bleed condition. Figure 56 depicts the same irregular flow field as in the one-half bleed and no bleed conditions at station 1. Figures 57, 58 and 59 show a somewhat larger region of separation in each corner than at the one-half bleed condition. There is once again no detectable zone of separation at station 5 in Figure 60.

It may be concluded therefore that the only difference induced in diffuser flow mechanisms by varying the mass bleed rate occur in the size of the zone of separation in the corners of the diffuser.

5.5 Variations in Diffuser Efficiency With Mass Flow Rate

The basic purpose behind the present study was to determine the magnitude of the change in diffuser efficiency that could be induced by varying the bleed rate in the upstream jets through their entire bleed range. Two tests were performed, one at a maximum upstream velocity of 86 ft/sec, and a second at one-half that value. The results are shown in Figures 61 and 62.

In Figure 61 the bleed mass, M_b, has been normalized with respect to the upstream mass flow of the mainstream, M_∞. If the apparatus had performed as anticipated the bleed range should have varied from zero to 3.0%. As it was however, a 9.22% decrease in diffuser efficiency was achieved with a 2.3% bleed range. In Figure 61, the bleed rate was varied from zero to full bleed and then back to zero again. There is a definite indication of

hysterisis in the system as depicted by the lower curve on the plot. It is not a significant effect (amounting to only a fraction of 1% of efficiency) but it is consistent.

In Figure 62, the fan has been throttled until the velocity upstream of the diffuser was approximately one-half of its former value. The static pressure in the tunnel increased significantly and therefore the mass flow rate in the jet should be significantly decreased. The maximum bleed rate however dropped to only 2.1% and the change in diffuser efficiency amounted to 8.91%. This would tend to indicate that the mass injection system would be equally efficient at contrclling the diffuser performance over a wide range of upstream conditions.

A more complete analysis of the design considerations of the mass injection system for the full scale wind tunnel is presented in Appendix B.

6. GENERAL CONCLUSIONS

The development of the mass injection apparatus through the various stages to its present form necessitated a comparison between slotted, rectangular and circular jets. Diffuser efficiency could be decreased as much as 50% with a 1" slot. However, when these three configurations were compared on a percentage decrease in efficiency per unit injected mass basis, the circular jet proved superior. After a lengthy experimental procedure, the circular jets were found to perform best in the corners of the duct just upstream of the diffuser inlet.

Having established the optimum form of injection, the characteristics of the flow about the jets in the corners were investigated. Using a liquid film technique, a single jet deflected by a flow at right angles to it was found to produce a three dimensional zone of recirculation directly behind and beneath it, as well as a horseshoe vortex which wrapped around either side of the jet. The flow about the double jet of the mass injection system was identical with that of the single jet, except that the horseshoe vortex of the upstream jet aids in supplying fluid to the horseshoe vortex of the downstream jet. Both the horseshoe vortex and the zone of separation in each jet persisted well below an $\dot{M}_b/\dot{M}_\infty = 0.25$.

It was also found that if the jets were spaced closely enough together so that the horseshoe vortices on one wall of the corner would interact with the horseshoe vortices on the other wall of the corner, a local separation was produced in that corner of the diffuser. Separation in the corner was found to persist throughout almost the entire length of the diffuser as these horseshoe vortices travelled downstream. Reattachment to the walls of the diffuser occurs near the downstream end of the diffuser at which point presumably most of the energy in the horseshoe vortices has been dissipated. The major effect of decreasing the bleed rate in the jet was a decrease in the magnitude of the separated region in the corners at each station.

Varying the bleed rate of the jet led to a decrease in the magnitude of the flow mechanisms within the diffuser. The resulting decrease in diffuser efficiency for the fan at full throttle over a bleed range of 2.3% was 9.22%. At one-half throttle, the bleed range was reduced to 2.1% and the corresponding change in diffuser efficiency was 8.91%. Therefore,

diffuser efficiency control within this range is relatively unaffected by the magnitude of the inlet velocity. The system does however have its limitations and cannot negate a 20 ft/sec speed fluctuation solely on its own. It would seem likely then that some other means of increasing the resistance to flow in the tunnel (possibly more base bleed cylinders) would have to be developed. This additional resistance, when combined with the variable resistance in the diffuser, would produce the required resistance to the flow in the tunnel.

APPENDIX A

A FLUIDIC WINDTUNNEL SPEED STABILIZATION SYSTEM

Measurements made on model aircraft in a closed circuit subsonic windtunnel are highly sensitive to variations in the airspeed in the test section (i.e. both pressures and forces are proportional to the square of the airspeed). Excluding high frequency variations due to turbulence level, the causes of low frequency variations are: (1) unsteady drive unit; (2) speed drift due to the heating of the air; (3) changed loading on the tunnel due to varying model incidence, yaw, or pitch.

The speed control at any set operating point is usually manually adjusted, but, due to large inertias of the rotating parts and the circulating air, response times are slow . Furthermore, a great deal of skill is required to maintain a constant speed within narrow limits. An automatic control system could be electro-mechanical, fluidic mechanical, or purely fluidic in nature. A fluidic system would use air to interfere directly with the tunnel air and therefore eliminate the large inertias of the drive unit and other mechanical components. A fluidic system would also boast rapid response times and a high degree of reliability as there are no moving parts.

The function of a fluidic system would be to sense the speed of the airflow and counteract the variations from the nominal setting by means of a variable fluid resistance in the tunnel circuit. The control system is shown in Figure A1 and would operate as follows.

A fluidic speed sensor placed at a convenient location in the tunnel would be connected to a fluidic comparator which would detect any change with respect to a set speed and give a pressure output as a function

of the speed error. A study of the static no-load performance of the speed sensor incorporating the comparator was reported [1]. Its principal of operation is based on two total head tubes placed at some distance apart in the fully developed portion of a high velocity jet issuing from a supply nozzle. When this apparatus is placed normal to a low velocity cross-flow the jet is deflected in the downstream direction. As one total head tube is farther downstream of the supply jet than the other, one will experience a different stagnation pressure due to the deflection of the jet. The difference in stagnation pressures is a measure of the cross-flow velocity.

The fluidic anemometer can also act as a comparator for the control system. The inclination of the supply nozzle to the cross-flow can be set in order to find a zero stagnation pressure difference at any cross-flow velocity up to a maximum of 40 ft/sec. Once there is a pressure deflection from this setting an error signal is amplified through several stages until the flow is sufficiently large enough to drive the variable resistances. In order not to change the air mass circulating in the tunnel, the air supply for the flow amplifier is to be taken from the tunnel settling chamber.

To vary the control resistances with this constant mass flow, two separate devices are to be used, one which increases the tunnel resistance with increase of control flow rate, and one which decreases resistance with flow rate. By dividing the total available flow rate through the fluidic amplifier between these two resistances as a function of the input from the comparator, the resulting change in resistance to the tunnel flow is additive.

The two modes of varying the resistance are: (1) variation of the drag of blunt based bodies by means of base bleed, and (2) control of the efficiency of the diffuser in the tunnel circuit by blowing. General characteristics of base bleed investigated by A.W.M. Bertels in his thesis, "The Reduction of the Drag of Two Dimenaions1 Blunt Based Bodies by Blowing" [3] show that drag decreases with bleed rate. The present thesis shows that the resistance to flow in the diffuser section of the windtunnel will increase with increasing amount of blowing. These two pieces of apparatus combined will yield the desired additive effect.

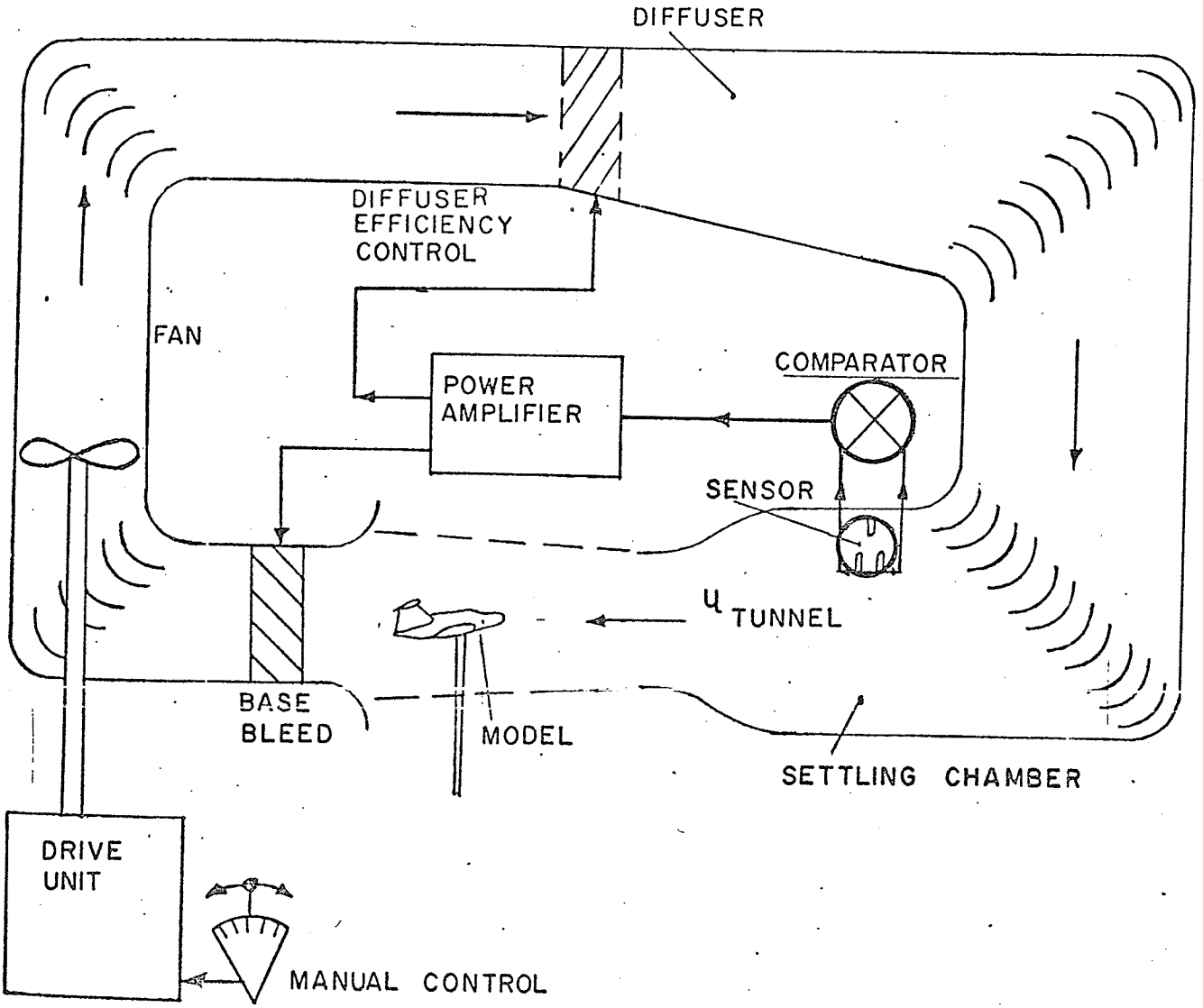

FIGURE A I FLUIDIC WINDTUNNEL STABILIZATION SYSTEM.

APPENDIX B

DESIGN CONSIDERATIONS FOR THE FULL SCALE WINDTUNNEL

The closed circuit windtunnel in the Mechanical Engineering Laboratory at the University of Manitoba is driven by a gas engine whose speed may drift during the course of a test. For the design of a suitable control system, a maximum speed error of ± 20 ft/sec was assumed. The working section of the tunnel is 18" in diameter and operates at a maximum velocity of 150 ft/sec. A power analysis is performed in order to determine the change in diffuser efficiency required to nullify a fluctuation in velocity of 40 ft/sec. It is assumed that one-half of the power requirements are absorbed by the diffuser and one-half by the base cylinders apparatus.

The K.E. of the flow in the working section

$$= \tfrac{1}{2}\rho A V^3$$

$$= \tfrac{1}{2} \times \frac{1}{420} \times \frac{\Pi}{4} \times \left(\frac{18}{12}\right)^2 \times (150)^3$$

$$= 7110 \ \frac{\text{ft-lbf}}{\text{sec}} .$$

Applying a power factor of 3/4, the rate of supply of K.E.

$$= 3/4 \times 7110 \simeq 5330 \ \frac{\text{ft-lbf}}{\text{sec}} .$$

The volume flow rate $\dot{Q} = AV$

$$= \frac{\Pi}{4} \times (1.5)^2 \times 150$$

$$= 265 \ \text{ft}^3/\text{sec}.$$

The power lost in the diffuser $= \dot{Q} (H_1 - H_2)$

where H_1 = total pressure at the diffuser inlet (1)

H_2 = total pressure at the diffuser outlet (2)

Making use of Bernoulli's equation:

$$H_1 = P_1 + \tfrac{1}{2}\rho u_1^2 \qquad H_2 = P_2 + \tfrac{1}{2}\rho u_2^2$$

$$\therefore H_1 - H_2 = P_1 - P_2 + \tfrac{1}{2}\rho u_1^2 - \tfrac{1}{2}\rho u_2^2$$

$$= P_1 - P_2 + \tfrac{1}{2}\rho u_1^2 \left(1 - \frac{u_2}{u_1}\right)^2 \quad \ldots\ldots\ldots\ldots (1)$$

However from continuity $\rho A_1 u_1 = \rho A_2 u_2$

$$\therefore \frac{u_2}{u_1} = \frac{A_1}{A_2} \quad \ldots\ldots\ldots\ldots\ldots\ldots\ldots\ldots (2)$$

Using the pressure definition, diffuser efficiency

$$\eta = \frac{P_2 - P_1}{\tfrac{1}{2}\rho u_1^2 [1 - (A_1/A_2)^2]} \quad \ldots\ldots\ldots\ldots\ldots\ldots (3)$$

Substituting equations (2) and (3) into (1)

$$H_1 - H_2 = -\eta \tfrac{1}{2}\rho u_1^2 [1 - (A_1/A_2)^2] + \tfrac{1}{2}\rho u_1^2 [1 - (A_1/A_2)^2]$$

$$= \tfrac{1}{2}\rho u_1^2 [1 - A_1/A_2)^2] [1 - \eta].$$

Assume that the tunnel speed is stabilized at 100 ft/sec. The minimum tunnel speed would then be 80 ft/sec, the maximum 120 ft/sec. The minimum input power would be

$$5330 \times \left(\frac{80}{150}\right)^3 = 808 \text{ ft-lbf/sec.}$$

The maximum input power would be

$$5330 \times \left(\frac{120}{150}\right)^3 = 2720 \text{ ft-lbf/sec}$$

$\therefore$ Power at w/s = 2720 - 808 = 1912 ft-lbf/sec

where w/s ≡ working section.

It is assumed that one-half the power at the working section would equal the change in power in the diffusing section and one-half would equal the change in power at the base bleed cylinders.

Assume that the diffuser efficiency has changed to a new value η_2 in order that

$\frac{1}{2}\Delta$ Power at w/s = Δ Power in diffuser.

$$\eta_2 = \frac{P_2^1 - P_1^1}{\frac{1}{2}\rho u_1'^2 [1 - (A_1/A_2)^2]}$$

$$\therefore P_2^1 - P_1^1 = \eta_2 \tfrac{1}{2}\rho u_1'^2 [1 - (A_1/A_2)^2] \quad \ldots\ldots\ldots\ldots \quad (4)$$

Recalculating the change in total pressure across the diffuser

$$H_1^1 - H_2^1 = P_1^1 - P_2^1 + \tfrac{1}{2}\rho u_1'^2 [1 - (A_1/A_2)^2] \quad \ldots\ldots\ldots \quad (5)$$

Assume that the velocity at the diffuser inlet is the same in both cases. $\therefore u_1 = u_1^1$

Substituting (4) into (5)

$$H_1^1 - H_2^1 = \eta_2 \tfrac{1}{2}\rho u_1^2 [1 - (A_1/A_2)^2] + \tfrac{1}{2}\rho u_1^2 [1 - (A_1/A_2)^2]$$

$$= \tfrac{1}{2}\rho u_1^2 [1 - (A_1/A_2)^2] [1 - \eta_2]$$

Δ Power in diffuser = $\dot{Q}\Delta (H_1 - H_2)$

$$\Delta (H_1 - H_2) - (H_1^1 - H_2^1)$$

$$= \tfrac{1}{2}\rho u_1^2 [1 - (A_1/A_2)^2] [1 - \eta_1] - \tfrac{1}{2}\rho u_1^2 [1 - (A_1/A_2)^2] [1 - \eta_2]$$

$$= \tfrac{1}{2}\rho u_1^2 [1 - (A_1/A_2)^2] [1 - \eta_1 - 1 + \eta_2]$$

$$= \tfrac{1}{2}\rho u_1^2 [1 - (A_1/A_2)^2] [\eta_2 - \eta_1]$$

$$\therefore \Delta \text{ Power in diffuser} = \dot{Q} \tfrac{1}{2} \rho u_1^2 \left[1 - (A_1/A_2)^2\right] \left[\eta_2 - \eta_1\right]$$

$$\therefore \eta_2 - \eta_1 = \frac{\Delta \text{ Power in diffuser}}{\dot{Q} \tfrac{1}{2} \rho u_1^2 \left[1 - (A_1/A_2)^2\right]} \quad \ldots\ldots\ldots\ldots (6)$$

Substituting into equation (6) and noting that $A_1/A_2 = 1/4$

$$\eta_2 - \eta_1 = \frac{\tfrac{1}{2} \times 1912}{176.8 \times \tfrac{1}{2} \times 1/420 \times 100^2 \times (1 - 1/16)}$$

$$= 0.785$$

The required efficiency change to counteract a fluctuation of ± 20 ft/sec in the tunnel speed would be 78.5%. This figure was subsequently found to be unrealistic as the required bleed mass to create such a change in diffuser efficiency would produce undesirable disturbances in the settling chamber of the windtunnel.

REFERENCES

1. A. Pottin, An Experimental Fluidic Anemometer, B.Sc. Thesis, Department of Mechanical Engineering, University of Manitoba, 1969.

2. B.W. Wilton, The Effect of Base Bleed on Base Drag, B.Sc. Thesis, Department of Mechanical Engineering, University of Manitoba, 1969.

3. A.W.M. Bertels, The Reduction of Drag of Two Dimensional Blunt Based Bodies by Blowing, M.Sc. Thesis, Department of Mechanical Engineering, University of Manitoba, 1970.

4. R.C. Worster, The Efficiency of Diffusers and Some Test Results on the Effect of Wall Roughness. The British Hydrodynamics Research Association, Report No. R.R. 554, 1957.

5. A.H. Gibson, Hydraulics and Its Applications, Constable. On The Flow of Water Through Pipes and Passages Having Converging or Diverging Boundaries. Proc. Roy. Soc. Series A, Vol. 83, 1910.

6. H. Peters, Diffusers at Different Angles of Expansion, Engineering Archives, 11 Band, Erstes Heft, März, 1931.

7. G.N. Patterson, Modern Diffuser Design. Aircraft Engineering, Sept., 1938.

8. F.B. Gessner & J.B. Jones, On Some Aspects of Fully Developed Turbulent Flow in Rectangular Channels. Journal of Fluid Mechanics, Vol. 23, Part 4, 1965.

9. B.S. Stratford, The Prediction of Separation of the Turbulent Boundary Layer. Journal of Fluid Mechanics, May, 1959.

10. S.J. Kline, C.A. Moore & D.L. Cochran, Wide Angle Diffusers of High Performance and Diffuser Flow Mechanisms. Journal of Aerospace Sciences, Vol. 24(b), 1957.

11. S.J. Kline, Some New Conceptions of the Mechanism of Stall in Turbulent Boundary Layers. Journal of Aerospace Sciences, Vol. 24(b), 1957.

12. C. Bourque & B.G. Newman, Reattachment of a Two Dimensional Incompressible Jet to an Adjacent Flat Plate. Aeronautical Quarterly, Vol. 11, 1960.

13. N. Gregory & W.S. Walker, The Effect on Transition of Isolated Surface Excrescences in the Boundary Layer. R. & M. Aero. Res. Coun. London 2779 [36, 551, 554], 1951.

14. G.N. Abramovich, The Theory of Turbulent Jets. M.I.T. Press Massachusetts Institute of Technology, Cambridge, Massachusetts, 1963.

15. D.B. Spalding, A Unified Theory of Friction, Heat Transfer and Mass Transfer in the Turbulent Boundary Layer and Wall Jet. A.R.C., C.P. 829, December, 1964.

16. H. Schlicting, Boundary Layer Theory. McGraw-Hill, Toronto, 1968.

17. R.L. Daugherty & J.B. Franzini, Fluid Mechanics with Engineering Applications. McGraw-Hill, Toronto, 1965.

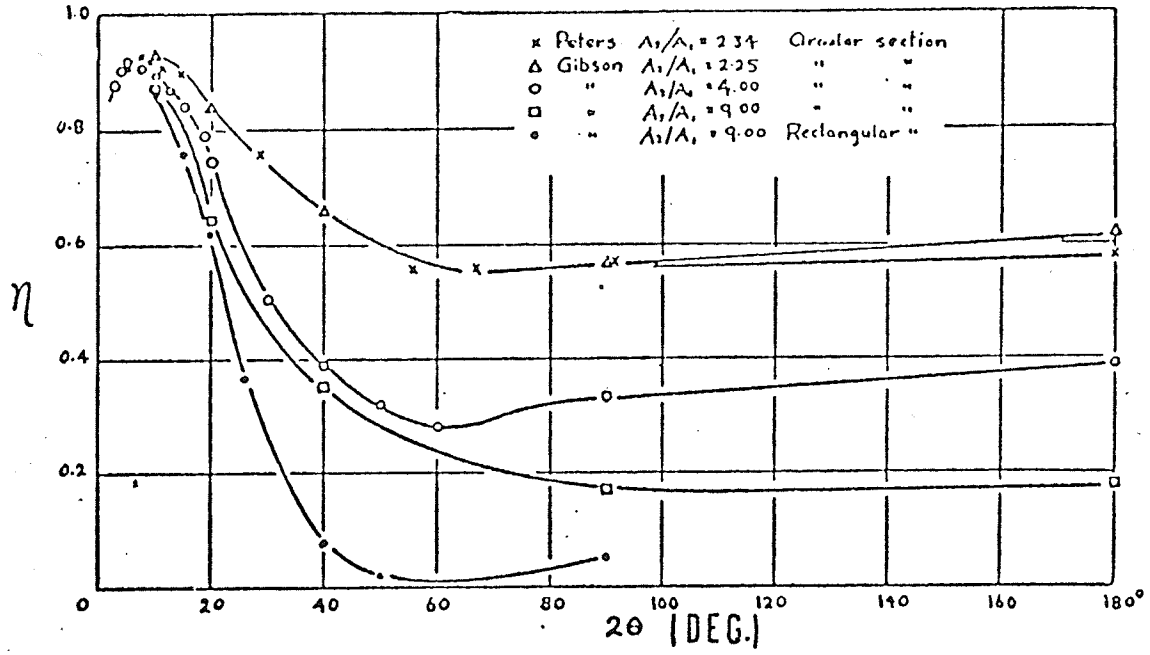

FIGURE 1 VARIATION OF THE EFFICIENCY WITH THE ANGLE OF EXPANSION — PATTERSON.

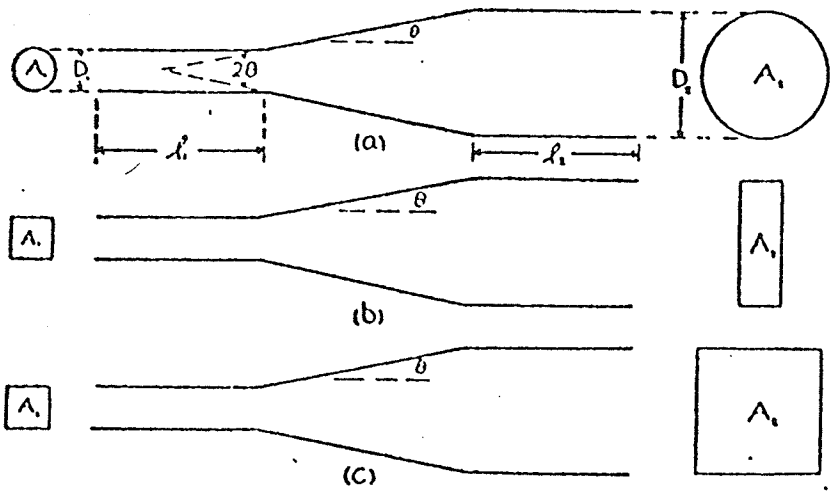

FIGURE 2 VARIOUS TYPES OF DIFFUSERS — PATTERSON.

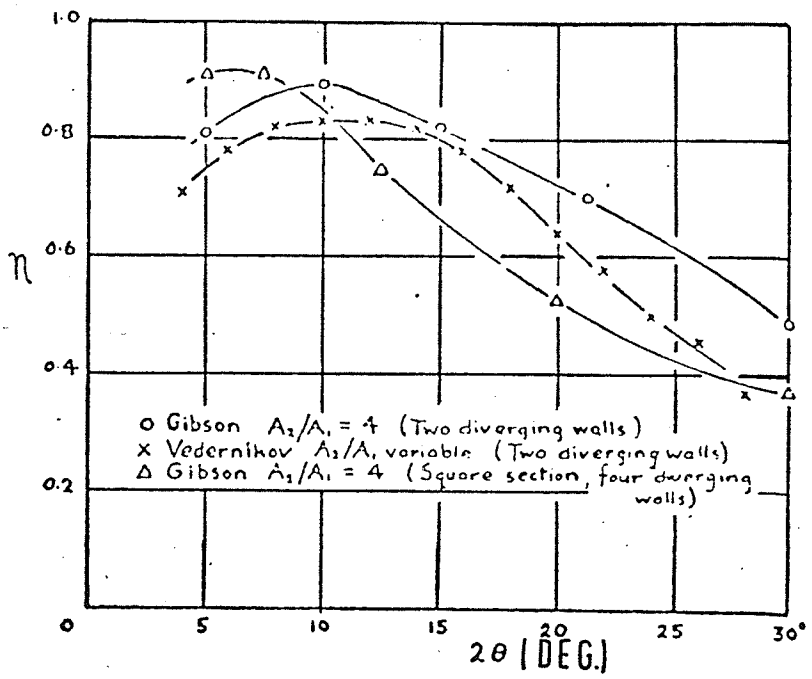

FIGURE 3 MAXIMUM EFFICIENCY OF SQUARE AND RECTANGULAR DIFFUSERS.— PATTERSON

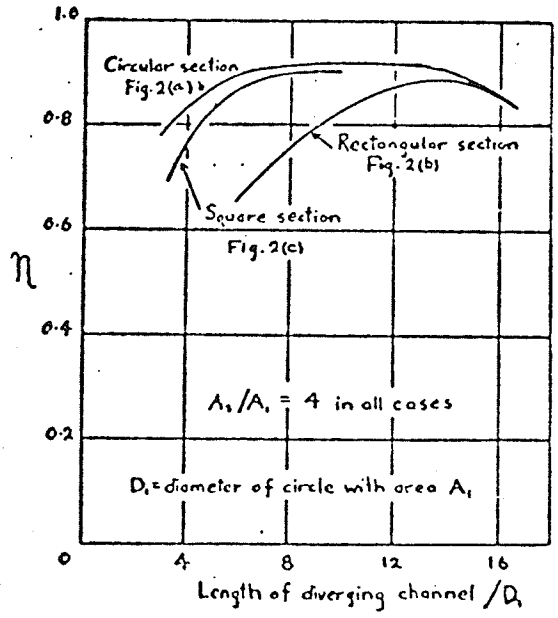

FIGURE 4 DEPENDENCE OF EFFICIENCY ON SECTIONAL SHAPE.— PATTERSON

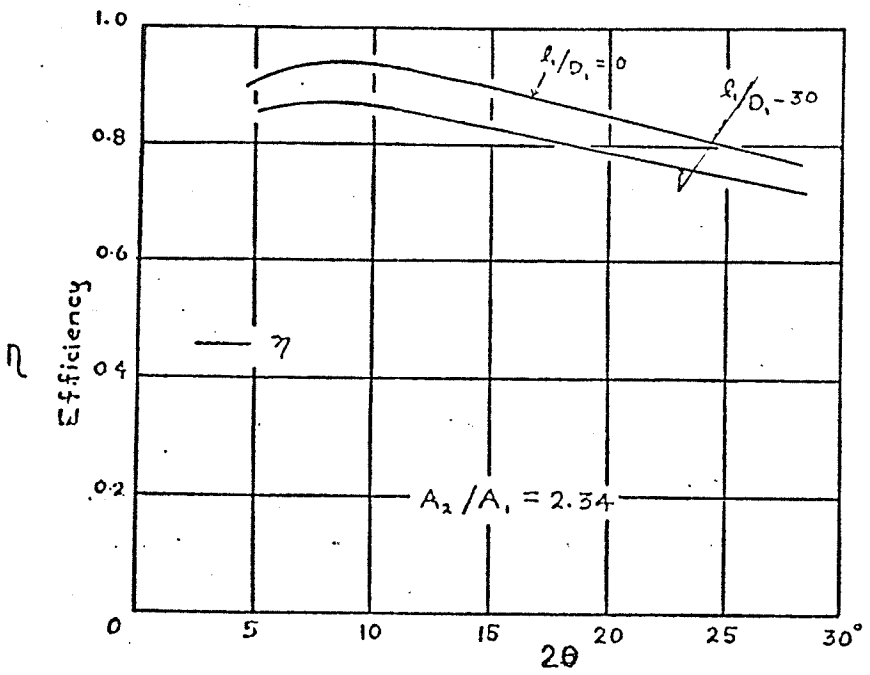

FIGURE 5 EFFECT OF INLET AND OUTLET CONDITIONS —— PATTERSON.

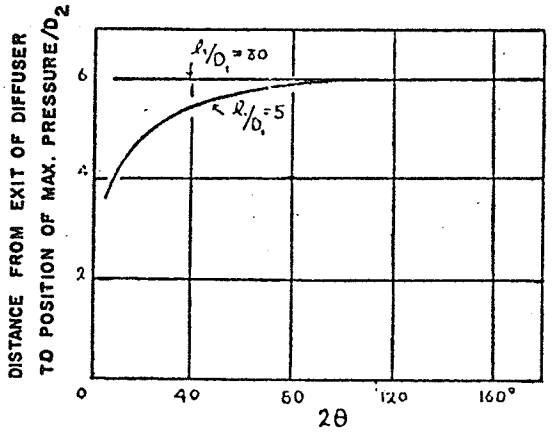

FIGURE 6 POSITIONS OF MAXIMUM PRESSURE —— PATTERSON.

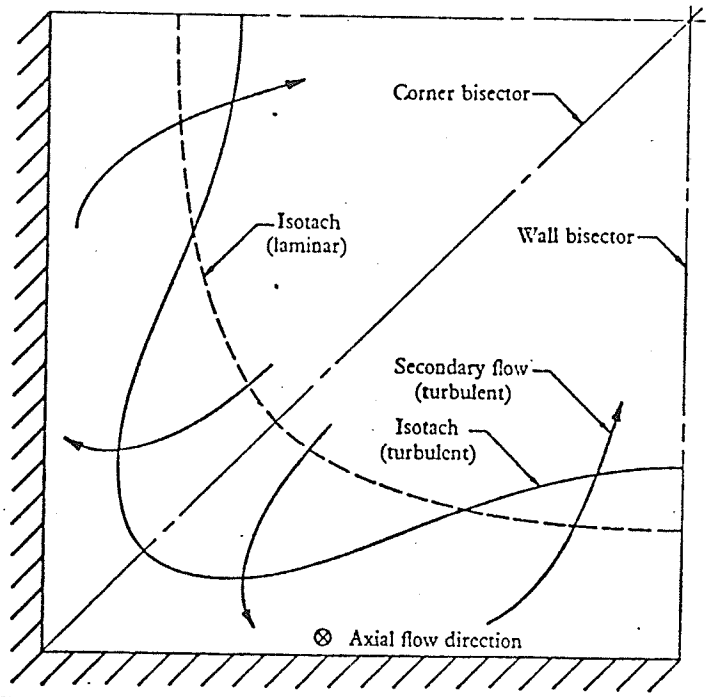

FIGURE 7 TYPICAL ISOTACH PATTERNS IN A SQUARE CHANNEL — GESSNER AND JONES.

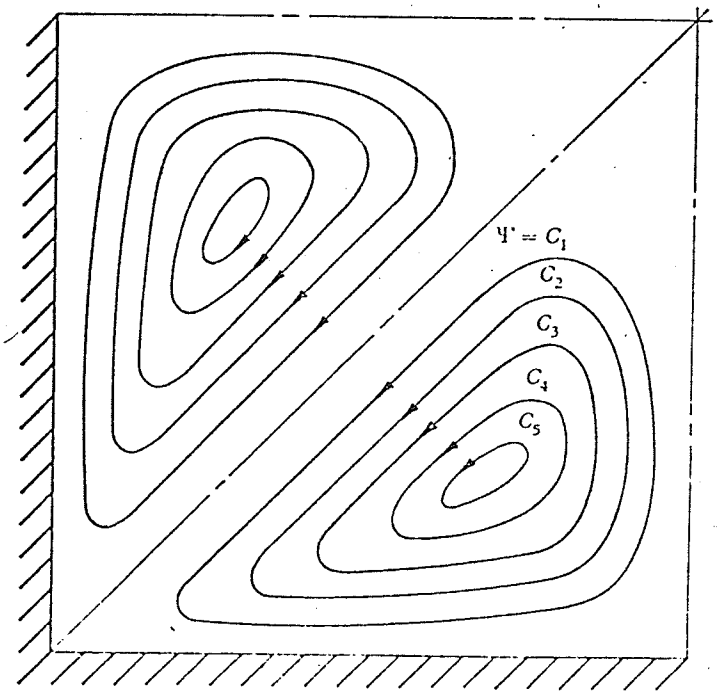

FIGURE 8 TYPICAL SECONDARY-FLOW STREAMLINE PATTERNS IN A SQUARE CHANNEL — GESSNER AND JONES.

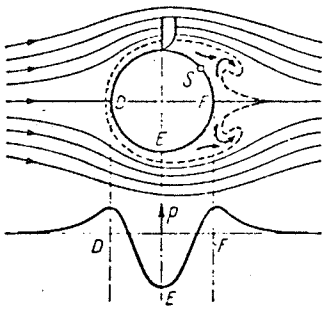

FIGURE 9 BOUNDARY-LAYER SEPARATION AND VORTEX FORMATION ON A CIRCULAR CYLINDER. — SCHLICHTING

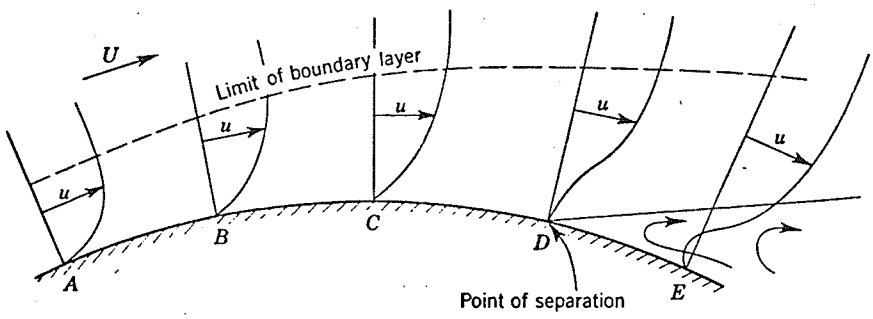

FIGURE 10 GROWTH AND SEPARATION OF BOUNDARY LAYER DUE TO INCREASING PRESSURE GRADIENT.—DAUGHERTY AND FRANZINI.

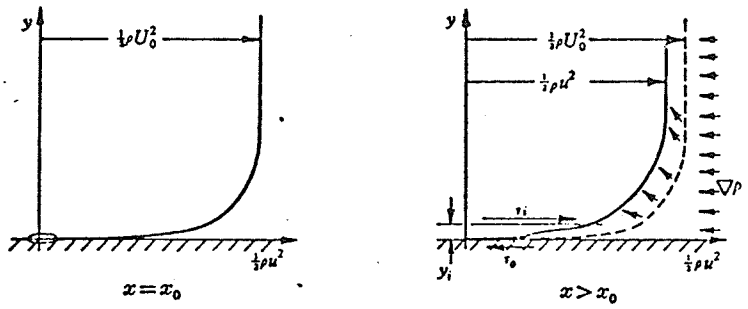

FIGURE 11 DEVELOPMENT OF A BOUNDARY LAYER IN A PRESSURE GRADIENT. —STRATFORD.

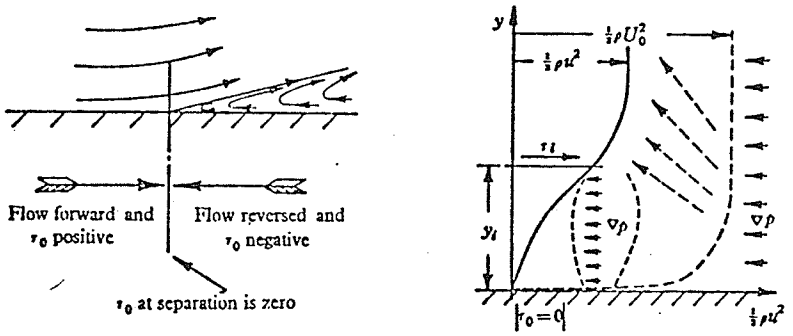

FIGURE 12 THE SEPARATION POSITION.——STRATFORD

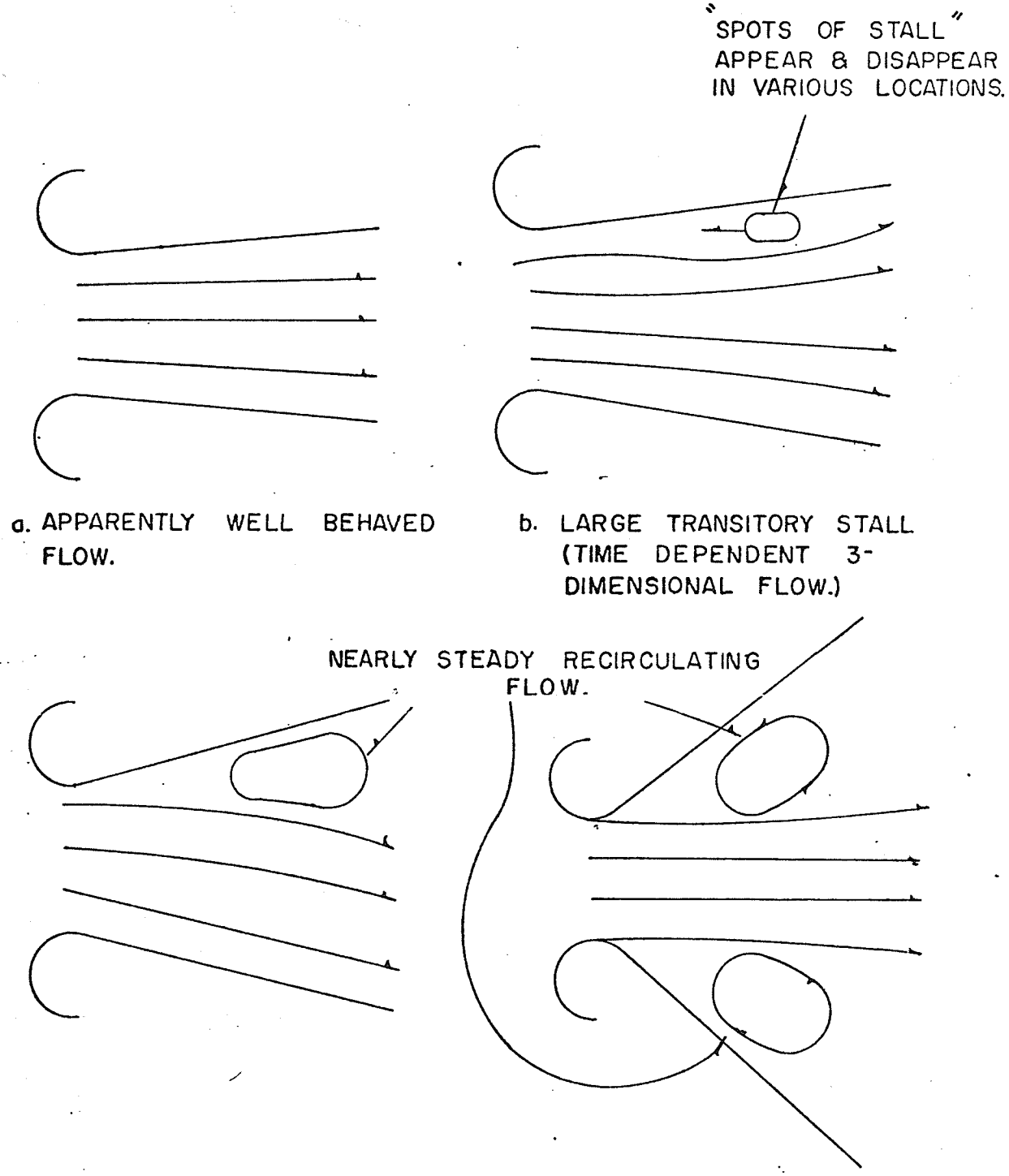

a. APPARENTLY WELL BEHAVED FLOW.

b. LARGE TRANSITORY STALL (TIME DEPENDENT 3-DIMENSIONAL FLOW.)

c. STEADY 2-DIMENSIONAL STALL.

d. JET FLOW.

FIGURE 13 SCHEMATIC DIAGRAMS OF THE REGIMES OF DIFFUSER FLOW—KLINE, MOORE, AND COCHRAN.

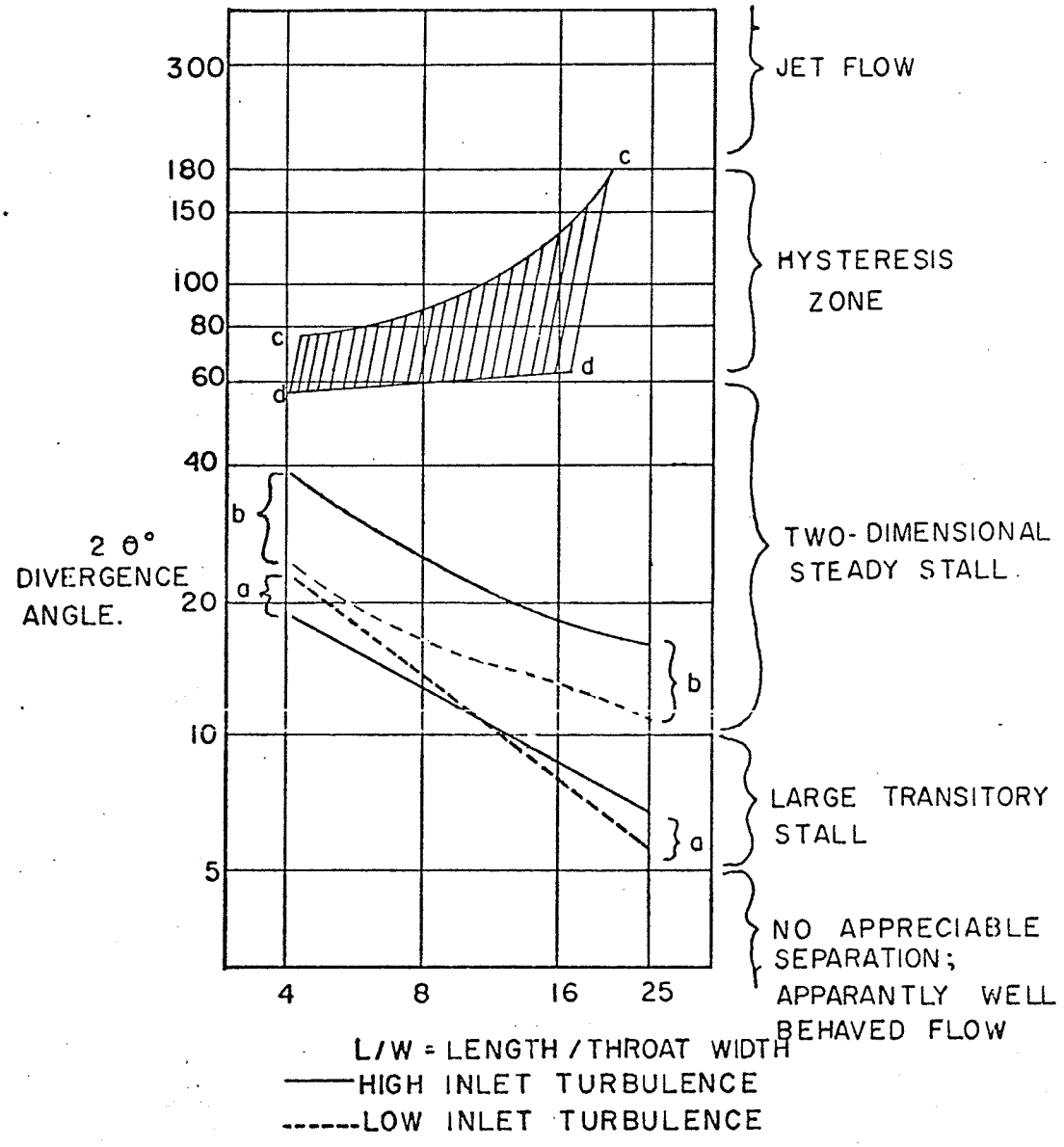

FIGURE 14 ZONES OF DIFFUSER FLOW IN TERMS OF GOVERNING PARAMETERS FOR FIXED MEAN INLET VELOCITY PROFILE.—KLINE, MOORE, AND COCHRANE.

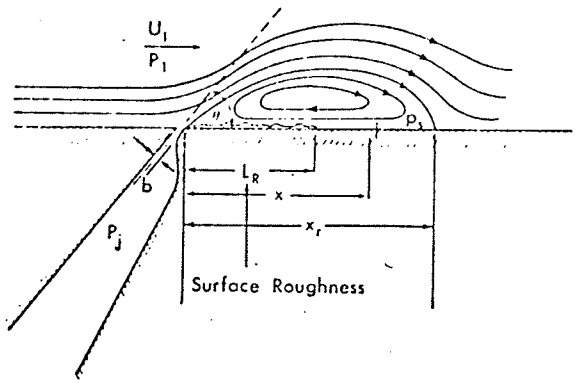

FIGURE 15 THE REATTACHMENT OF AN INCLINED TWO DIMENSIONAL JET TO A FLAT SURFACE. WYGNANSKI AND NEWMAN.

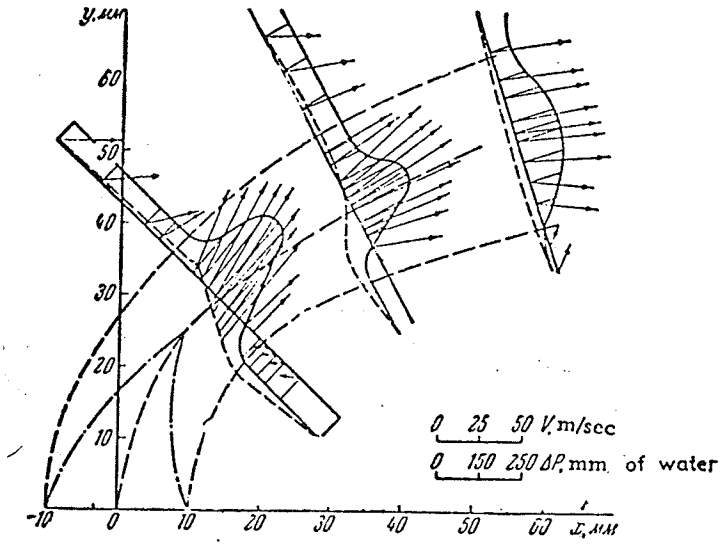

FIGURE 16 FIELDS OF VELOCITY AND PRESSURE IN THE PLANE OF SYMMETRY OF A JET DEFLECTED BY LATERAL FLOW. —— ABRAMOVICH.

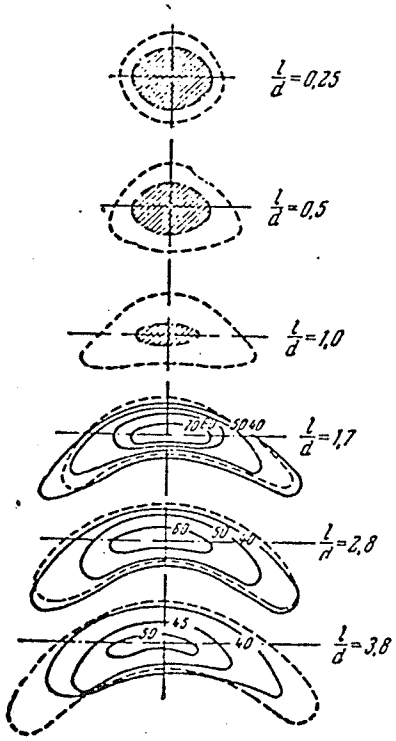

FIGURE 17 A JET IN A LATERAL DEFLECTING FLOW. — AMBRAMOVICH.

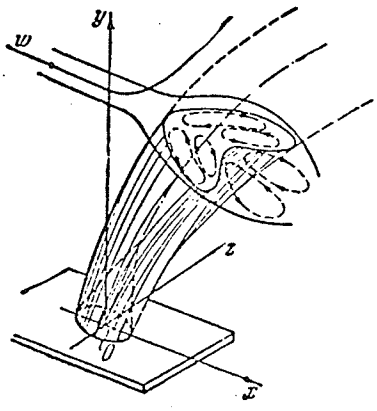

FIGURE 18 THE CROSS SECTIONAL CONFIGURATION OF A JET IN A LATERAL FLOW AT VARIOUS DISTANCES FROM THE FIRST SECTION. — AMBRAMOVICH.

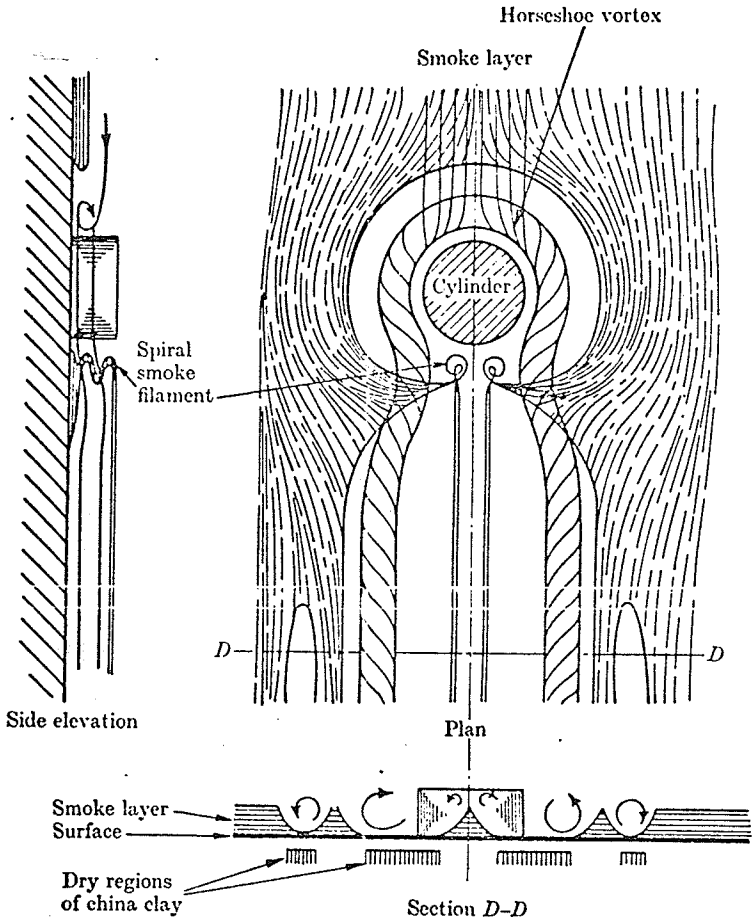

FIGURE 19 SHEAR FLOW PAST A SMALL CIRCULAR CYLINDER ON A PLANE, BASED ON THE OBSERVATION OF A LAYER OF SMOKE.—THWAITES

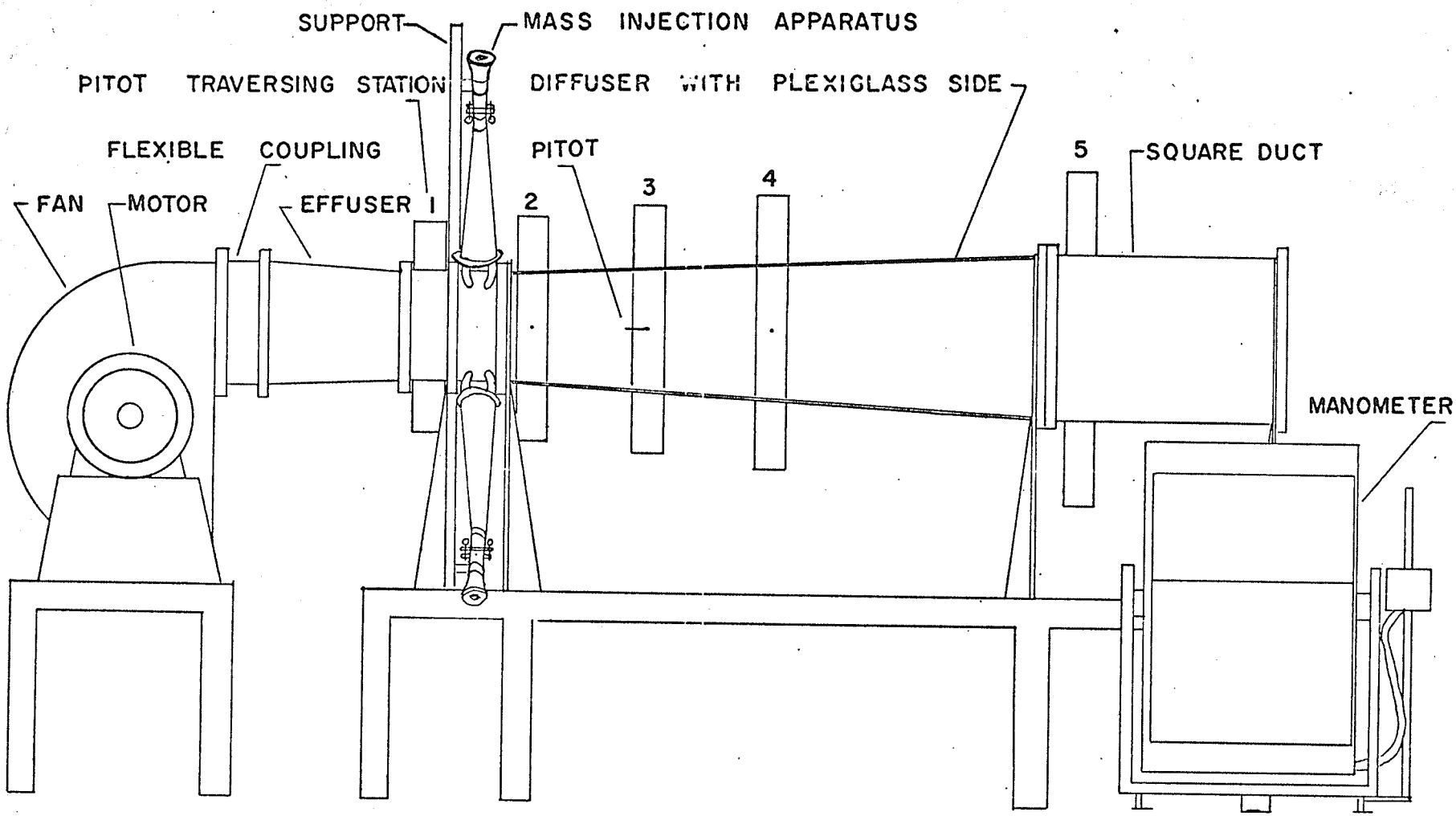

FIGURE 20 SCHEMATIC DIAGRAM OF APPARATUS

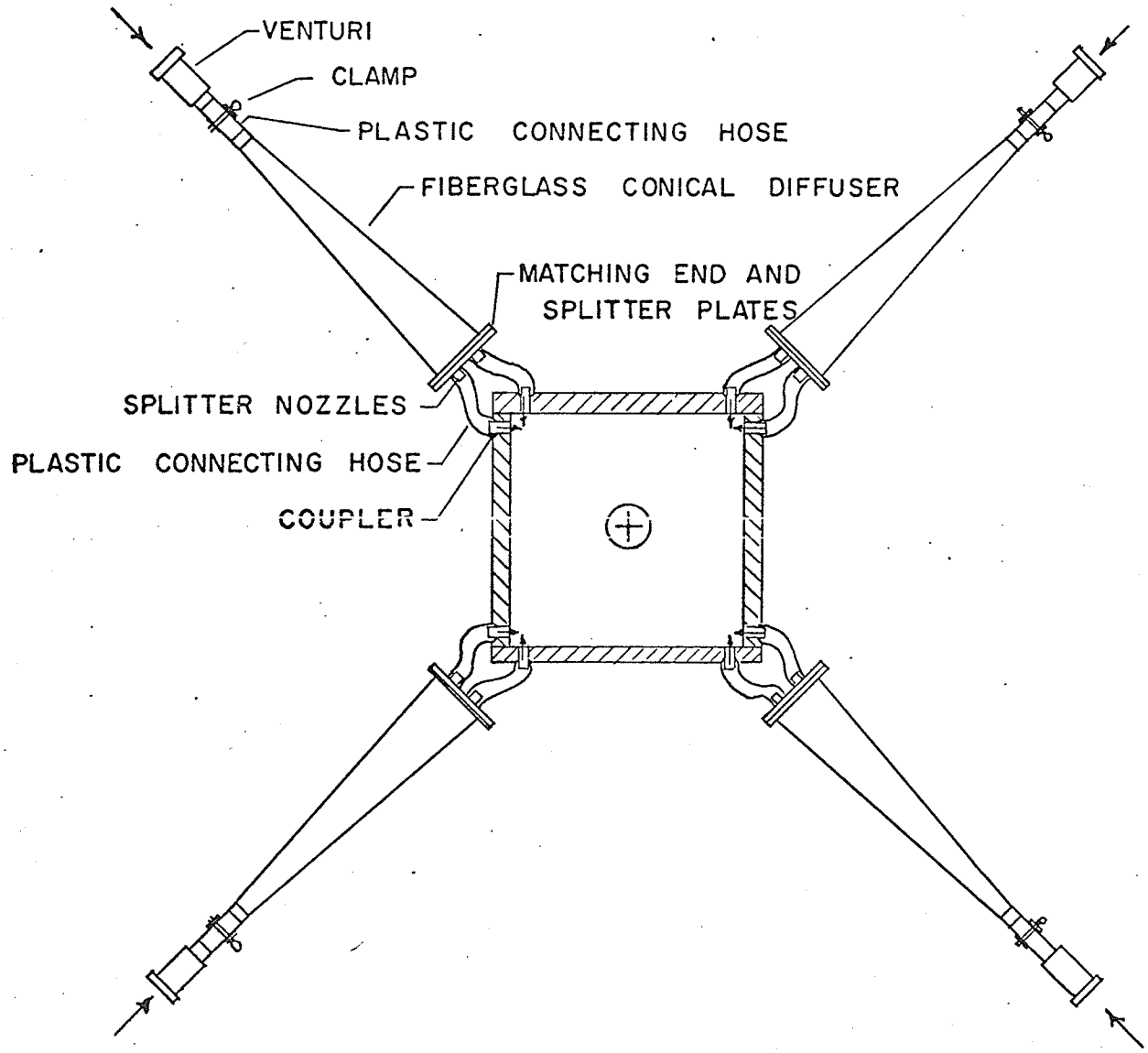

FIGURE 21 — SCHEMATIC DIAGRAM OF MASS INJECTION APPARATUS.

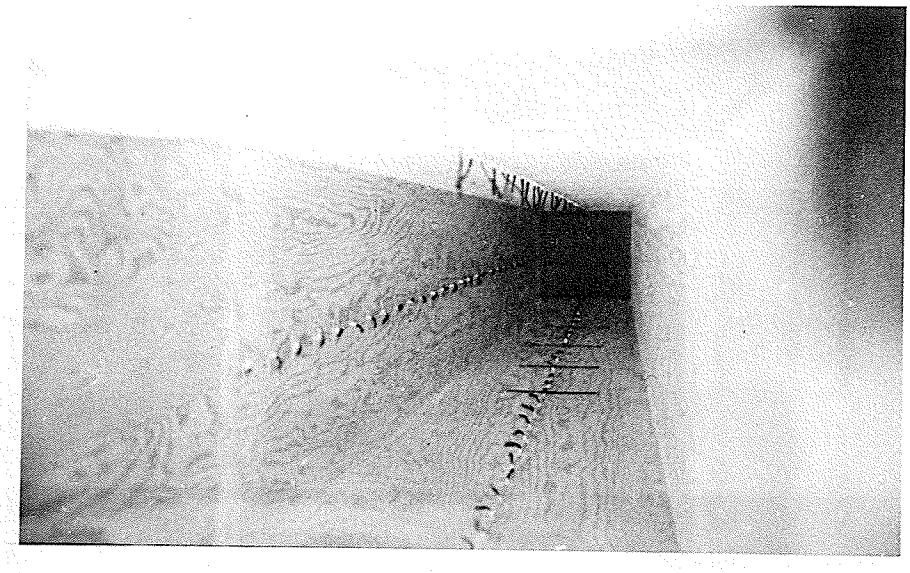

FIGURE 22 TUFTS INDICATING SEPARATION.

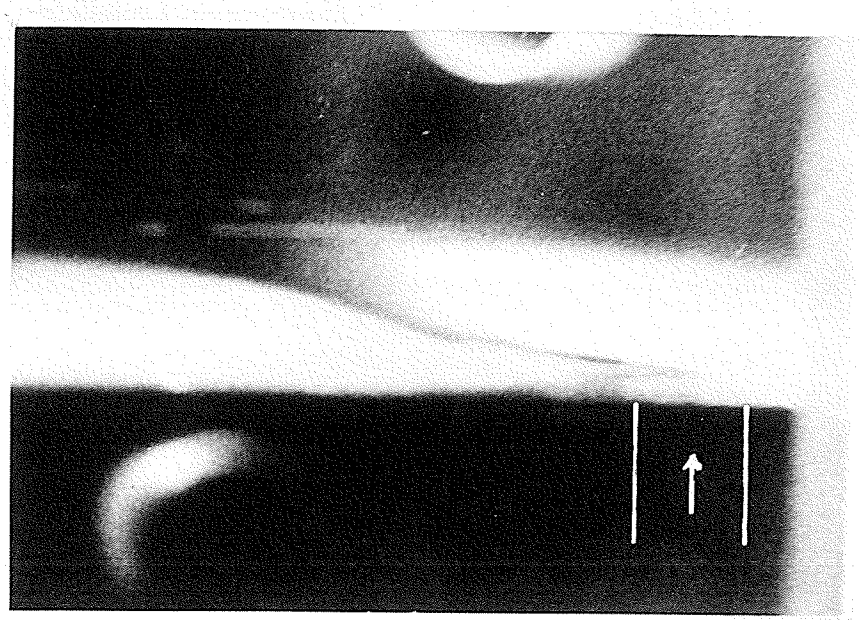

FIGURE 23 SMOKE TRACE IN JET.

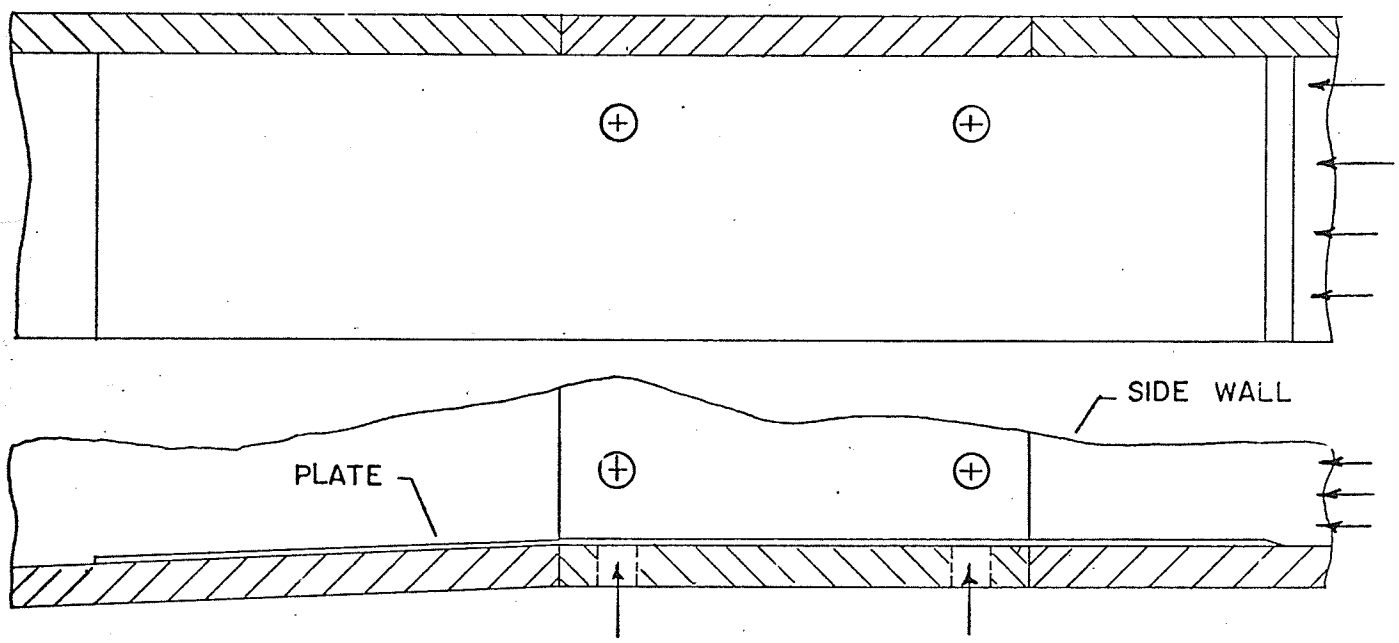

PLATE IN THE HORIZONTAL PLANE.

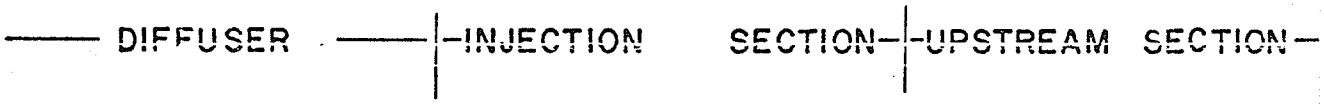

PLATE IN VERTICAL PLANE OF SYMMETRY.

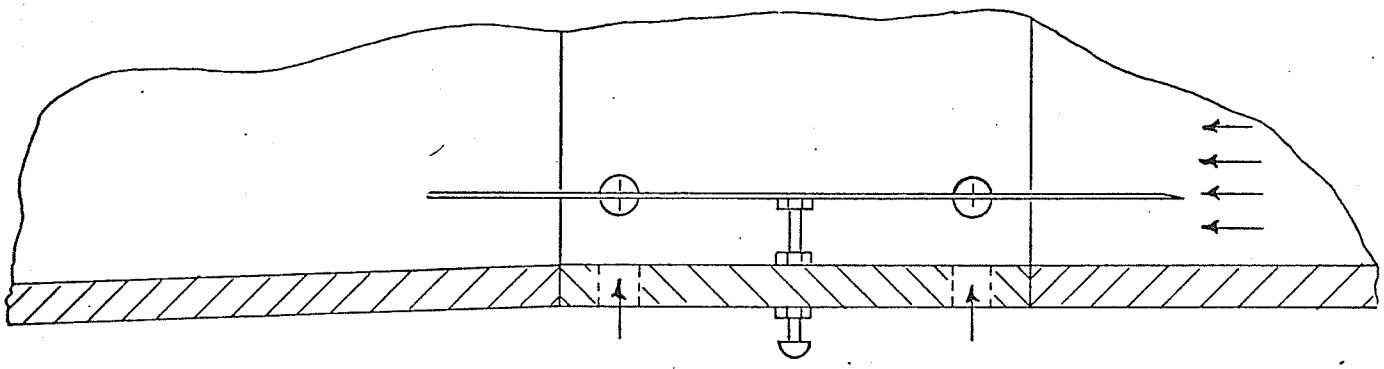

FIGURE 24 — STAINLESS STEEL PLATES FOR FLOW VISUALIZATION.

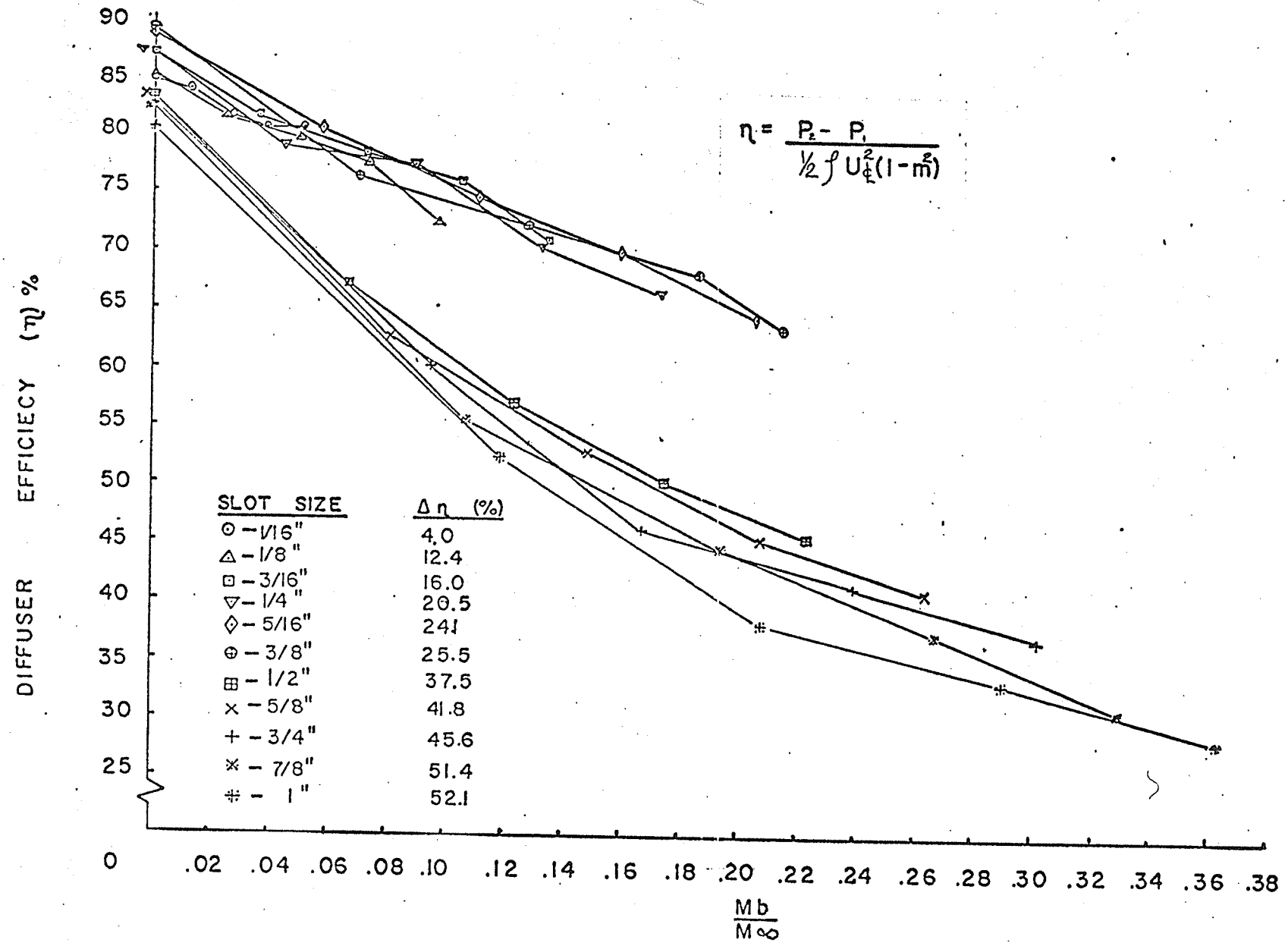

FIGURE 25 — DIFFUSER EFFICIENCY vs BLEED MASS FLOW RATE FOR SLOT SIZES 1/16"→1"

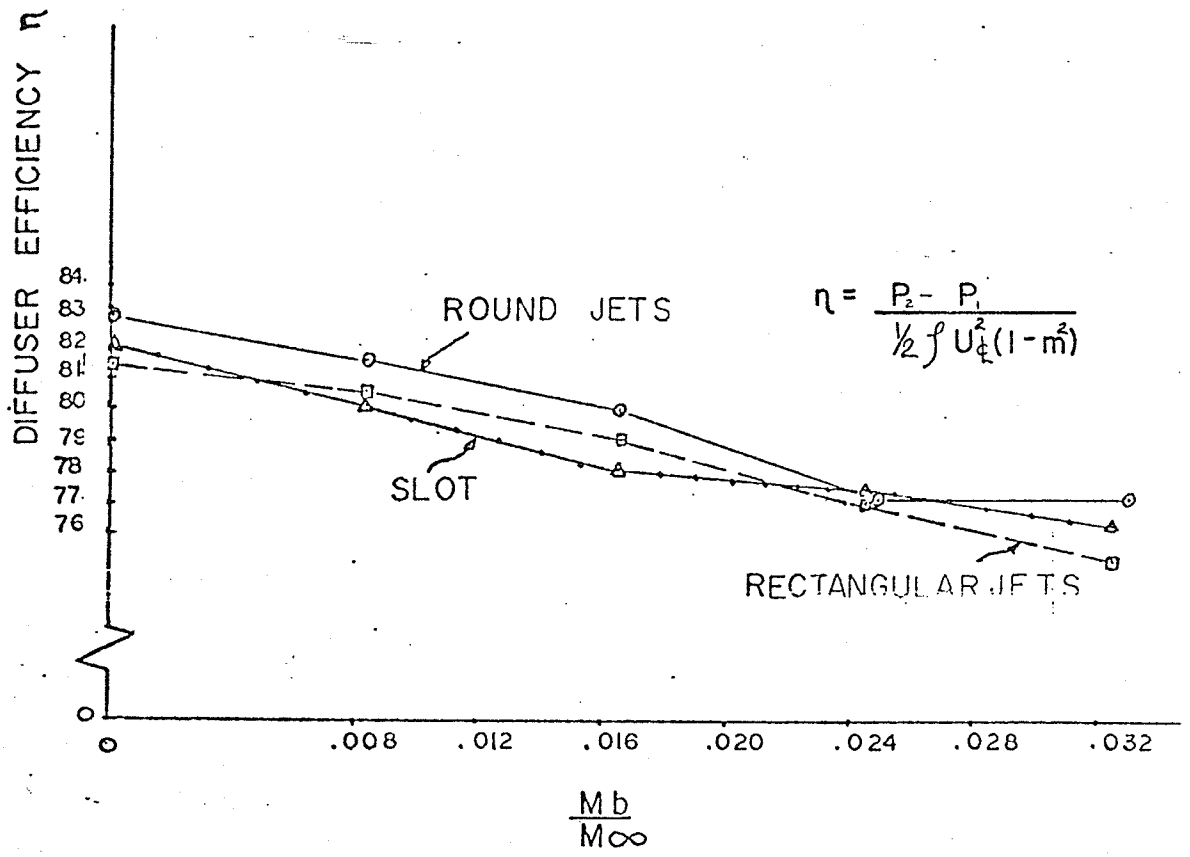

Δ η(%)

Rd. JETS	6.8
Rec. JETS	6.1
Slot.	5.6

FIGURE 26 DIFFUSER EFFICIENCY vs MASS FLOW RATE for DIFFERENT INJECTION CONFIGURATIONS.

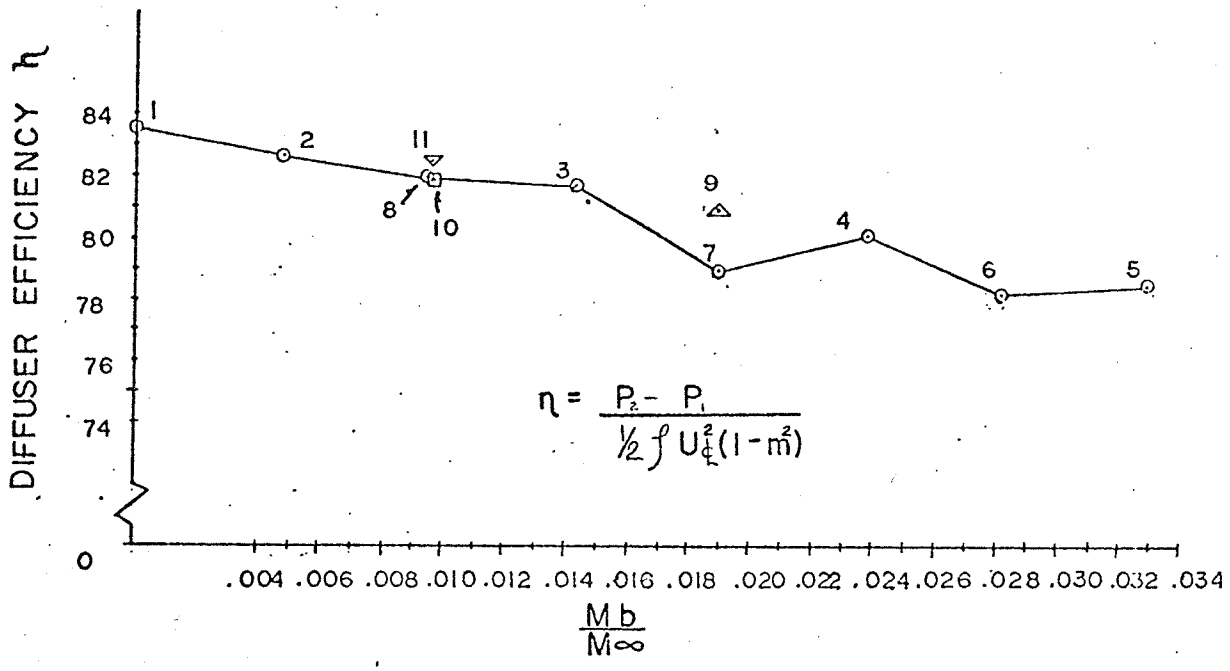

CONFIGURATION

1-XXXXXXX
2-XXXOXXX
3-XXOOOXX
4-XOOOOOX
5-OOOOOOO
6-OOOXOOO
7-OOXXXOO
8-OXXXXXO
9-XOOXOOX
10-XOXXXOX
11-XXOXOXX

FIGURE 27 SYMMETRIC BLOWING CONFIGURATION

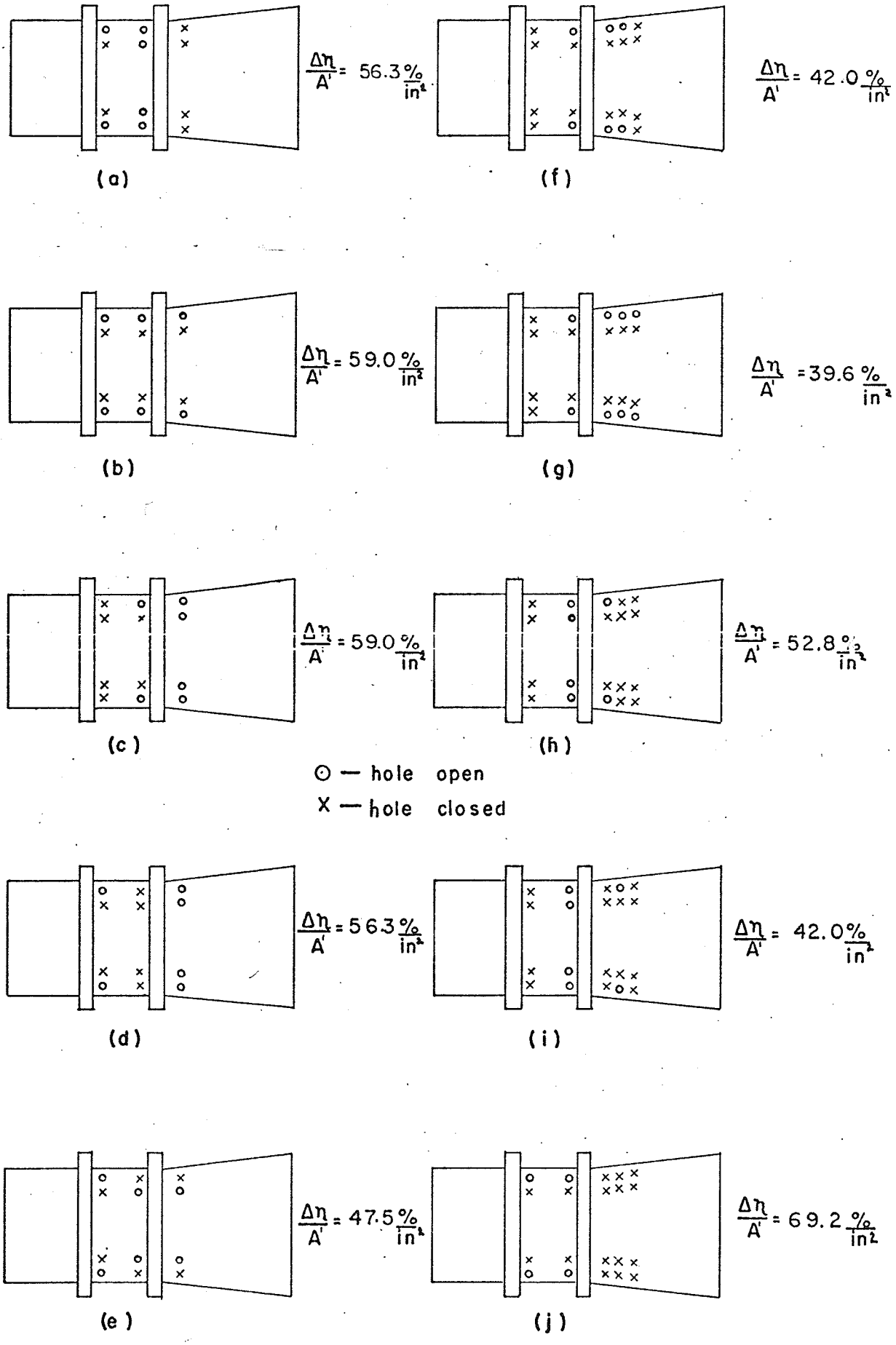

FIGURE 28—VARIATIONS IN CONFIGURATION FOR CORNER BLOWING.

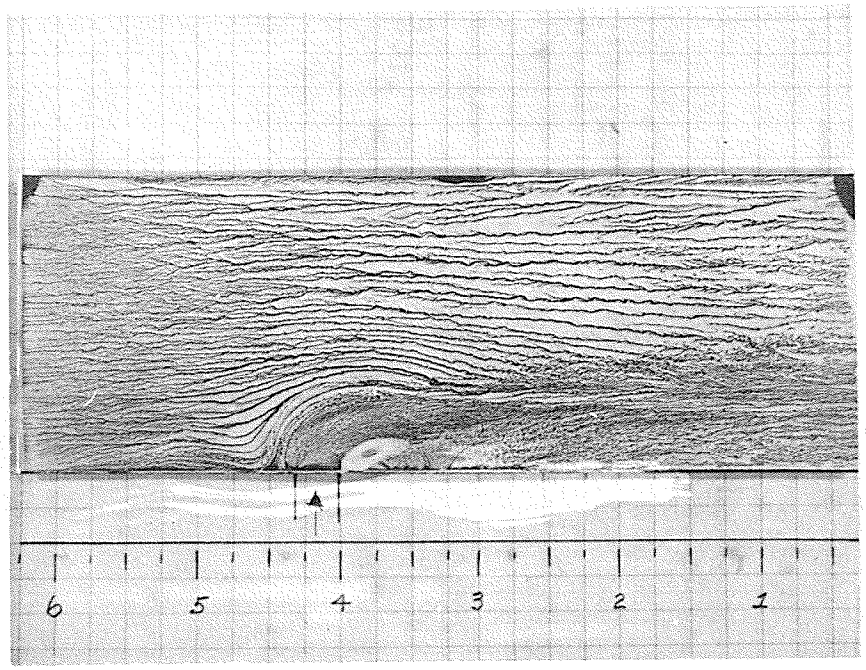

FIGURE 29 SINGLE JET — FULL BLEED — VERTICAL PLANE OF SYMMETRY

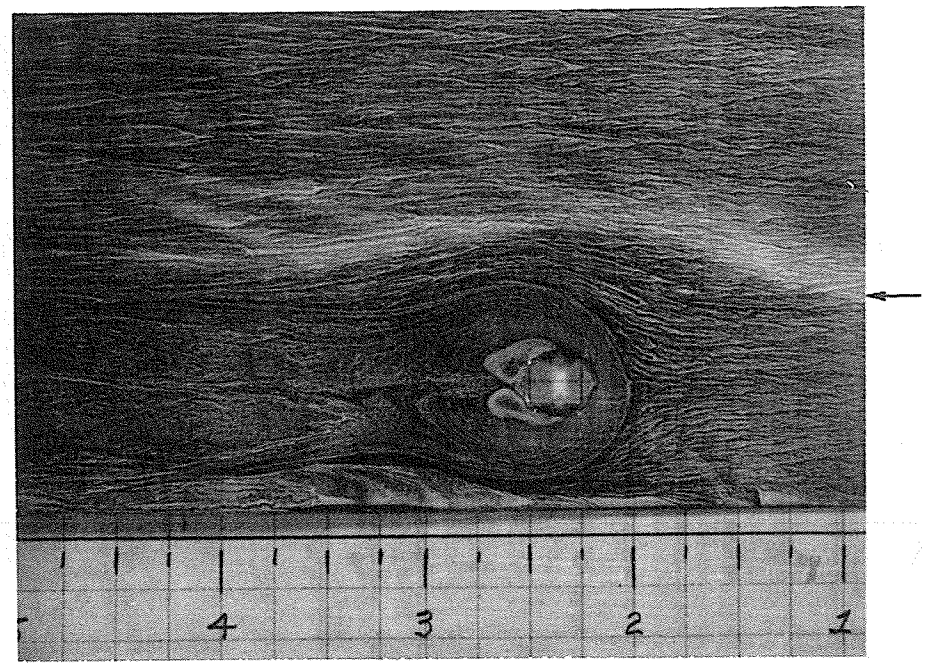

FIGURE 30 SINGLE JET — FULL BLEED — HORIZONTAL PLANE

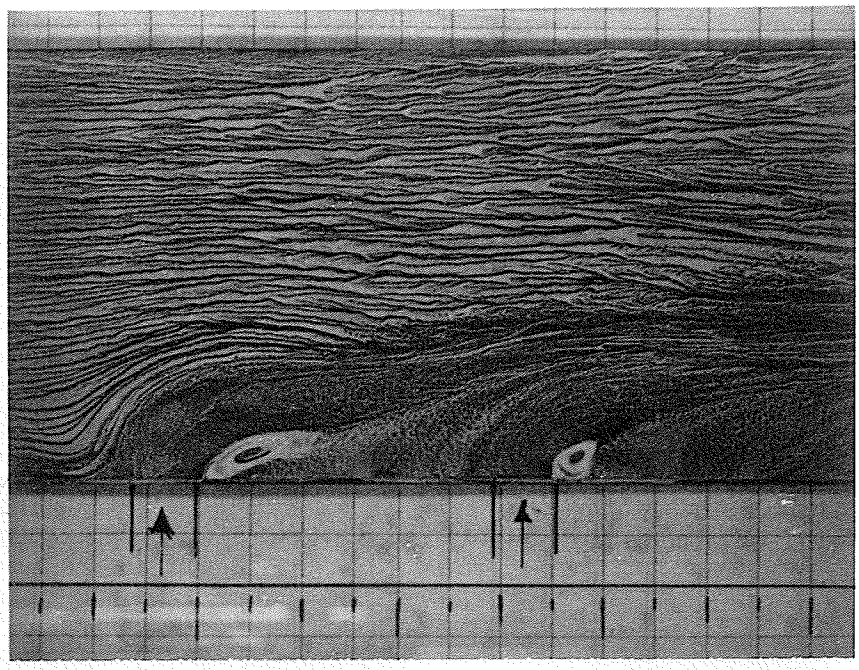

FIGURE 31 DOUBLE JET — FULL BLEED — VERTICAL PLANE OF SYMMETRY

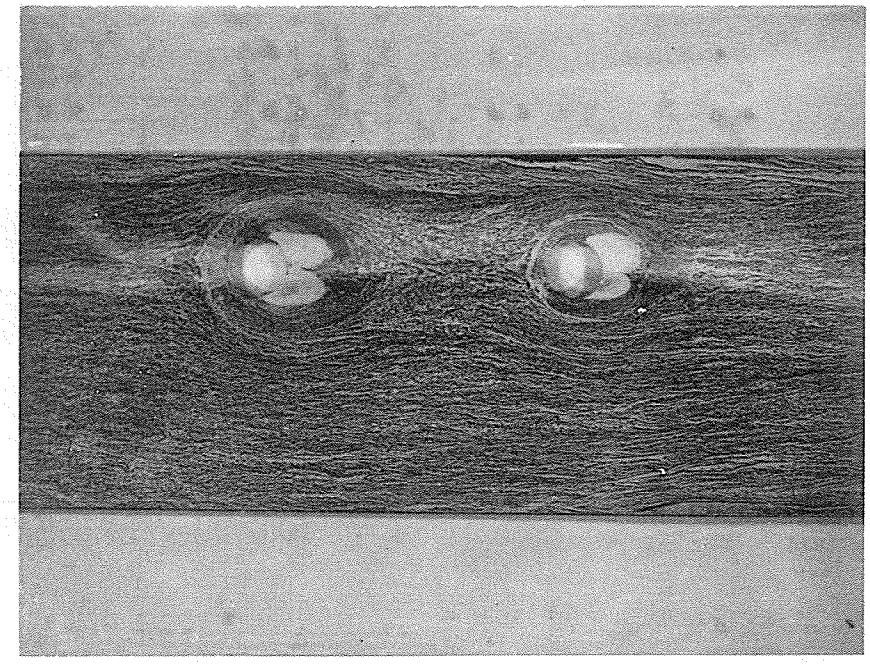

FIGURE 32 DOUBLE JET— FULL BLEED — HORIZONTAL PLANE

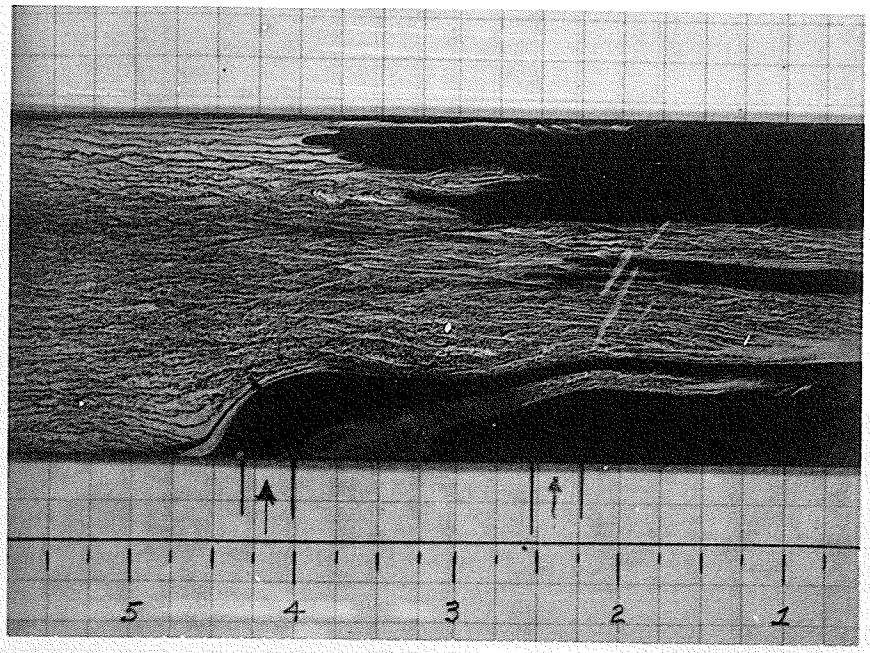

FIGURE 33

DOUBLE JET — FULL BLEED — VERTICAL PLANE OF SYMMETRY.
FLUID ADDED AT X = 3.3"

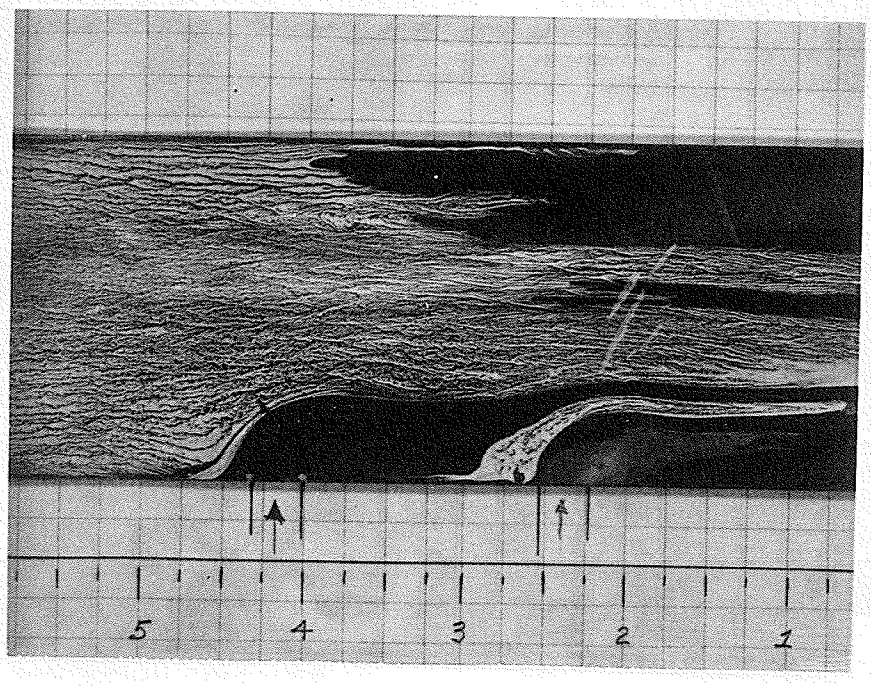

FIGURE 34

DOUBLE JET — FULL BLEED — VERTICAL PLANE OF SYMMETRY.
FLUID ADDED AT X = 2.75" AND 2.35"

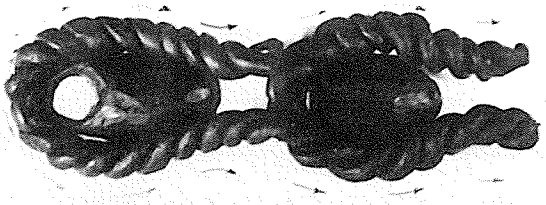

FIGURE 35

THREE DIMENSIONAL MODEL OF JET AND MAINSTREAM INTERACTING.

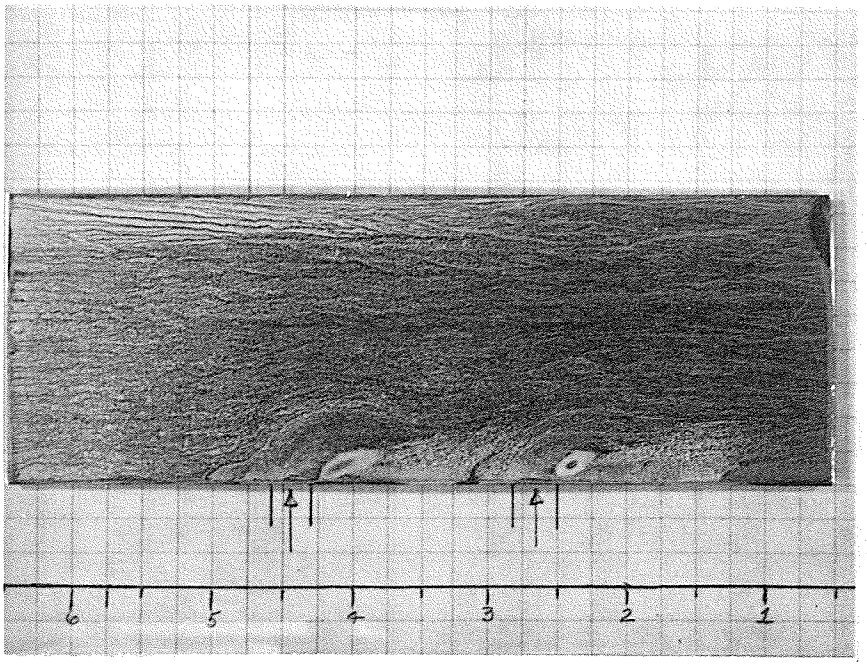

FIGURE 36

DOUBLE JET — FULL BLEED — VERTICAL PLANE OF SYMMETRY.

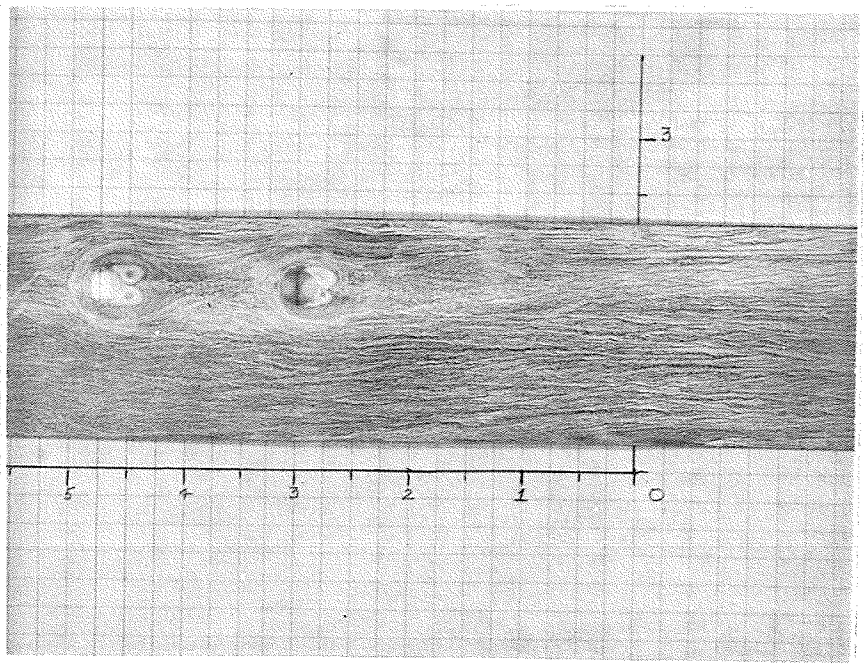

FIGURE 37

DOUBLE JET — FULL BLEED — HORIZONTAL PLANE

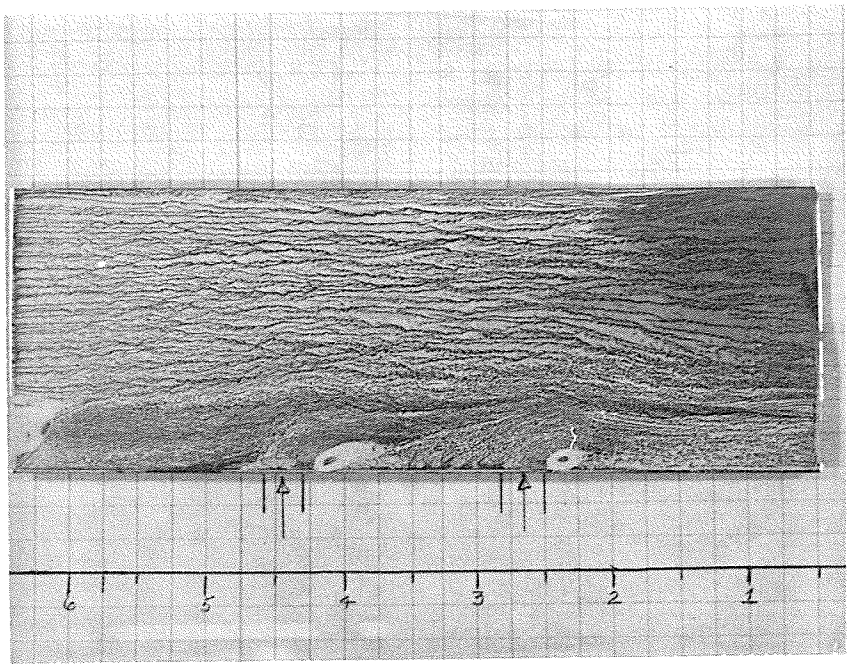

FIGURE 38

DOUBLE JET — THREE QUARTERS BLEED
VERTICAL PLANE OF SYMMETRY

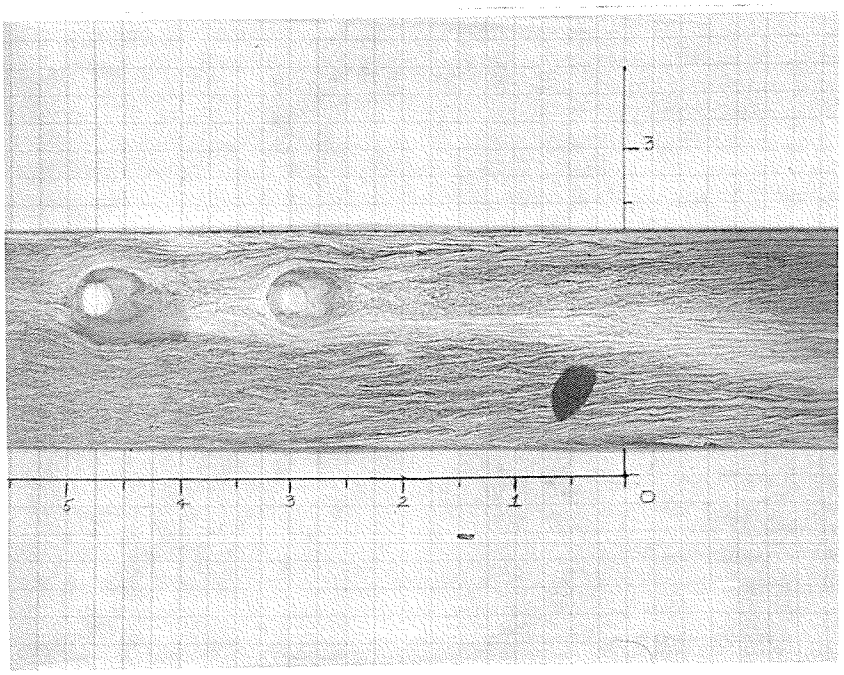

FIGURE 39

DOUBLE JET — THREE — QUARTERS BLEED
HORIZONTAL PLANE.

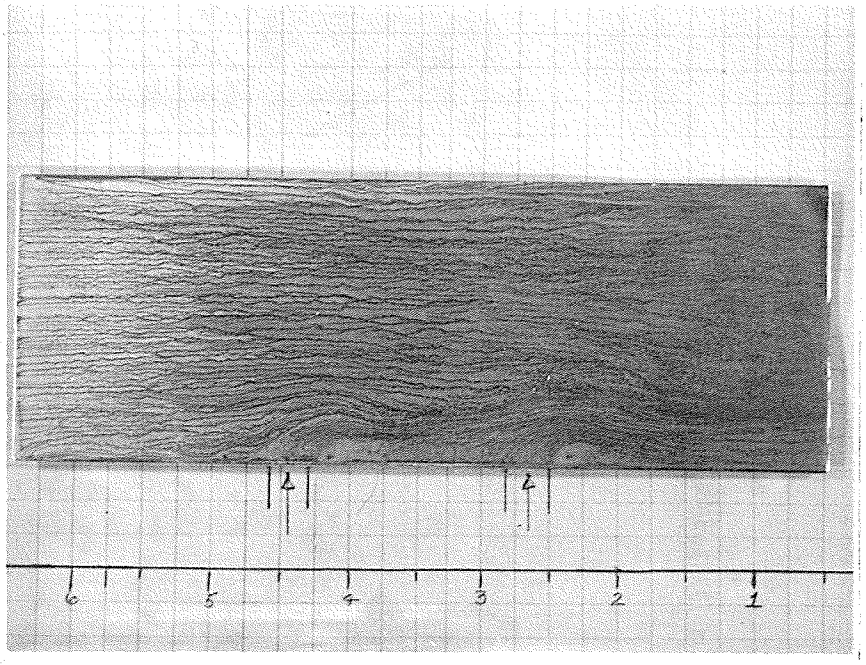

FIGURE 40

DOUBLE JET — ONE-HALF BLEED — VERTICAL PLANE OF SYMMETRY.

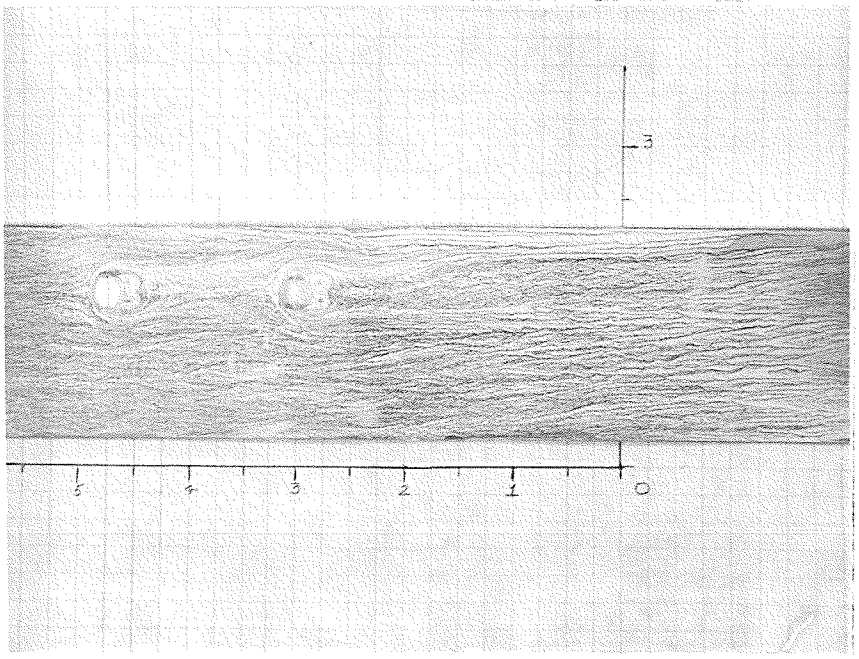

FIGURE 41

DOUBLE JET — ONE-HALF BLEED — HORIZONTAL PLANE.

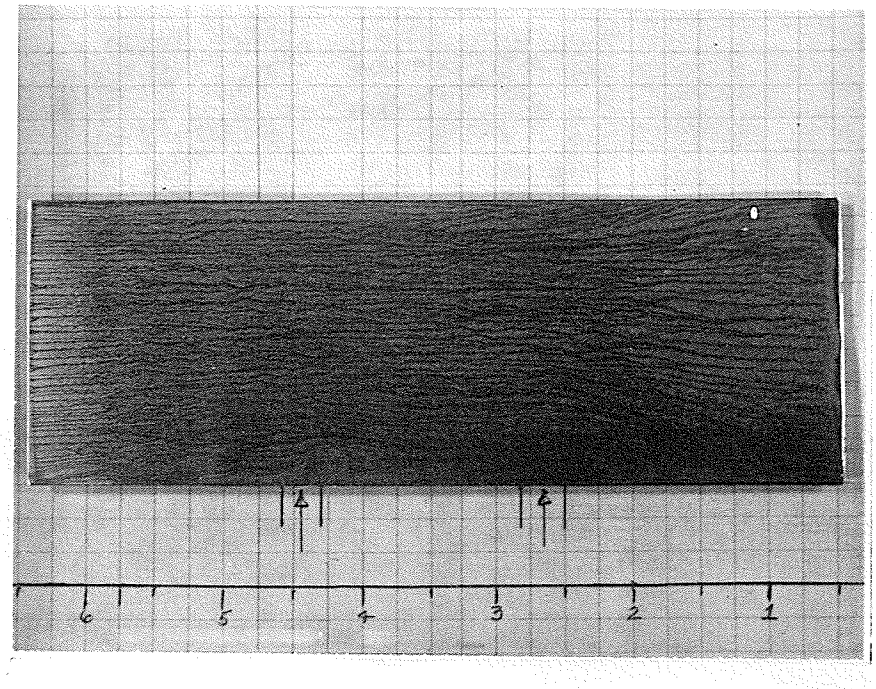

FIGURE 42

DOUBLE JET — ONE-QUARTER BLEED — VERTICAL PLANE OF SYMMETRY.

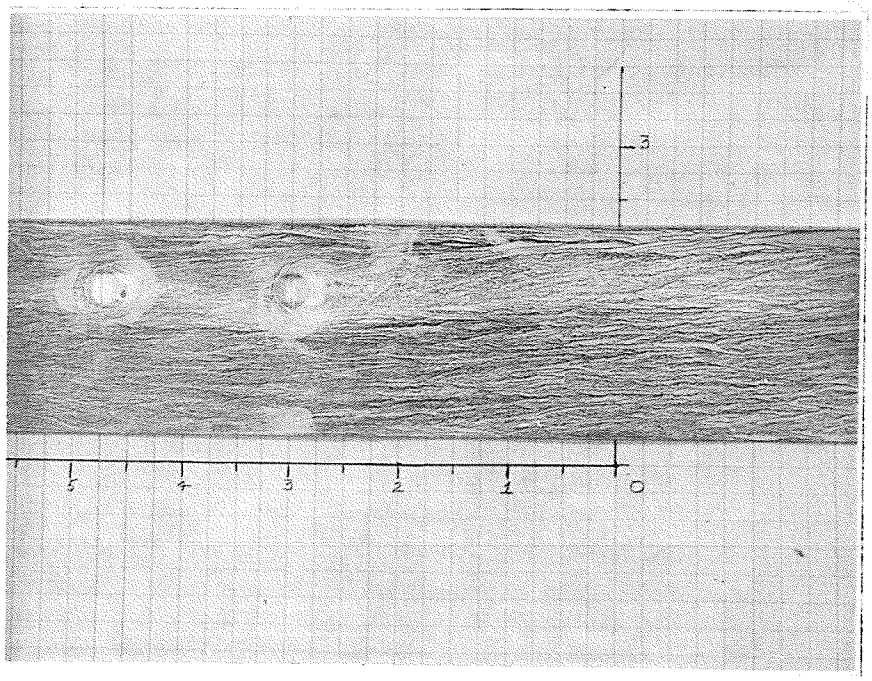

FIGURE 43

DOUBLE JET — ONE-QUARTER BLEED HORIZONTAL PLANE.

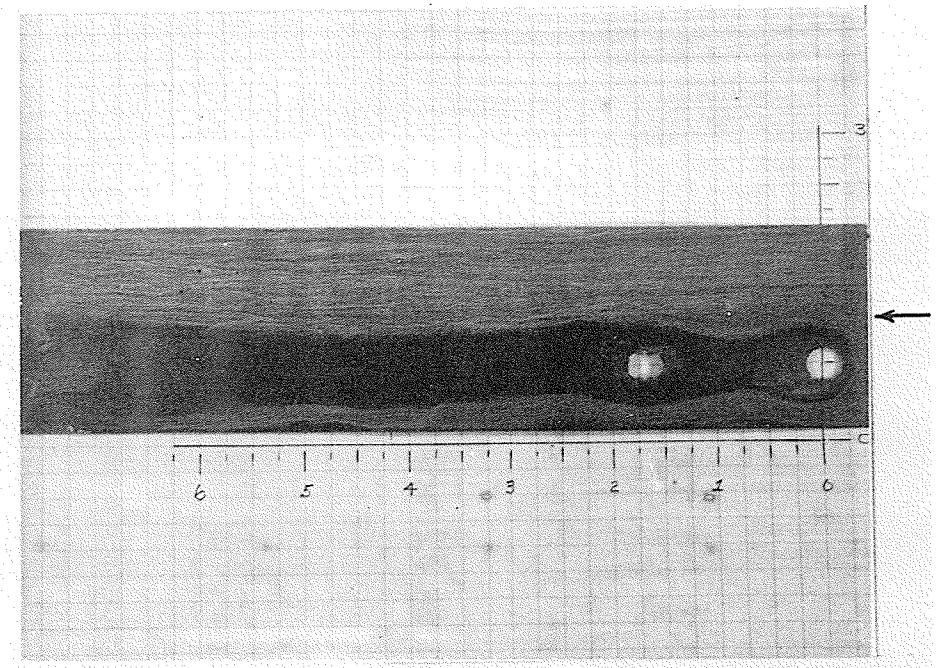

FIGURE 44 DOUBLE JET—FULL BLEED—HORIZONTAL PLANE—CORNER SEPARATION.

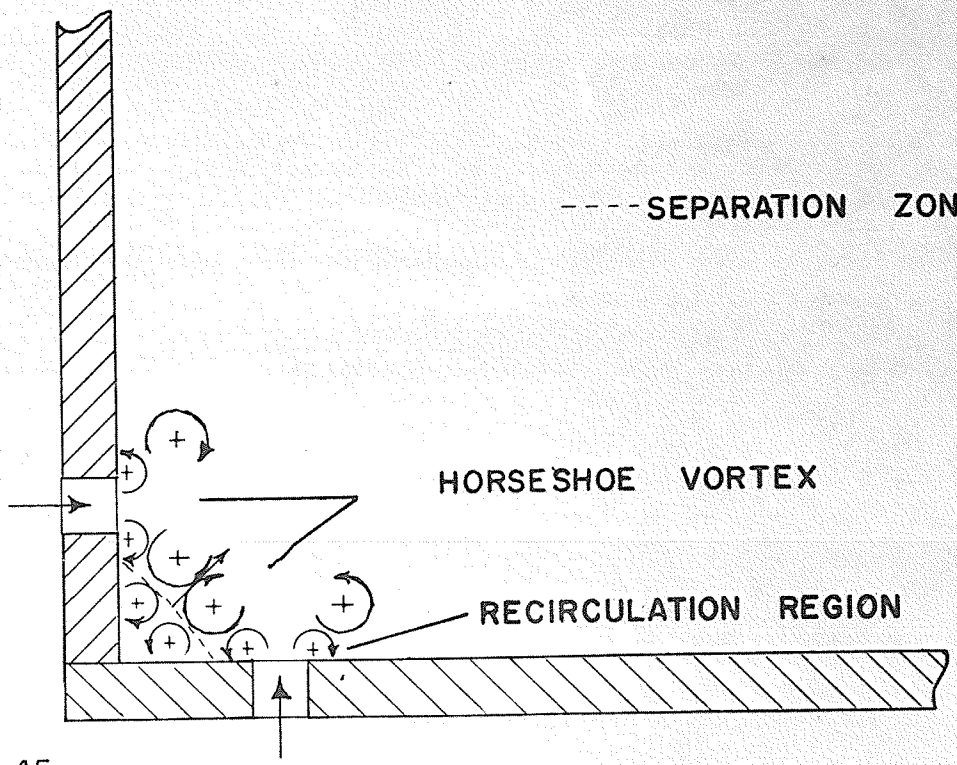

FIGURE 45 SEPARATION IN A CORNER.

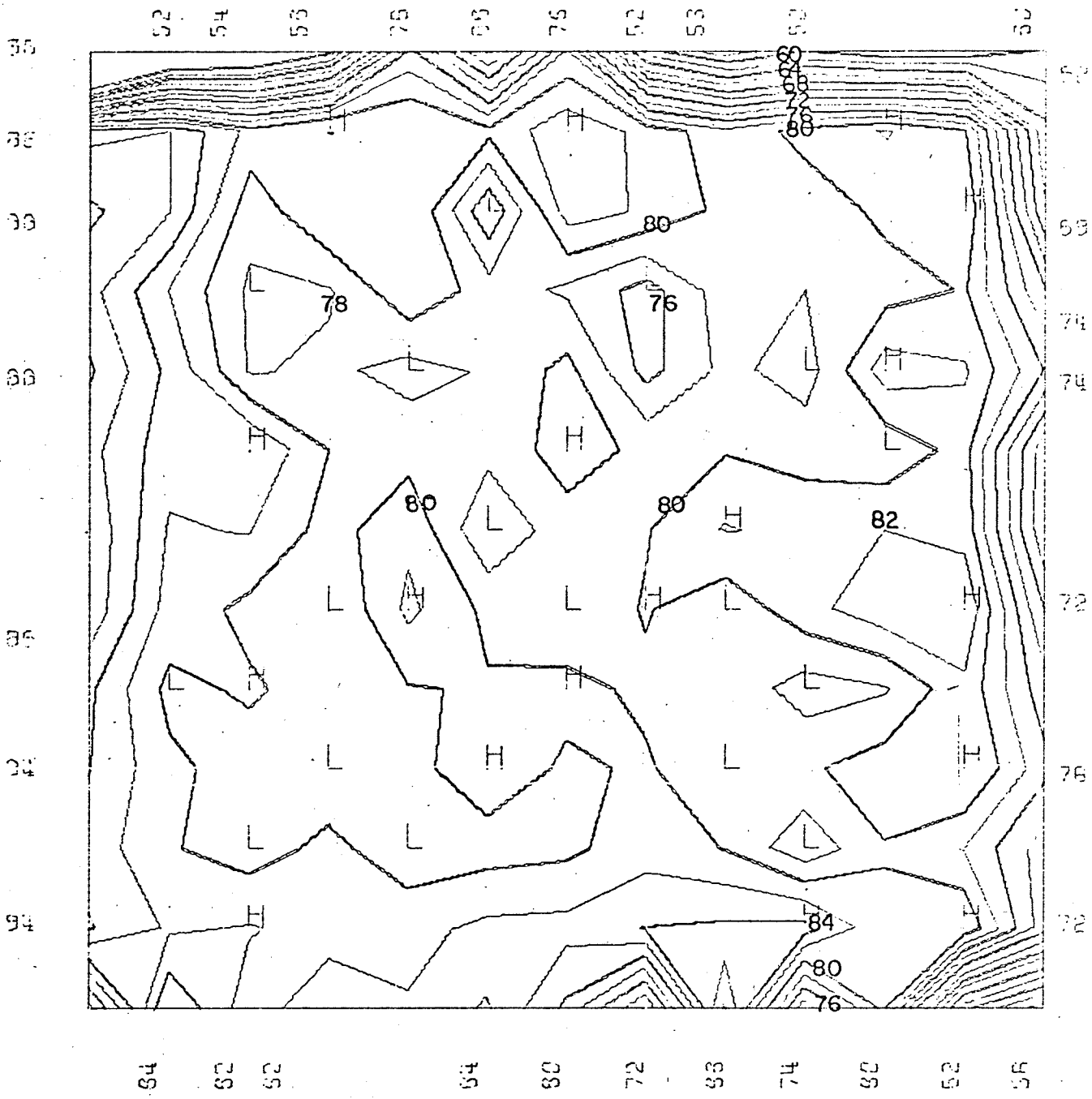

FIGURE 46

CONTOUR PLOT AT STATION I
NO BLEED.
(AXIAL VELOCITY- FT./ SEC.)

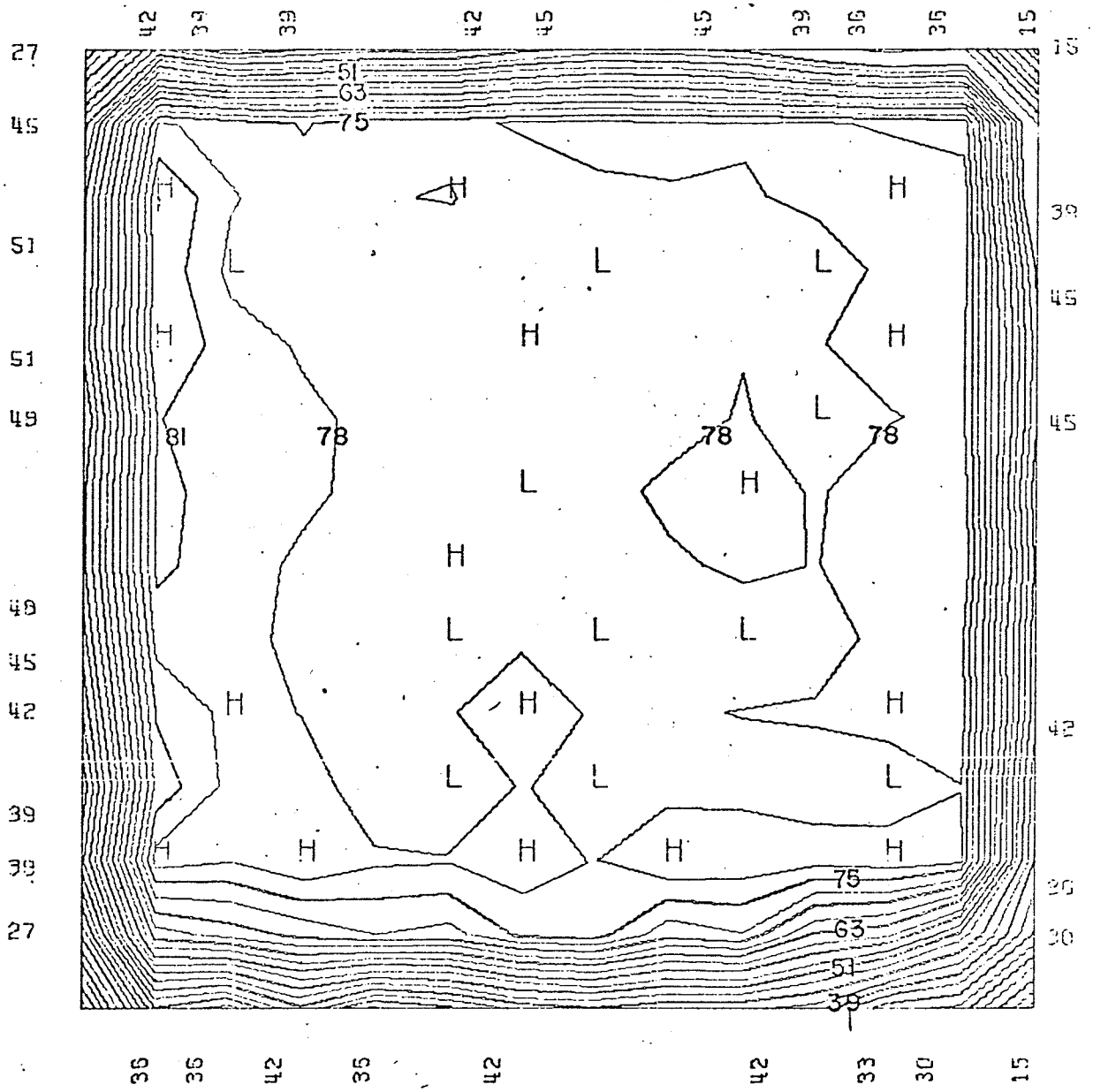

FIGURE 47

CONTOUR PLOT AT STATION 2
NO BLEED.
(AXIAL VELOCITY - FT / SEC)

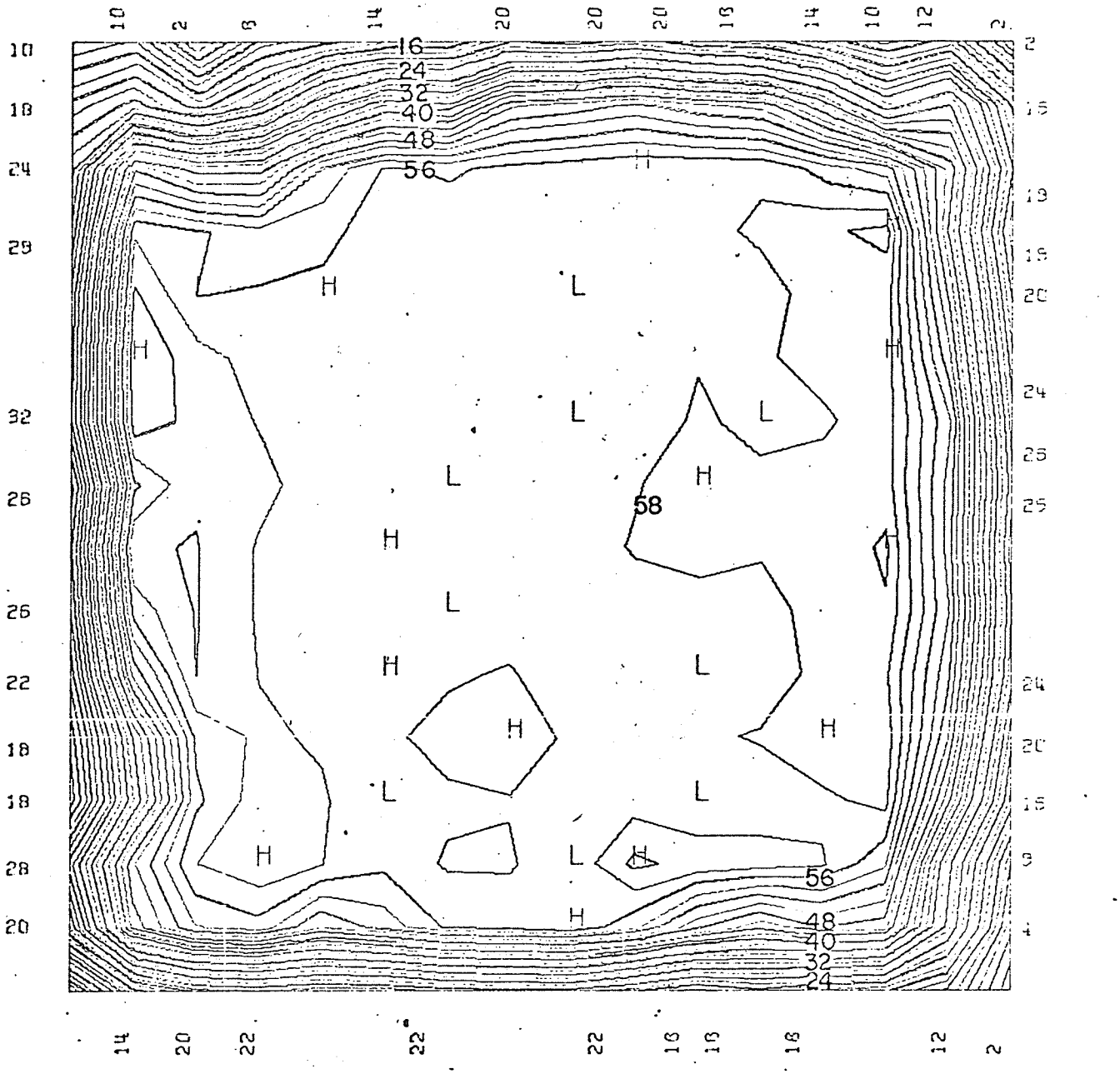

FIGURE 48

CONTOUR PLOT AT STATION 3
NO BLEED.

(AXIAL VELOCITY - FT./SEC.)

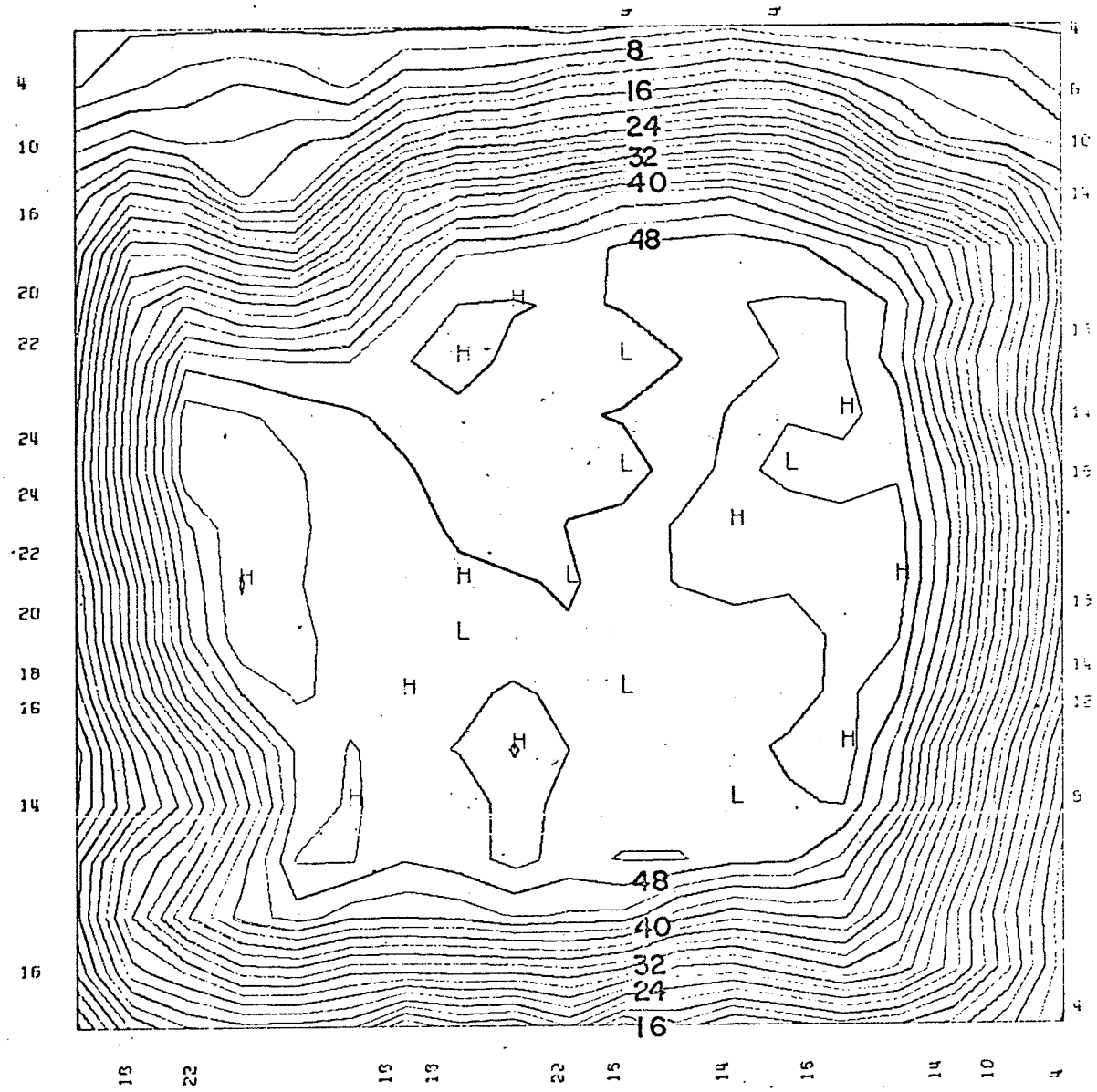

FIGURE 49

CONTOUR PLOT AT STATION 4
NO BLEED.
(AXIAL VELOCITY - FT./SEC.)

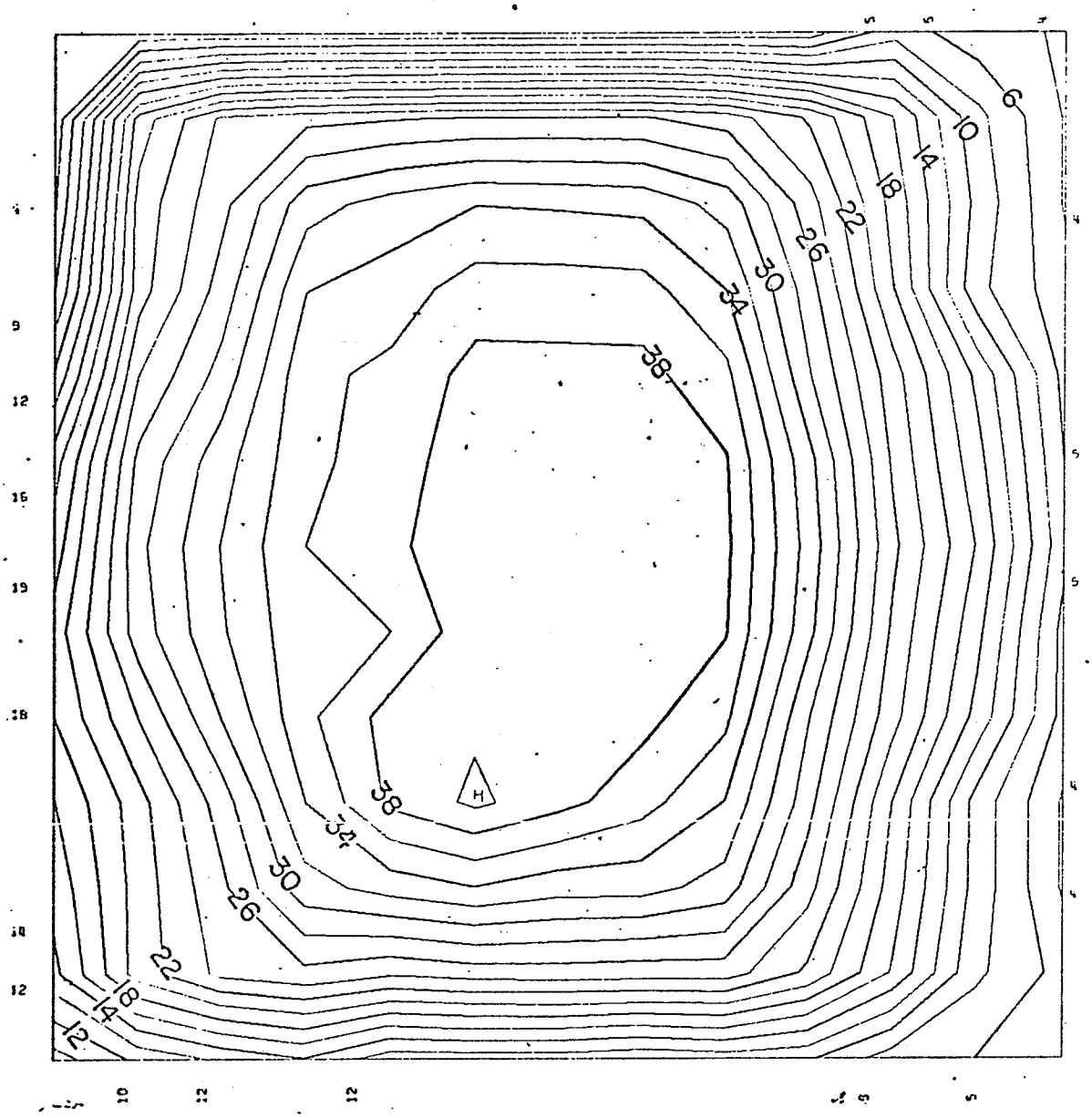

FIGURE 50

CONTOUR PLOT AT STATION 5
NO BLEED.
(AXIAL VELOCITY - FT. / SEC.)

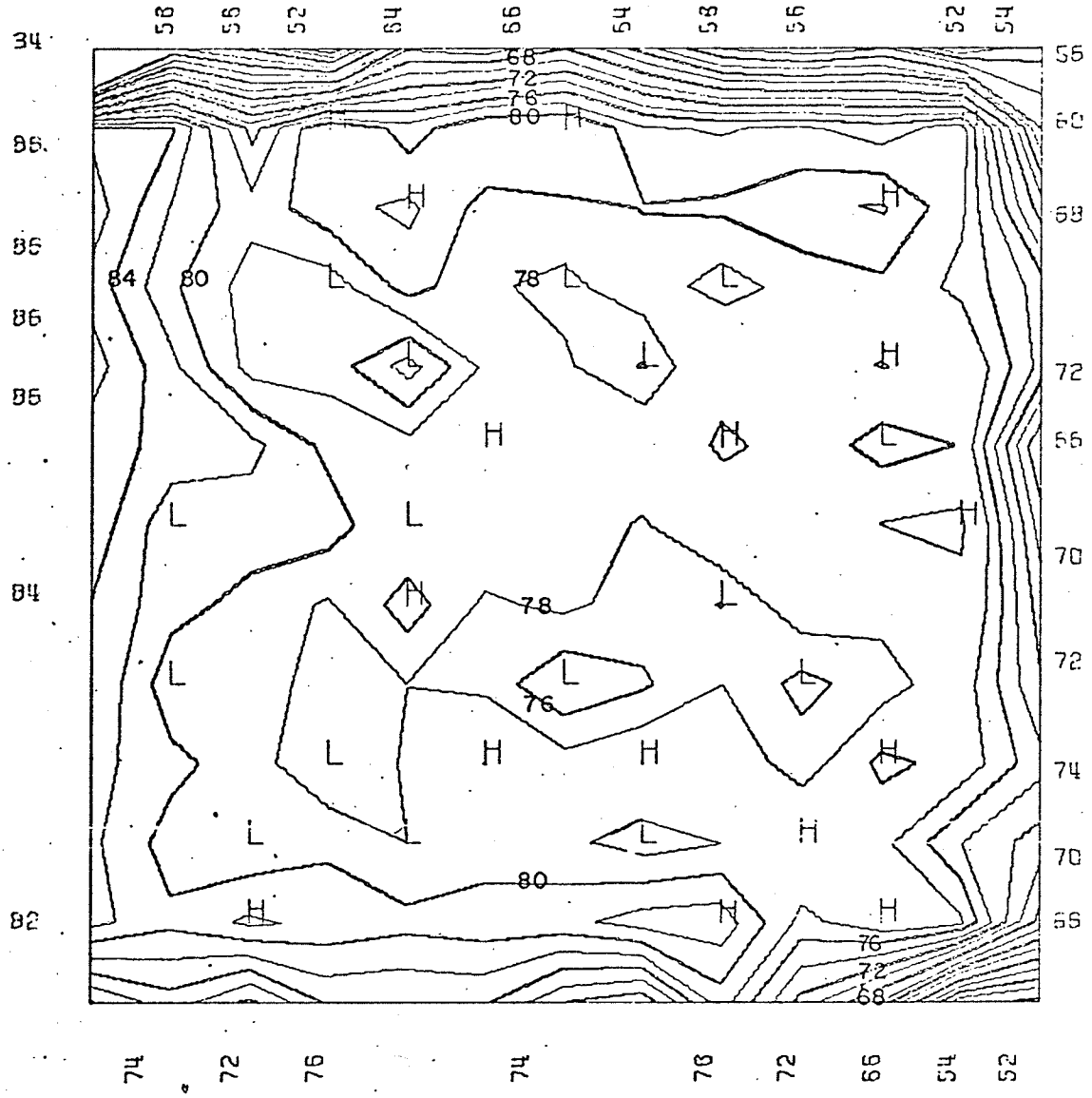

FIGURE 51

CONTOUR PLOT AT STATION I
ONE-HALF BLEED
(AXIAL VELOCITY - FT / SEC.)

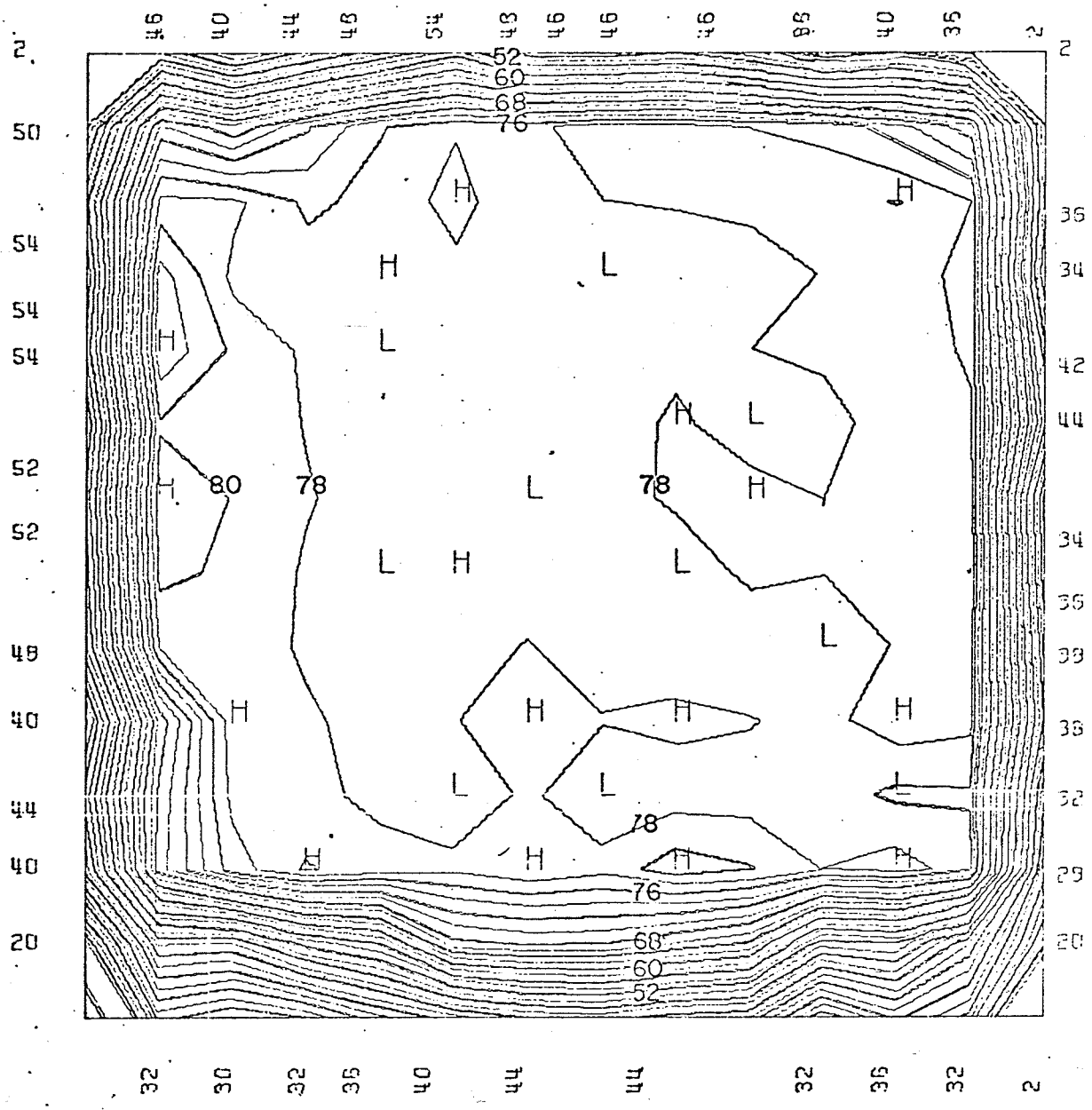

FIGURE 52

CONTOUR PLOT AT STATION 2
ONE-HALF BLEED.

(AXIAL VELOCITY - FT/SEC.)

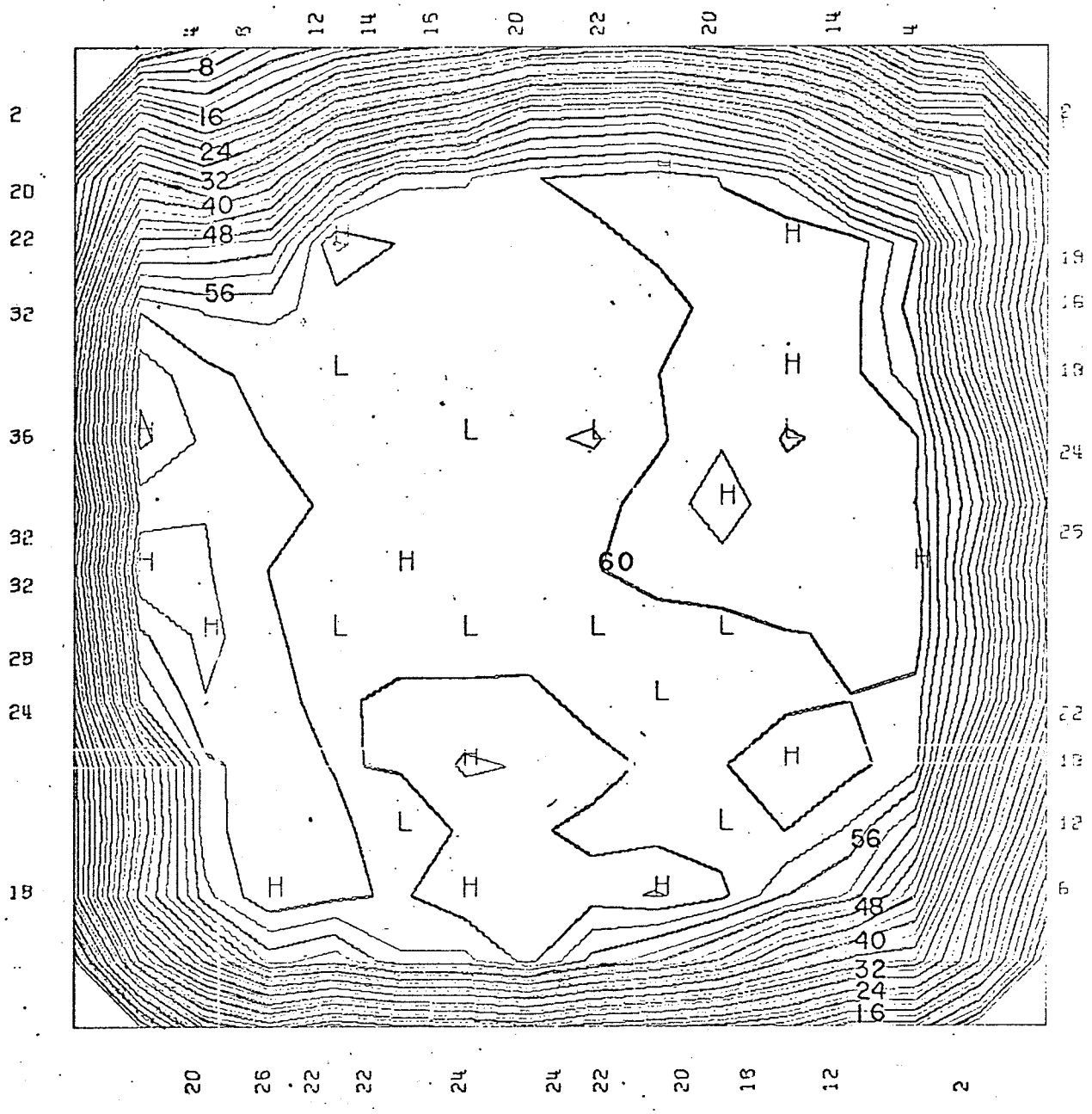

FIGURE 53

CONTOUR PLOT AT STATION 3
ONE-HALF BLEED.
(AXIAL VELOCITY - FT./ SEC.)

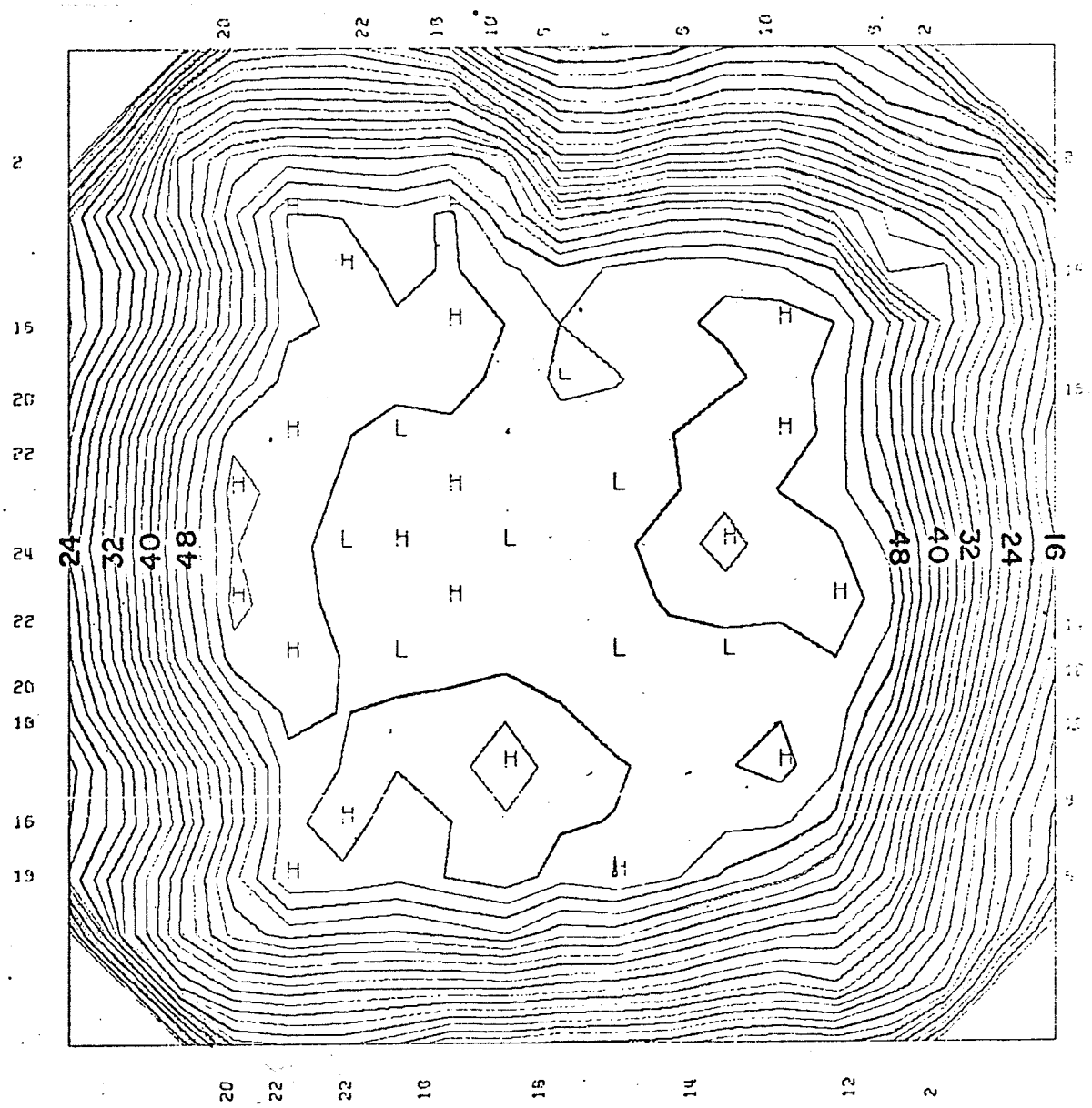

FIGURE 54

CONTOUR PLOT AT STATION 4
ONE HALF BLEED.
(AXIAL VELOCITY - FT / SEC.)

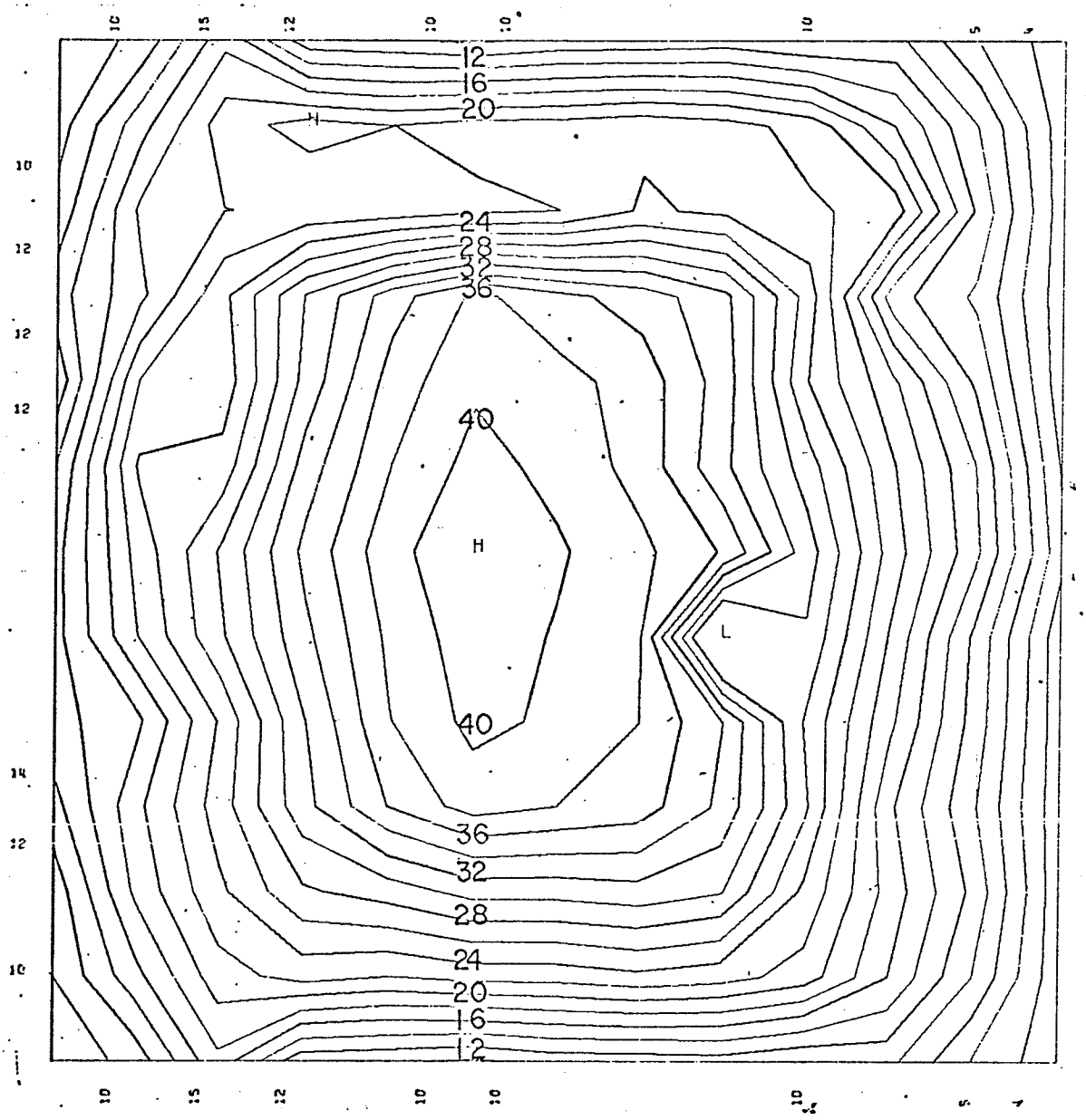

FIGURE 55

CONTOUR PLOT AT STATION 5
ONE-HALF BLEED
(AXIAL VELOCITY – FT./-SEC.)

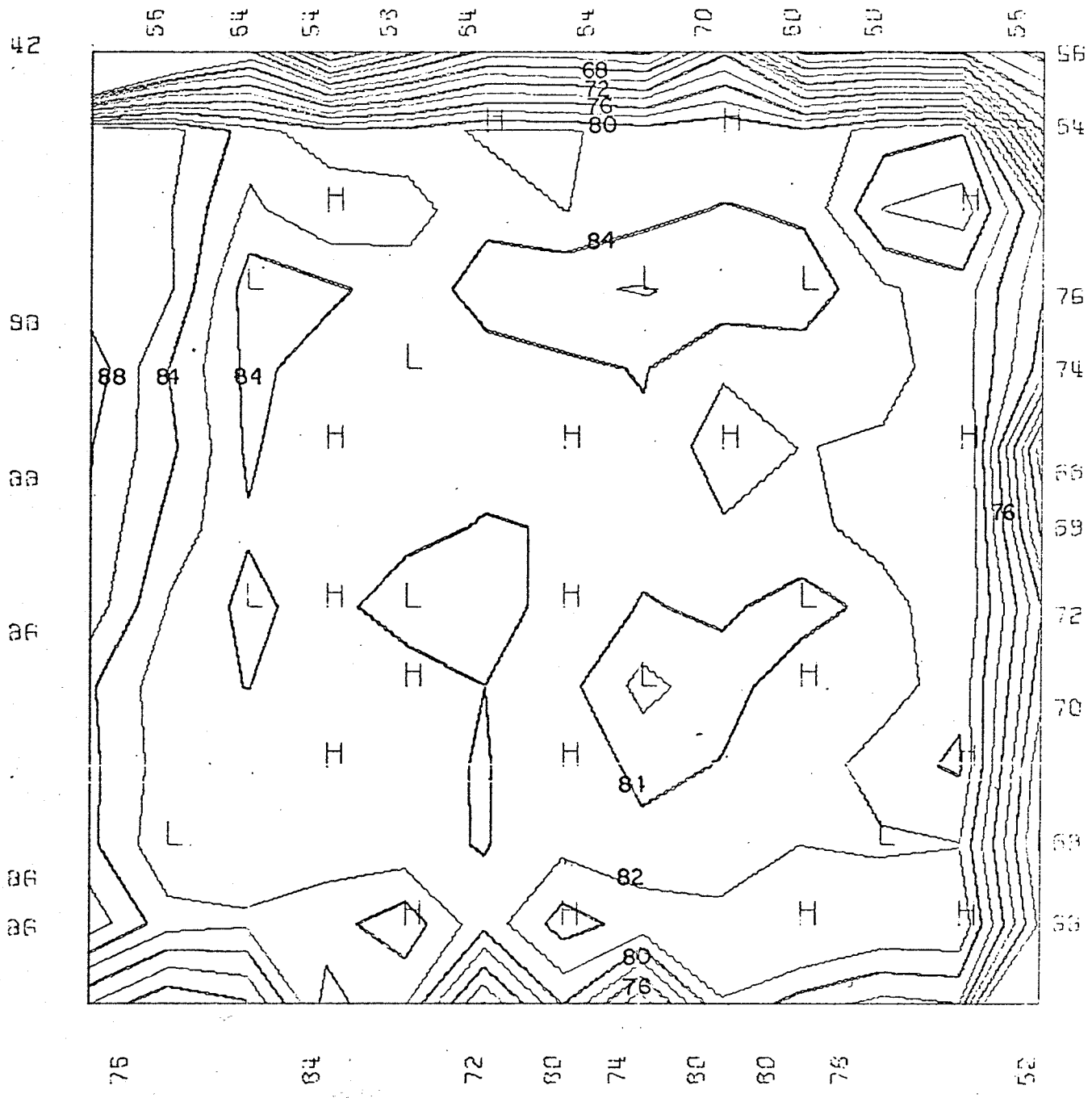

FIGURE 56

CONTOUR PLOT AT STATION 1
FULL BLEED.
(AXIAL VELOCITY - FT./SEC.)

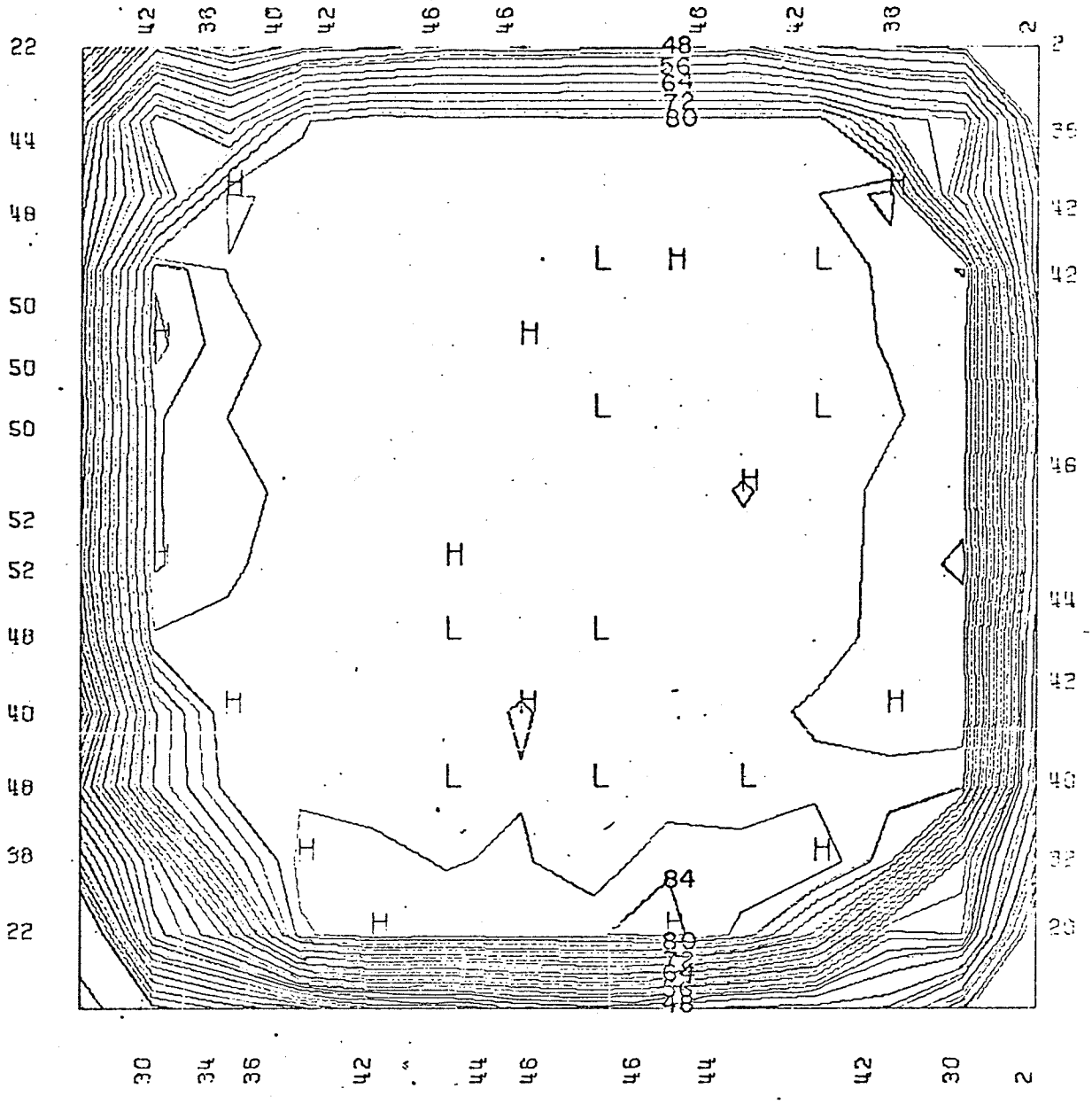

FIGURE 57

CONTOUR PLOT AT STATION 2
FULL BLEED.
(AXIAL VELOCITY- FT./SEC.)

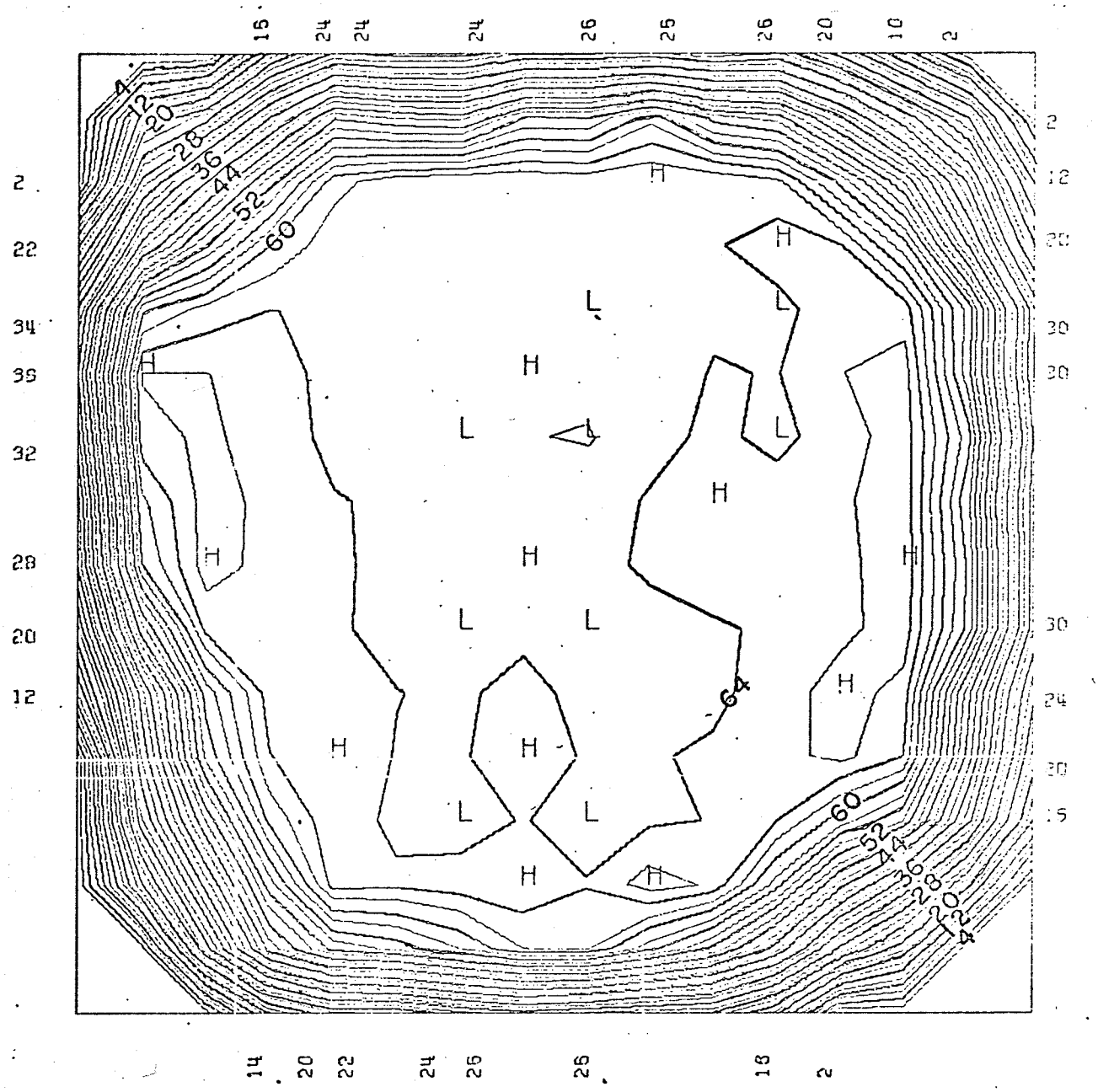

FIGURE 58

CONTOUR PLOT AT STATION 3
FULL BLEED.

(AXIAL VELOCITY - FT./SEC.)

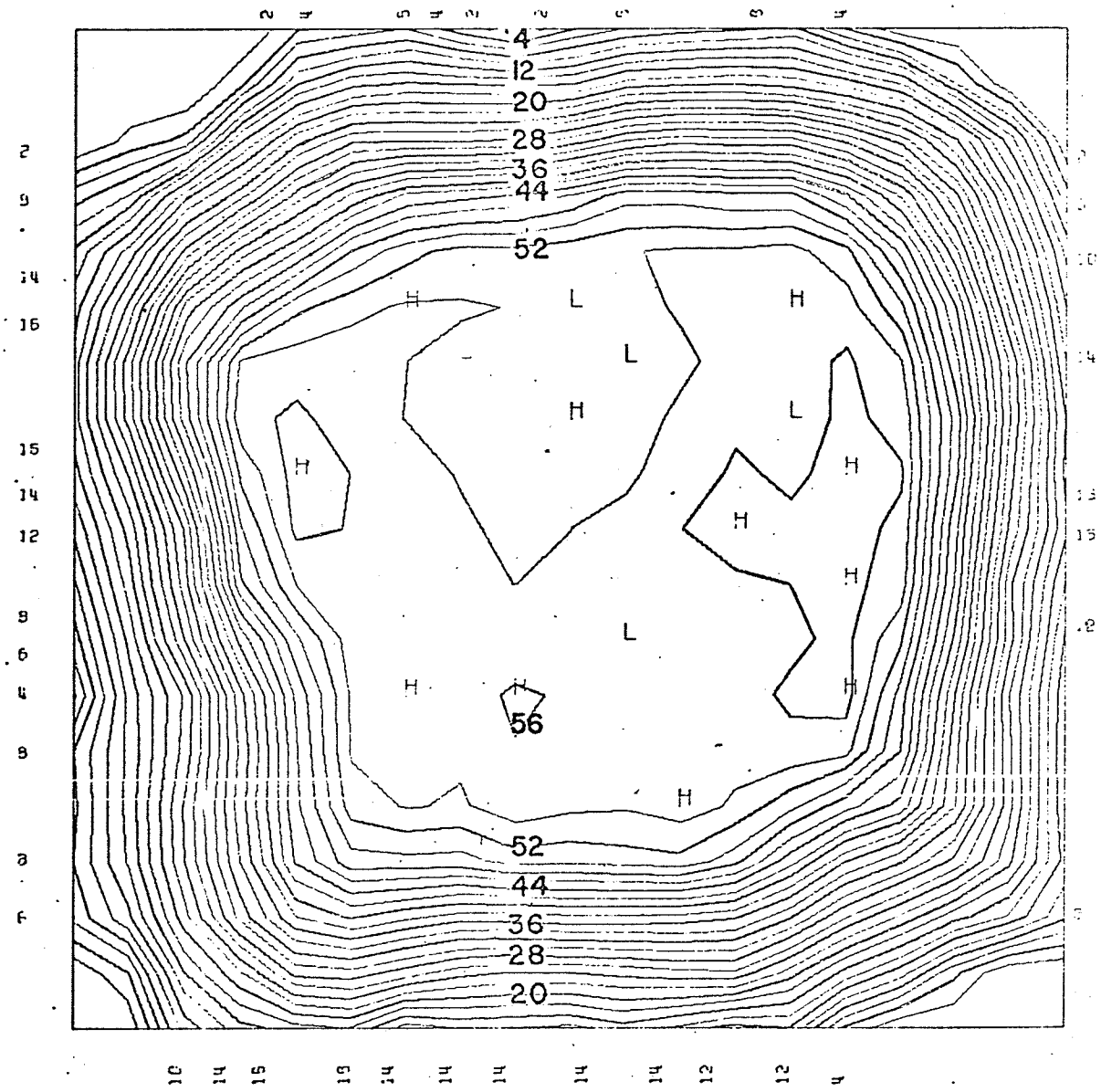

FIGURE 59

CONTOUR PLOT AT STATION 4
FULL BLEED.

(AXIAL VELOCITY - FT./SEC.)

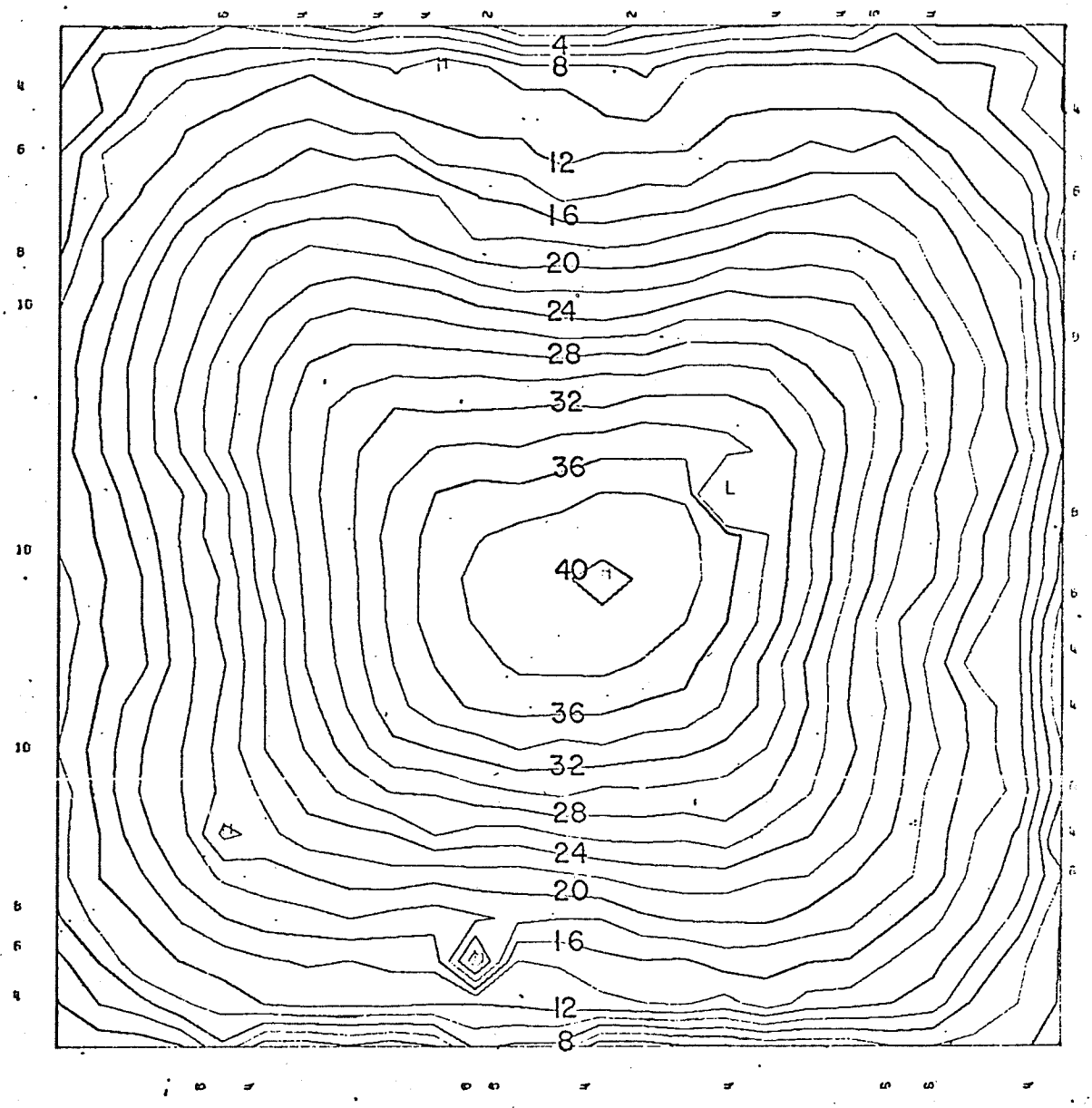

FIGURE 60

CONTOUR PLOT AT STATION 5
FULL BLEED.
(AXIAL VELOCITY - FT./SEC.)

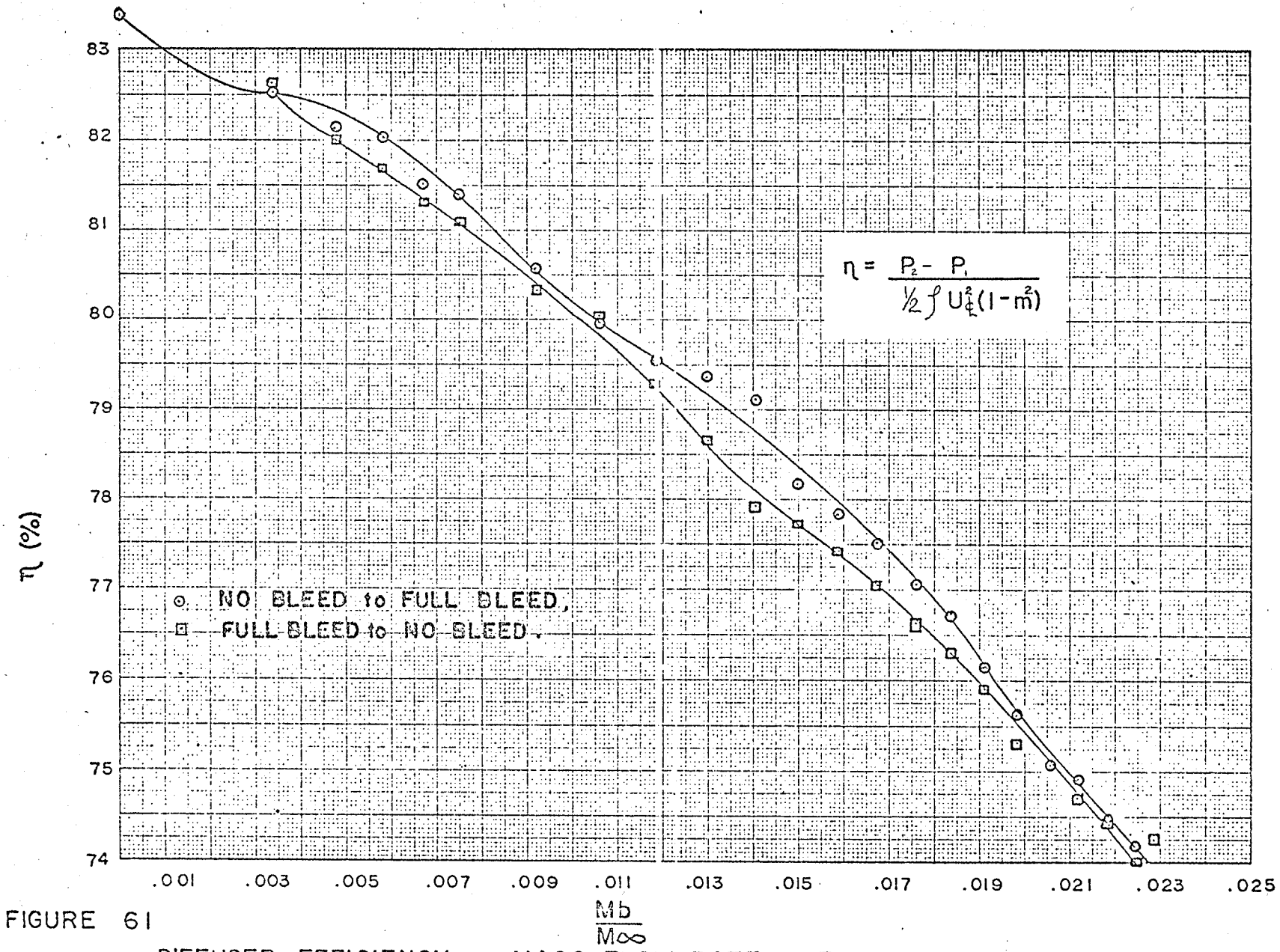

FIGURE 61

DIFFUSER EFFICIENCY vs MASS FLOW RATE — FULL THROTTLE.

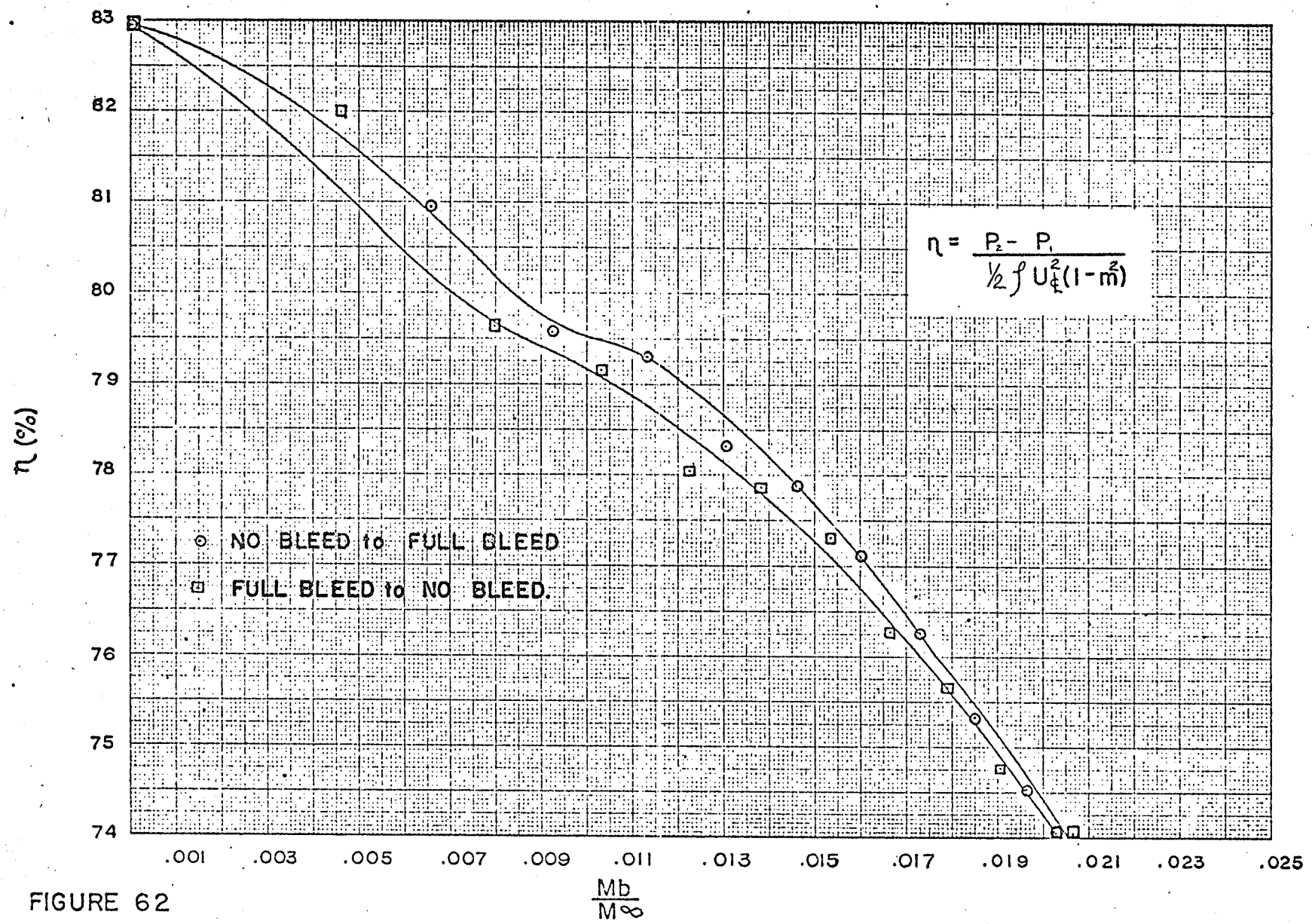

FIGURE 62

DIFFUSER EFFICIENCY vs MASS FLOW RATE — ONE-HALF THROTTLE.